AFRL-AFOSR-VA-TR-2016-0252

Cellular Mechanisms of Transcranial Direct Current Stimulation

Marom Bikson
RFCUNY - CITY COLLEGE
CONVENT AVE & 138TH ST
NEW YORK, NY 100319101

07/14/2016
Final Report

Air Force Research Laboratory
AF Office Of Scientific Research (AFOSR)/RTB2

Arlington, Virginia 22203
Air Force Materiel Command

REPORT DOCUMENTATION PAGE

Form Approved
OMB No. 0704-0188

PLEASE DO NOT RETURN YOUR FORM TO THE ABOVE ORGANIZATION.

1. REPORT DATE *(DD-MM-YYYY)*	2. REPORT TYPE	3. DATES COVERED *(From - To)*
13/06/2016	Final	March 15, 2013 to March 14, 2016

4. TITLE AND SUBTITLE

Cellular Mechanisms of Transcranial Direct Current Stimulation

5a. CONTRACT NUMBER

FA9550-13-1-0073

5b. GRANT NUMBER

5c. PROGRAM ELEMENT NUMBER

6. AUTHOR(S)

Marom Bikson

5d. PROJECT NUMBER

5e. TASK NUMBER

5f. WORK UNIT NUMBER

7. PERFORMING ORGANIZATION NAME(S) AND ADDRESS(ES)

RESEARCH FOUNDATION OF THE CITY UNIVERSITY OF NEW YORK
RFCUNY - CITY COLLEGE
CONVENT AVE & 138TH ST NEW YORK NY 10031-9107

8. PERFORMING ORGANIZATION REPORT NUMBER

9. SPONSORING/MONITORING AGENCY NAME(S) AND ADDRESS(ES)

Air Force Office of Scientific Research
875 North Randolph Street
Suite 325, Room 3112
Arlington VA, 22203

10. SPONSOR/MONITOR'S ACRONYM(S)

11. SPONSOR/MONITOR'S REPORT NUMBER(S)

12. DISTRIBUTION/AVAILABILITY STATEMENT

DISTRIBUTION A: Distribution approved for public release.

13. SUPPLEMENTARY NOTES

14. ABSTRACT

During transcranial Direct Current Stimulation (tDCS), low-intensity DC current is applied across the scalp to enhance specific performance or training efficacy on a range of complex cognitive tasks; moreover tDCS has been suggested to produce minimal side-effects (undesired cognitive changes). The central premise of this proposal is that tDCS achieves task-specific modulation through a cellular mechanism where only neuronal circuits primed during tDCS (for example by training) are modulated by tDCS, while non-primed mechanisms are not modulated. The specific goal of this proposal is thus to establish a cellular substrate for DCS mediated activation-specific changes. This proposal addresses two independent, but not exclusive, cellular mechanisms: Can DCS lead to plastic changes by direct modulation of neuronal membrane excitability, dependent on action potential activity but not necessarily dependent on synaptic function (Aim 1)? How does DCS modulation of synaptic efficacy depend on ongoing synaptic activity (Aim 2)?

15. SUBJECT TERMS

16. SECURITY CLASSIFICATION OF:			17. LIMITATION OF ABSTRACT	18. NUMBER OF PAGES	19a. NAME OF RESPONSIBLE PERSON
a. REPORT	b. ABSTRACT	c. THIS PAGE			19b. TELEPHONE NUMBER *(Include area code)*

Reset

Standard Form 298 (Rev. 8/98)
Prescribed by ANSI Std. Z39.18
Adobe Professional 7.0

INSTRUCTIONS FOR COMPLETING SF 298

1. REPORT DATE. Full publication date, including day, month, if available. Must cite at least the year and be Year 2000 compliant, e.g. 30-06-1998; xx-06-1998; xx-xx-1998.

2. REPORT TYPE. State the type of report, such as final, technical, interim, memorandum, master's thesis, progress, quarterly, research, special, group study, etc.

3. DATES COVERED. Indicate the time during which the work was performed and the report was written, e.g., Jun 1997 - Jun 1998; 1-10 Jun 1996; May - Nov 1998; Nov 1998.

4. TITLE. Enter title and subtitle with volume number and part number, if applicable. On classified documents, enter the title classification in parentheses.

5a. CONTRACT NUMBER. Enter all contract numbers as they appear in the report, e.g. F33615-86-C-5169.

5b. GRANT NUMBER. Enter all grant numbers as they appear in the report, e.g. AFOSR-82-1234.

5c. PROGRAM ELEMENT NUMBER. Enter all program element numbers as they appear in the report, e.g. 61101A.

5d. PROJECT NUMBER. Enter all project numbers as they appear in the report, e.g. 1F665702D1257; ILIR.

5e. TASK NUMBER. Enter all task numbers as they appear in the report, e.g. 05; RF0330201; T4112.

5f. WORK UNIT NUMBER. Enter all work unit numbers as they appear in the report, e.g. 001; AFAPL30480105.

6. AUTHOR(S). Enter name(s) of person(s) responsible for writing the report, performing the research, or credited with the content of the report. The form of entry is the last name, first name, middle initial, and additional qualifiers separated by commas, e.g. Smith, Richard, J, Jr.

7. PERFORMING ORGANIZATION NAME(S) AND ADDRESS(ES). Self-explanatory.

8. PERFORMING ORGANIZATION REPORT NUMBER. Enter all unique alphanumeric report numbers assigned by the performing organization, e.g. BRL-1234; AFWL-TR-85-4017-Vol-21-PT-2.

9. SPONSORING/MONITORING AGENCY NAME(S) AND ADDRESS(ES). Enter the name and address of the organization(s) financially responsible for and monitoring the work.

10. SPONSOR/MONITOR'S ACRONYM(S). Enter, if available, e.g. BRL, ARDEC, NADC.

11. SPONSOR/MONITOR'S REPORT NUMBER(S). Enter report number as assigned by the sponsoring/ monitoring agency, if available, e.g. BRL-TR-829; -215.

12. DISTRIBUTION/AVAILABILITY STATEMENT. Use agency-mandated availability statements to indicate the public availability or distribution limitations of the report. If additional limitations/ restrictions or special markings are indicated, follow agency authorization procedures, e.g. RD/FRD, PROPIN, ITAR, etc. Include copyright information.

13. SUPPLEMENTARY NOTES. Enter information not included elsewhere such as: prepared in cooperation with; translation of; report supersedes; old edition number, etc.

14. ABSTRACT. A brief (approximately 200 words) factual summary of the most significant information.

15. SUBJECT TERMS. Key words or phrases identifying major concepts in the report.

16. SECURITY CLASSIFICATION. Enter security classification in accordance with security classification regulations, e.g. U, C, S, etc. If this form contains classified information, stamp classification level on the top and bottom of this page.

17. LIMITATION OF ABSTRACT. This block must be completed to assign a distribution limitation to the abstract. Enter UU (Unclassified Unlimited) or SAR (Same as Report). An entry in this block is necessary if the abstract is to be limited.

Final Report Contents

Executive Summary

Main Result and Impact

The overall aim of this proposal (FA9550-13-1-0073) was to address the cellular mechanisms of transcranial Direct Current Stimulation (DCS). Indeed, the scale and pace on tDCS trials in humans (hundreds published per year, and hundreds ongoing) has vastly outpaced our understanding of cellular mechanisms. There are so many human trials *because* various investigators have proposed that tDCS may be used to enhanced wide range of cognitive functions and also treat a wide range of neuro-psychiatric disease. The breadth of these applications is *almost* unbelievable – it is based on the general concept that tDCS is paired with a task (some kind of training) and that tDCS produces an enhancement in only that task. The ability of tDCS to selectively promote performance on trained tasks is essential but unaddressed at the cellular level. The combination of tDCS with training *implies interactions of DCS with ongoing task-specific activity leading to task-specific plasticity*. This proposal showed that DCS can induce lasting (plastic) changes selectivity in co-activated synaptic processes and provided a cellular substrate for these changes. This proposal therefore provided a detailed cellular-level explanation for how tDCS can enhance (theoretically) any task it is paired with. This proposal thus not only provides a cellular explanation for tDCS, it also showed why tDCS could be applied to so many applications. This is a fundamental advance in rationalizing the use of tDCS, and together is a new theory we call “functional targeting”.

Report Sections

This summary report is organized on chapters that approximated papers either published or in preparation that resulted from this proposal. Related to the overall cellular explant ion for tDCS summarized above, the salient results of each chapter are simply [Mapping to Aims in the original proposal indicated]:

Section 1: Identifies a new cellular target of tDCS. Whereas prior work has focused on the soma of neurons, we show the axon is in fact more sensitivity. [Aim 1].

Section 2: tDCS is diffuse (current going to much of the brain) and weak (low-intensity). Whereas prior work tried to explain away this "deficit" we in fact show these feature of tDCS can be "benefits" – including making the effects of tDCS specific to a matched training task. [Aim 1, Aim 2].

Section 3: tDCS is thought to boost the learning of tasks or therapy applied at the same time. We provide a cellular mechanism for this. Moreover, we show that thus "boosting" is specific to the trained task. [Aim 2]

Section 4: tDCS is though to boost learning by promoting synaptic plasticity. We show the mechanism of this plasticity. [Aim 2]

Publications and Chapters deriving form this proposal:

Rahman A, Bikson M. et al. Diffuse and sustained electrical stimulation amplifies synaptic cooperativity. Submitted. In review.

Rahman A, Bikson M. et al. Electrical stimulation accelerates and boosts the capacity for synaptic learning. In preparation.

Kronberg G, Bikson M. et al. Modulation of synaptic plasticity with direct current stimulation is activity-dependent and differs with dendritic location. Submitted. In review.

Rahman A, Reato D, Arlotti M, Gasca F, Datta A, Parra LC, Bikson M. Cellular Effects of Acute Direct Current Stimulation: Somatic and Synaptic Terminal Effects. Journal of Physiology 2013; 591.10: 2563-2578

Rahman A, Lafon B, Bikson M. Multilevel computational models for predicting the cellular effects of noninvasive brain stimulation. Prog Brain Res. 2015;222:25-40. doi:10.1016/bs.pbr.2015.09.003

Bikson M, Truong DQ, Mourdoukoutas AP, Aboseria M, Khadka N, Adair D, Rahman A. Modeling sequence and quasi-uniform assumption in computational neurostimulation. Prog Brain Res. 2015;222:1-23 doi:10.1016/bs.pbr.2015.08.00

Rahman A, Bikson M. Origins of specificity during tDCS: anatomical, activity-selective, and input-bias mechanisms Frontiers of Human Neuroscience 2013; doi 10.3389/fnhum.2013.00688

Reato D, Rahman A, Bikson M, Parra LC. Effects of weak transcranial Alternating Current Stimulation on brain activity – a review of known mechanisms from animal studies. Frontiers of Human Neuroscience 2013; doi 10.3389/fnhum.2013.00687

Section 1: Somatic and synaptic terminal effects of acute direct current stimulation

Abstract

Transcranial Direct Current Stimulation (tDCS) is a non-invasive brain stimulation technique to modulate cortical excitability. Although increased/decreased excitability under the anode/cathode electrode is nominally associated with membrane depolarization/hyperpolarization, which cellular compartments (somas, dendrites, axons and their terminals) mediate changes in cortical excitability remains unaddressed. Here we consider the acute effects of direct current stimulation on excitatory synaptic efficacy. Using multi-scale computational models and rat cortical brain slices we show: 1) Typical tDCS montages produce predominantly tangential (relative to the cortical surface) direction currents (4-12 times radial direction currents), even directly under electrodes. 2) Radial current flow (parallel to the somatodendritic axis) modulates synaptic efficacy consistent with somatic polarization, with depolarization facilitating synaptic efficacy. 3) Tangential current flow (perpendicular to the somatodendritic axis) modulates synaptic efficacy acutely (during stimulation) in an afferent pathway specific manner that is consistent with terminal polarization, with hyperpolarization facilitating synaptic efficacy. 4) Maximal polarization during uniform direct current stimulation is expected at distal (branch length is >3 times the

membrane length constant) synaptic terminals, independent of and 2-3 times more susceptible than pyramidal neuron somas. We conclude that during acute direct current stimulation the cellular targets responsible for modulation of synaptic efficacy are concurrently somata and axon terminals, with the direction of cortical current flow determining the relative influence.

Introduction

During tDCS, current flow (~1 mA) from an anode to a cathode electrode generates weak electric fields (<1 V/m) across the cortex (Datta et al., 2009; Salvador et al., 2010). tDCS modulates cortical excitability in the primary motor cortex (Nitsche and Paulus, 2000, 2001; Antal et al., 2004), with anodal stimulation enhancing and cathodal stimulation diminishing corticospinal excitability, as measured by motor evoked potentials (MEPs) elicited by transcranial magnetic stimulation (TMS) (Nitsche et al., 2005). Similarly, in animal models of DCS spontaneous and evoked cortical potentials were acutely facilitated under the anode and inhibited under the cathode (Creutzfeldt et al., 1962; Bindman et al., 1964; Purpura and McMurtry, 1965b). The acute changes in synaptic efficacy by DCS may translate to enduring effects (short or long-term plasticity) lasting over one hour after stimulation, dependent on the duration of stimulation (typically minutes) (Bindman et al., 1962, 1964; Gartside, 1968) and the nature of ongoing (synaptic) activity (Fritsch et al., 2010; Ranieri et al., 2012). Additionally, the acute effects of DCS are not homogeneous since the cellular effects of stimulation depend on neuronal morphology, stimulation intensity, neuronal orientation relative to the induced electric field, and on the nature of the spontaneous/evoked activity(Tranchina and Nicholson, 1986; Chan et al., 1988; Andreasen and Nedergaard, 1996; Bikson et al., 2004; Joucla and Yvert, 2009; Radman et al., 2009b). Here, we consider if characterizing the cellular targets of DCS may help reconcile acute neuromodulation patterns in a single framework. We specifically focus on the role of acute cortical DCS on presynaptic (afferent axon) versus postsynaptic (soma/dendrites) cellular compartments in modulating synaptic efficacy (Jefferys, 1981; Bikson et al., 2004; Fritsch et al., 2010; Kabakov et al., 2012; Ranieri et al., 2012).

Neuronal excitability in resting neurons is modulated by subthreshold DCS through cell membrane polarization (< 1 mV polarization per V/m) (Radman et al., 2009). While, the increase in excitability under the anode is attributed to “membrane depolarization” and the decrease in excitability under the cathode is attributed to “membrane hyperpolarization” (Bindman et al., 1962, 1964; Purpura and McMurtry, 1965b), in fact, during DCS there are an equal number of cellular elements that are hyperpolarized or depolarized in any given brain region (Joucla & Yvert, 2009), including directly under the anode and cathode. For example, during DCS of cortical pyramidal neurons, somatic depolarization is associated with concurrent apical dendritic hyperpolarization, and somatic hyperpolarization is associated with apical dendritic depolarization (Chan and Nicholson, 1986; Tranchina and Nicholson, 1986; Chan et al., 1988; Andreasen and Nedergaard, 1996; Radman et al., 2009b). Additionally, afferent axons and their terminals are also polarized during DCS with varied polarity depending on morphology (BeMent and Ranck, 1969; Ranck, 1975; Tranchina and Nicholson, 1986; Arlotti et al., 2012; Kabakov et al., 2012; Marquez-Ruiz et al., 2012). Finally, membrane compartment-specific polarization affects the capacity of presynaptic input to influence postsynaptic output (synaptic efficacy) in both acute and long-lasting effects of DCS (Bikson et al., 2004; Fritsch et al., 2010; Kabakov et al., 2012; Marquez-Ruiz et al., 2012). The diversity of cellular targets of DCS raises a number of mechanistic questions. Which membrane compartments (somas, dendrites, or axons/terminals) polarized during DCS contributes to changes in excitability, including synaptic efficacy? Does depolarization/hyperpolarization of the implicated compartments in fact correlate with facilitation/inhibition of synaptic efficacy?

Classical animal research has implicated somatic polarization during transcortical DCS (Terzuolo and Bullock, 1956; Purpura and McMurtry, 1965a, b). Accordingly, local field potentials and intracellular recordings suggest that facilitation/inhibition of spontaneous activity (Frohlich & McCormick, 2010; Reato et al., 2010) and synaptic efficacy during DCS may be associated with depolarization/hyperpolarization of the somatic membrane potential (Jefferys, 1981; Bikson et al., 2004; Radman et al., 2009). However, afferent axons, including corticocortical and thalamocortical connections, which are involved in synaptic processing, might additionally contribute to the effects of DCS (Purpura and McMurtry, 1965a, b; Bikson et al., 2004; Kabakov et al., 2012; Marquez-Ruiz et al., 2012). For example, modulation of presynaptic

transmitter release at thalamocortical sensory afferents has been attributed to the effects of DCS in vivo (Marquez-Ruiz et al., 2012). Whether hyperpolarization or depolarization of axon terminals enhances efficacy may vary across synaptic pathways. Finally, DCS of the apical dendrites of pyramidal neurons, which polarize opposite to somas, may further influence synaptic processing (Bikson et al., 2004). Thus, it remains unclear, which compartments influence modulation by DCS (somas, dendrites, or axons/terminals) and whether depolarization or hyperpolarization is associated with enhanced synaptic efficacy. Understanding the cellular targets of tDCS is considered pre-requisite to rational electrotherapy design and optimization (Bikson et al., 2012b).

The cellular targets of TES remain unclear. Afferent axons, somas, and dendrites are all susceptible to polarization depending on the directionality of the induced electric field and the orientation of the neuronal compartment. The well-established approach to characterize the cellular effects of electrical stimulation is to determine the electric field produced in the brain target and then reproduce the electric field in animal models or neuron compartment models; for transcranial stimulation, including with DCS, the quasi-uniform assumption is widely applied (Bikson et al., 2012b). We extended previous MRI-derived models of tDCS generated brain current flow (Datta et al., 2009; Salvador et al., 2010) to quantify the directionality of the induced electric field in the cortex – specifically the relative radial and tangential components of the cortical electric field. In the second part of this study, we aimed to characterize the role of uniform electric fields on modulating the excitability of extracellular field potentials using brain slices, which facilitate control of electric-field direction (radial and tangential to the somatodendritic axis) and isolated activation of pathway-specific synaptic activity. Finally, compartment models of morphologically reconstructed cortical pyramidal neurons were used to predict which neuronal elements are polarized by uniform DC fields.

We report that during tDCS both radial and tangential (relative to the cortical surface) direction currents are induced, however, tangential currents are prevalent across the cortex. Fields radial to the cortical surface modulated synaptic efficacy independent of synaptic pathway and consistent with somatic polarization, with depolarization/hyperpolarization facilitating/inhibiting synaptic efficacy, while tangential

fields modulated synaptic efficacy in a pathway-specific manner, such that axon terminal hyperpolarization/depolarization was associated with facilitation/inhibition of synaptic efficacy. The acute effects of DCS on synaptic efficacy may be reconciled through (concurrent) contributions from these two cellular targets.

The overall goal of this study was to systematically characterize the cellular target of action for DC stimulation. Our approach was to first determine the prevalence of radial and tangential EFs in the cortex using MRI-derived computational models. Secondly, effects of radial and tangential DC fields on synaptic efficacy were characterized in cortical brain slices in four distinct synaptic pathways corresponding to different orientations of afferent axons. Synaptic efficacy was shown to be pathway-specific and synaptic terminal polarization by tangential fields can lead to facilitation/inhibition independent of somatic polarization. These findings motivated us to determine a general rule to describe sensitivity of axon terminals to polarization in the form of a coupling constant.

Methods

MRI-derived electric field models

Complete methods for MRI-derived head models of electric field (EF) distributions are detailed elsewhere (Datta et al., 2009). Briefly, EF distributions in the brain were computed using individualized head models created from the T1-weighted MRI scans of a healthy individual. The head was segmented into compartments representing gray matter, white matter, cerebrospinal fluid (CSF), skull, scalp, eye region, muscle, air, and blood vessels using a combination of tools from the FSL and Simpleware (Exeter, UK). The finite element (FE) mesh generated from the segmentation masks was exported to COMSOL Multiphysics 4.2 (Burlington, MA) for computation of electric fields.

Electric field magnitudes were calculated for the conventional tDCS montage over M1-SO (one anode over the primary motor cortex and one cathode over the supraorbital region, 5x5 cm sponge electrodes, Fig. 1A1, 2A) and the High-Definition tDCS (HD-tDCS) montage (center anode over the primary motor

cortex and four surround cathode electrodes, 1 cm electrode diam. with 6 cm separation between center and surround electrodes) (Datta et al., 2009). The relative magnitude of the two components of the EF (E_x = radial and E_y = tangential) are considered and quantified on multiple scales (Fig. 10), including global field distributions in the brain, regionally under/between electrodes, and in sub-regions on gyral crowns/walls. We use the ratio of tangential to radial (E_y / E_x) field magnitudes to describe the relative magnitudes in each region, such that $E_y / E_x > 1$ corresponds to greater tangential fields on average and $E_y / E_x < 1$ corresponds to greater radial fields on average (Fig. 9A2, A3). The E_y / E_x metric is represented in Fig. 1A1 with a schematic representation of the voltage distribution overlaid on each region of interest along a cortical gyrus.

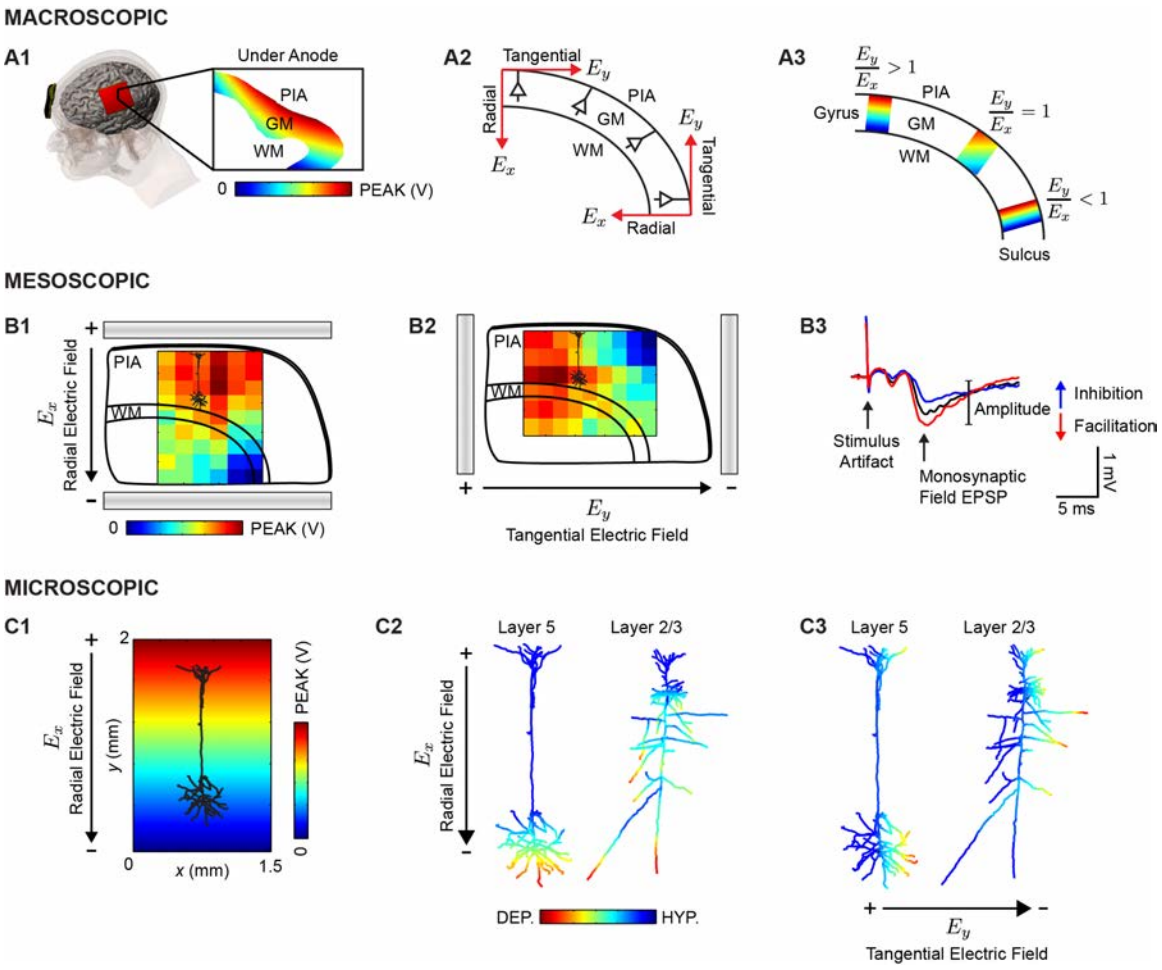

Figure 1. Multi-scale methods and outcome measures of uniform electric field directionality and effects. *A1*, Gyri-precise finite element models of current flow during tDCS indicate a uniform voltage gradient in cortical grey matter (GM) directly under the anode. *A2*, The induced electric

field in the cortex can be decomposed into a radial component (E_x) that is parallel to the somatodendritic axis and a tangential component (E_y) that is orthogonal to the somatodendritic axis. *A3*, We quantified the relative occurrence of radial and tangential fields in cortical GM expressed as the ratio of the average of the field magnitude in the tangential direction to the average of the field magnitude in the radial direction (E_y / E_x). *B1-2*, The brain slice preparation was used to study the change in synaptic efficacy during a uniform radial or tangential field by recording evoked field potentials. The voltage gradient between parallel Ag/AgCl wires is superimposed on a schematic of a sagittal slice of the rat primary motor cortex. From the macroscopic to the mesoscopic scale we can approximate a uniform electric field along the length of a neuron (compare voltage gradients in A1 and B1). *B3*, The field EPSP provides a measure of synaptic efficacy through facilitation or inhibition of the response amplitude. *C1*, Compartment model simulations of morphologically reconstructed neocortical pyramidal neurons were used to provide a description of axon terminal polarization in a uniform electric field. *C2*, The polarization profile of a layer 5 pyramidal neuron in a radially directed uniform electric field indicates soma depolarization (red) corresponds to apical dendrite hyperpolarization (blue). Layer 2/3 neurons have a more complex polarization profile with long processes reaching maximal depolarization independent of the neuronal body. *C3*, Neurons in a uniform electric field directed tangential to the somatodendritic axis preferentially affects processes that are oriented along the tangential field.

Electrophysiology

Brain slices including a part of the motor cortex were prepared from male young adult Wistar rats aged 3 to 6 weeks old, which were deeply anesthetized with ketamine (7.4 mg/kg) and xylazine (0.7 mg/kg) applied intraperitoneally (i.p.) and sacrificed by cervical dislocation. The brain was removed and immersed in chilled (2-6 ºC) artificial cerebrospinal fluid (ACSF) containing (in mM): 126 NaCl, 3 KCl, 1.25 NaH_2PO_4, 2 $MgSO_4$, 2 CaCl, 24 $NaHCO_3$ and 10 D-glucose, bubbled with a mixture of 95% O_2-5% CO_2). Parasagittal slices (450 µm thick) were cut at the distance of 2.0-3.0 mm from the brain midline using a vibrating microtome and transferred to a holding chamber for at least 1 h in ambient temperature. Slices were then transferred to a fluid-gas interface chamber perfused with warmed ACSF (30.0±0.5 ºC) at 1.9 mL/min. The humidified atmosphere over the slices was saturated with a mixture of 95% O2-5% CO2. Recordings started 2-3 h after dissection.

To investigate the role of distinct cortical pathways on modulation of synaptic efficacy the recording electrode (a glass micropipette filled with 0.25 M NaCl, resistance 1-8 MΩ) was placed in either layer II/III or layer V of the rat primary motor cortex (Fig. 11A). Neocortical horizontal pathways (within a cortical layer) and vertical pathways (across lamina) represent functionally distinct connections that are well

characterized in the rat neocortex (Aroniadou and Keller, 1993; Keller, 1993). For instance, horizontal connections integrate information across sensory maps in the motor cortex by connecting related functional columns; however, extrinsic connections from distant cortical and subcortical regions have dominantly vertical projections (Hess and Donoghue, 1994; Sasaki et al., 2011). The synaptic circuits representing intrinsic connections between populations of neurons within the motor cortex was previously identified in the literature using current source density distributions, morphological analysis, and through studies of functional connectivity, including long-term potentiation and depression experiments (Aroniadou and Keller, 1993; Keller, 1993; Aroniadou and Keller, 1995; Castro-Alamancos et al., 1995; Hess et al., 1996; Rioult-Pedotti et al., 1998). Fig. 3B summarizes the identified pathways relevant for this study. In addition to probing the pathway-specific effects of electric fields on cortical field potentials, we use the synaptic organization of the cortex to test the effectiveness of radial and tangential fields in modulating synaptic efficacy in horizontal and vertical pathways.

Orthodromic stimulation targeting four distinct synaptic pathways previously identified in the rat primary motor cortex was applied with a bipolar platinum/stainless steel stimulating electrode placed either 400-800 μm (stimulating electrodes S1 and S2) or 1100-1300 μm (stimulating electrodes S3 and S4) below the pial surface to activate fibres running within layer II/III or layer V, respectively (Fig. 11A). The stimulating electrodes were placed either laterally anterior or posterior to the recording electrode targeting horizontal afferent synaptic connections in either of the superficial (S1 and S2) or deep layers (S3) (Fig. 11A). Vertical connections were stimulated with a bipolar electrode (S4) in deep layer V and a recording electrode in layer II/III. Field excitatory postsynaptic potentials (fEPSPs), which provides a measure of localized extracellular currents generated from a population of pyramidal neurons in response to synaptic or antidromic activation, were evoked with constant-current pulses (0.2 ms) delivered once per minute. The test stimulus intensity (30-200 μA) was adjusted to evoke half-maximal responses based on input-output curves (Fig. 12A); no consistent relationship was found between fEPSP delay and stimulation amplitude or fEPSP peak. This relatively weak stimulation did not evoke population spikes, and usually elicited a fEPSP having a single peak in 84 of 92 slices tested. Responses were amplified, low pass

filtered (1000 Hz cutoff, Warner Instruments, CT, USA), acquired at a 10-kHz sampling rate (1401 interface, CED, UK) and analyzed on- and offline (Signal 3 software, CED, UK).

The stimulation protocol was designed to measure the acute (during field) changes in fEPSPs evoked during an applied electric field. fEPSP amplitudes were used as a measure of the change in synaptic efficacy during the field, such that an increase in the amplitude indicates facilitation and a decrease indicates inhibition. Uniform fields (±8 V/m) were generated by passing current (D/A driven analog current follower, A-M Systems, WA, USA) between two large parallel Ag-AgCl wires positioned in the bath across the slice for 1 sec starting 0.5 sec before bipolar stimulation. The field intensity was chosen based on pilot experiments to produce approximately a 5% change in fEPSP amplitude such that a statistically significant change could be observed within slices with a practical sample size (Fig. 12B).

The quasi-uniform EF assumption (Bikson et al., 2012b), which considers the applied EF amplitude may be uniform on the scale of the membrane length constant, allowed us to evaluate synaptic efficacy in a population of neurons in a uniform EF in vitro as well as in single neuron models (compare Fig. 1A1, B1 and C1). Specifically, tDCS produces approximate uniform fields across select regions of grey matter (Fig. 12A, linear voltage gradients) that can be reproduced in vitro (Fig. 12B) and simulated in silico (Fig. 12C). Consideration of uniform electric fields allows analysis in this study across the macroscopic (brain current flow using FEM), mesoscopic (synaptic efficacy in brain slice), and microscopic scales (neuron compartment polarization). Indeed, representation of electric fields is ubiquitous in FEM computational studies (Miranda et al., 2006; Datta et al., 2009; Salvador et al., 2010; Datta et al., 2011), and uniform electric fields are used in mechanistic studies of tDCS (Radman et al., 2009a; Anastassiou et al., 2010; Fritsch et al., 2010; Arlotti et al., 2012; Kabakov et al., 2012; Ranieri et al., 2012). To our knowledge this is the first study to integrate analysis across these three scales.

All the statistical data are expressed as mean ± SD, unless stated otherwise. The statistical difference between groups (critical value=0.05) was estimated using the Student's t-test considering normally distributed fEPSP amplitudes (Lilliefors test for normality).

Compartment model simulation

Numerical and analytical solutions of 3D reconstructed neurons and simplified cable models, respectively, were used to infer a general rule of steady-state axon terminal polarization under a uniform electric field based on axonal morphology. With thousands of axonal afferents, with diverse morphologies for any given cortical neuron, a range of axon terminal polarization values are expected; but our goal was to approximate the *maximum* polarization expected in the most sensitive axon terminals. Specifically, we aimed to characterize the sensitivity of axon terminals by their coupling constant (which linearly relates steady-state membrane polarization to electric field); this then allows comparison of maximal axon terminal sensitivity with previously characterized coupling constants for neuron somas (Radman et al., 2009a).

Numerical solutions for realistic neurons. Complex neuronal geometries require numerically solving the cable equation (Basser and Roth, 2000). Eight morphologically reconstructed layer II/III and layer V rat somatosensory pyramidal neurons from the NeuroMorpho.org database (ID: NMO_0116, NMO_00348, NMO_00410, NMO_00417, NMO_01134, NMO_01132, NMO_01135, NMO_01112) were used to approximate membrane polarization in a uniform EF using Neuron (version 7.2) (Wang et al., 2002; Ascoli, 2006). The built-in function extracellular(x) was used to apply 1 V/m uniform electric fields in the radial direction (parallel to the somatodendritic axis, Fig. 1C1, C2), tangential direction (perpendicular to the somatodendritic axis, Fig. 1C3), and in optimal polarization angles along individual axons to produce the maximum terminal polarization in that axon. The membrane resistance R_m was 70 kΩcm^{-2} and the intracellular axial resistance R_i was 155 Ωcm (Markram et al., 1998). The median axonal length constant ($\lambda = \sqrt{\frac{r \times \rho_m}{2 \times \rho_i}}$, where r is the radius ρ_m is the membrane resistivity and ρ_i is the intracellular resistivity) was 0.56 mm (0.05 mm interquartile range). In all compartment neuron models, passive resistive parameters were used to approximate steady state membrane polarization.

Branched semi-infinite axon. Next, we considered a bent semi-infinite axon in a uniform EF to establish a relationship between terminal polarization and fibre morphology, extending previous derivations (Tranchina and Nicholson, 1986; Basser and Roth, 2000; Miranda et al., 2007b). We previously derived the analytical steady-state solution to the classic cable equation for a passive terminating straight branch of an axon (Eq. 1, for a complete derivation see (Arlotti et al., 2012).

Equation 1. $$V_t = E\lambda\cos(\theta)\tanh(\ell/\lambda) + V_0\frac{1}{\cosh(\ell/\lambda)}$$

The terminal polarization varies with the physical length ℓ of the final segment and depends on the angle θ of the electric field E relative to the final branch and the membrane polarization at the bend V_0. The relative contribution of $E\lambda$ vs. V_0 depends on the electrotonic (dimensionless) length ℓ/λ.

Straight semi-infinite axon. A simple analytical solution of polarization of a straight semi-infinite axon in a uniform EF is well known (and is in fact a special case of the axon branch with infinite length); Equation 2 relates polarization at the fibre terminal with the membrane space constant λ (Hause, 1975). The terminal membrane polarization is a function of the uniform extracellular EF relative to the axon, such that $\theta = 0$ corresponds to an EF along the longitudinal axis of the fibre. Interestingly, in this formulation λ is analogous to the coupling constant, and we intend to establish if and when this approximation is valid for realistic axon morphologies.

Equation 2. $$\ell \gg \lambda \Rightarrow V_t = E\lambda\cos\theta$$

Results

Quantitative analysis of electric field directionality in finite element models

Consistent with previous computational studies, tDCS and HD-tDCS are predicted to generate weak EFs (<1 V/m per mA applied current) in the cortex, with a complex spatial pattern determined by the electrode montage and the details of brain anatomy, notably cortical surface idiosyncrasies (Datta et al., 2009). Under the assumption that the voltage gradient in each region of the grey matter was locally linear, we summarized the (uniform) EF in each region (Fig 12A, Fig 13). Cortical EFs generated during stimulation have components both radial (E_x , normal) and tangential (E_y , parallel) to the cortical surface (Fig. 9B). Radial fields that are oriented along the somatodendritic axis of cortical pyramidal neurons produce somatic polarization. Tangential fields are transverse to the somatodendritic axis of cortical pyramids, and will polarize horizontally directed corticocortical axons. High-resolution modeling shows that current flowing across grey matter will have both radial and tangential components in conventional (Fig. 10A, top) and High-Definition (Fig. 10A, bottom) tDCS. We previously reported interindividual variations of peak cortical electric field of ~two fold across anatomically normal adult heads (Datta et al., 2012) but focus here on relative directional distribution. The global prevalence of tangential fields motivated further analysis of field directionality on additional levels including regions under/between electrodes and sub-regions of gyral crown/walls.

The distribution of radial and tangential components (Fig. 10B; density plots show relative occurrence) under the anode (E_y / E_x tDCS: 7.9, HD-tDCS: 4.8), cathode (E_y / E_x tDCS: 7.0, HD-tDCS: 8.0), and between electrodes (E_y / E_x tDCS: 11.7, HD-tDCS: 7.6) indicate most elements have both field components but with (significantly) stronger tangential than radial field (Fig. 10B, inset histograms). Interestingly, the few isolated highest EFs are radial (Fig. 10B, axis histograms).

Cortical folding greatly influenced the EF distribution under the electrodes (Fig. 10C). For example, on the scale of a single gyrus in the primary motor strip, the gyral crown has a dominantly tangential component (E_y / E_x tDCS: 16.6, HD-tDCS: 7.3) and the strongest fields are tangentially oriented. In contrast, motor strip gyral walls have a relatively equal distribution of field components using the

conventional tDCS electrode montage and slightly stronger radial components in HD-tDCS (E_y / E_x tDCS: 1.1, HD-tDCS: 0.33). The maximal EF in gyral walls is typically radial to the cortical surface, but a few elements have negligible tangential components as well.

In all regions, under and between electrodes, there is a higher density of elements with stronger tangential than radial fields, and few elements had purely radially oriented fields. Given the prevalence of tangential EFs, we next considered field direction sensitive changes in synaptic efficacy in cortical pathways of the rat primary motor cortex.

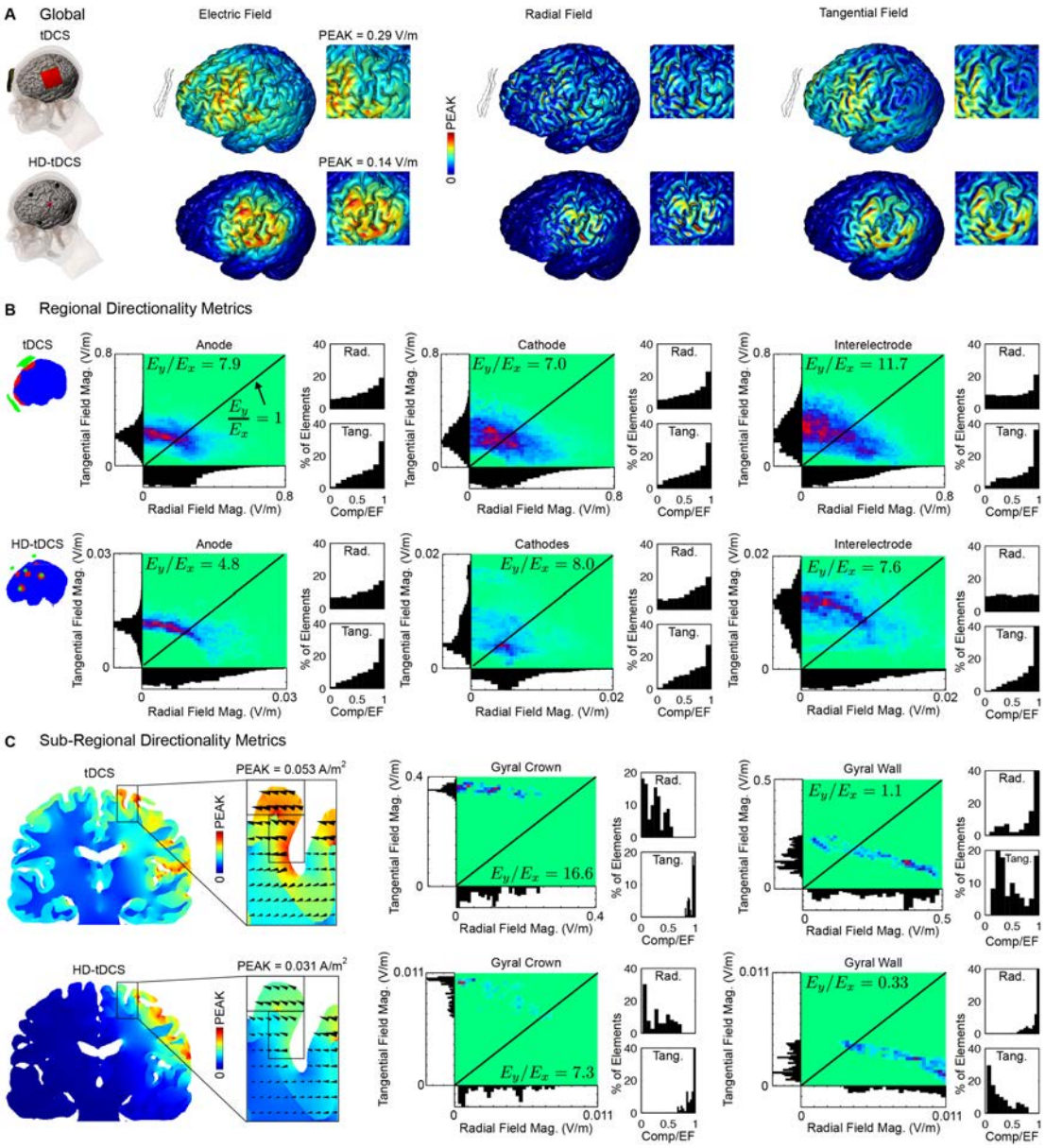

Figure 2. Forward model of tDCS and HD-tDCS quantifying electric field direction metrics. During tDCS, current may be dominantly tangential (along the cortical surface) rather than radial, even in brain regions directly under the electrodes. *A*, MRI-derived finite element models of current distribution in a gyri-precise head model are used to quantify the relative occurrence of radial (normal to the cortical surface) and tangential (along the cortical surface) components of the electric field. Both conventional (top) and high definition (HD, bottom) tDCS montages produce radial (E_x, normal to the cortical surface) and tangential current (E_y, along the cortical surface) indicated by the global electric field distribution (V/m) across the head. In the HD-tDCS montage, current is focalized within the ring configuration (inset) with radial currents under the center electrode and tangential currents between the surround electrodes. Qualitative comparison of the electric field components indicate greater radial field magnitudes in the gyral wall and greater tangential field magnitudes in the gyral crown (compare insets). *B*, Regionally, the distribution of field component magnitudes indicate prevailing tangential currents under the anode, cathode and between electrodes as described by the ratio of tangential to radial field magnitude (E_y / E_x ratio,

see methods). However, most elements have both radial and tangential components, and the isolated highest electric fields are radial. The tangential and radial component for individual elements is shown for each sub-region in false color density plots, which show relative occurrence (relative density from absent (green) to maximal (red)). Axis histograms show relative distribution of elements with a given tangential or radial component electric field. Inset histograms describe the distribution of the % of elements in a region as a function of the normalized component magnitude (such that 1 indicates elements with dominant radial or tangential component). *C*, Cortical folding further influences the distribution of the electric field, therefore, sub-regional field component distributions are indicated for a gyral crown and wall. Tangential fields are dominant in magnitude in the gyral crown but are weaker in the walls where radial magnitudes are stronger, as observed in *A*.

Effects of parallel and perpendicular electric fields on field potentials

The primary motor cortex is characterized by functionally distinct afferent synaptic pathways with specific axonal morphologies and orientations (Aroniadou and Keller, 1993; Keller, 1993). Using the rat primary motor cortex slice preparation we tested the acute effects of uniform EFs on synaptic efficacy in four distinct cortical pathways for electric fields applied parallel to the somatodendritic axis (radial fields) and perpendicular to the somatodendritic axis (tangential fields). Field excitatory postsynaptic potentials were monitored in layer II/III or layer V in response to activity evoked by stimulation of posterior or anterior afferent synaptic pathways in layer II/III (stimulating electrodes S1 and S2, respectively) and horizontal or vertical afferents in layer V (stimulating electrodes S3 and S4, respectively) (Fig. 11A, B). In addition to monosynaptic fEPSPs (4-7 ms peak), a fiber volley was observed in some slices that was non-synaptically mediated as indicated by the time course (<2 ms peak) and insensitivity to bath application of the non-NMDA receptor antagonist 6,7-dinitroquinoxaline-2,3-dione (DNQX, 20 µM) (Fig. 11D). We tested the hypothesis that synaptic efficacy increases with somatic depolarization and/or axon terminal hyperpolarization; thus in a defined polarity, field direction, and pathway-specific manner (Fig 11C).

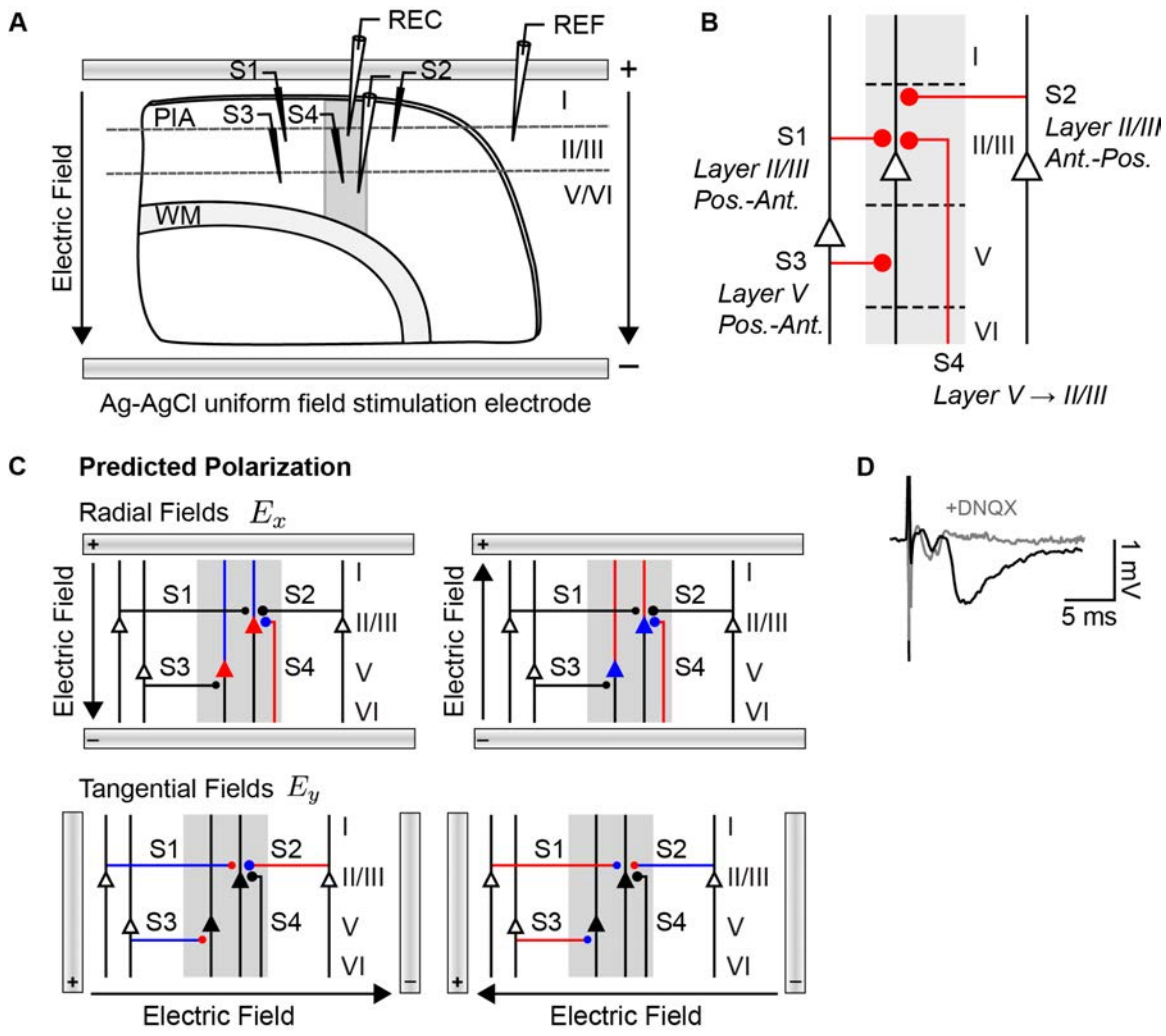

Figure 3. Electrophysiology of direction-specific uniform DC electric fields in synaptic pathways of the rat motor cortex. *A*, Schematic of electrophysiology setup where uniform extracellular electric fields were generated in all experiments by passing constant current across parallel Ag-AgCl wires positioned in the bath across the slice. Activity was monitored in layer II/III (REF) or layer V with a glass microelectrode. An additional field electrode (REF) was positioned in an iso-potential to remove the uniform field artifact. Activity was evoked with a bipolar stimulating electrode (S1-S4) positioned 500 µm from the recording electrode in either layer II/III or layer V targeting one of four distinct synaptic pathways corresponding to different orientations of afferent axons: posterior horizontal layer II/III (S1), anterior horizontal layer II/III (S2), posterior horizontal layer V (S3), and vertical layer V to II/III (S4). *B*, Diagram summarizing the primary synaptic circuits in this study. Line thickness and diameter of the filled circles, which represent synapses, are correlated with the strength of the synaptic input. *C*, Schematic of the expected polarization in distinct synaptic pathways exposed to radial and tangential fields. Somas, dendrites, axons and axon terminals are depolarized (red), hyperpolarized (blue), or not affected (black) by DC fields. *D*, Characteristic fEPSP and field spike waveforms from the layer V pathway. The fEPSPs, but not earlier field-spike, were suppressed by the non-NMDA receptor antagonist DNQX.

Radial EFs (parallel to the somatodendritic axis of cortical pyramidal neurons) typically leads to 'excitation' for positive fields (anode proximal to pia) and 'inhibition' for negative fields (cathode proximal to pia) (Fig. 9B3). In three of the afferent pathways tested fEPSP amplitudes were significantly facilitated (Fig. 12C; S1: posterior horizontal layer II/III, 5.2±3%, p=0.031, n=7; S3: horizontal layer V, 7.3±8%, p=0.02, n=7; S4: vertical layer II/III, 9.4±4% p=0.023, n=11) by radial positive EFs (+8 V/m), with no significant effect in one pathway (S2: anterior horizontal layer II/III, p=0.251, n=6). Radial negative fields (-8 V/m) reduced responses in the same three pathways (S1: -8±1%, p=0.022, n=7; S3: -6.4±6.9%, p=0.024, n=7; S4: -10.2±1.5%, p=0.01, n=11) with no significant effect in the anterior horizontal layer II/III pathway (S2: p=0.98, n=6). A change in fEPSP timing was not resolved. Importantly, grouping across all pathways (e.g. not controlling pathway selectivity), 8 V/m radial positive fields significantly facilitated (7±1%, p=0.004) and radial negative fields inhibited (-6.1±4%, p=0.04) fEPSP amplitudes (Fig. 12C).

tDCS also induces tangential fields that are not expected to polarize neurons with a somatodendritic axis radial to the cortical surface (Fig. 12C) (Bikson et al., 2006). Yet, we found tangential positive fields significantly modulated three of four pathways tested; moreover, the direction of change in excitability was pathway-specific. Tangential positive fields (+8 V/m, oriented posterior to anterior) reduced fEPSP responses in two pathways (Fig. 12D; S1: posterior horizontal layer II/III, -10±3.7%, p=0.024, n=5; S3: posterior horizontal layer V, -5.6±4%, p=0.01, n=6), facilitated in one pathway (S2: anterior horizontal layer II/III, 9.7±2%, p=0.02, n=4), and had no significant effect on the fourth pathway (S4: vertical layer II/III, p=0.14, n=7). Tangential negative fields (-8 V/m, oriented anterior to posterior) facilitated responses in all horizontal pathways (S1: posterior horizontal layer II/III, 11.4±2.5%, p=0.007, n=5; S2: anterior layer II/III, -10.3±3%, p=0.009, n=4; S3: posterior horizontal layer V, 4.3±6.9%, p=0.024, n=6), with no significant modulation of synaptic efficacy in the vertical pathway (S4: vertical layer II/III, p=0.13, n=7). Across modulated afferent pathways, our results are consistent with tangential EFs that produce synaptic terminal hyperpolarization/depolarization leading to facilitation/inhibition of synaptic efficacy (compare Figures 11C and 12D). Though individual pathways were generally as sensitive to tangential fields as radial fields, tangential EFs had no average effect on synaptic efficacy averaging across pathways by virtue of anterior and posterior directed afferents (Fig. 12D). Afferent axon terminal polarization by

subthreshold DC fields was next explored using compartment models to understand morphological factors influencing terminal polarization.

Polarization of axon terminals in compartment neuron models

Synaptic terminal polarization by a uniform extracellular EF leads to changes in synaptic efficacy, consistent with observations in cortical brain slices. Therefore, we estimated the polarization of axonal terminals to weak DC stimulation using compartment and analytical models. The sensitivity of a given compartment to a sub-threshold field can be expressed as the coupling-constant (or polarization-length) in terms of membrane polarization per unit EF (mV per V/m) (Bikson et al., 2004; Radman et al., 2009a).

The relative terminal polarization was calculated numerically for fields oriented parallel (radial component of EF, Fig. 1C2) or perpendicular (tangential component of EF, Fig. 1C3) to the somatodendritic axis, as well as for fields oriented in the optimal angle that leads to maximal polarization at each terminal (Fig. 13A, B). Layer V neurons with passive properties exposed to a strong uniform electric field produces a bimodal polarization profile (Fig. 9C2, false color indicates relative depolarization (red) and hyperpolarization (blue)). However, layer II/III neurons demonstrate a complex polarization profile with distal axonal branches approaching maximal polarization at the terminals independently of the polarization along the neuronal axis (Fig. 9C2-3). Cortical axons are not straight even over microscopic scales but we considered the length of each terminating branch as the distance from the terminal to the bend (Fig. 13A). The final branch space constant varied with fibre radius. We considered relative terminal polarization (V_t normalized by the axonal length constant and by EF) to indicate sensitivity compared to the semi-infinite axon case (maximal polarization= $E\lambda$). For radial and tangential EFs, numerical simulations of cortical neuron polarization indicated that terminal polarization was a complex function of neuronal morphology and angle relative to the EF. Though varying within ±1 (i.e. $\pm E\lambda$), there was no apparent monotonic relationship between terminal coupling constant and branch length (Fig. 13A, B1-2). However, further consideration of branch angle reveals that, specifically for long branches, relative

terminal polarization approaches ±1 for branches oriented parallel to the EF and ~0 for branches perpendicular to the EF:

$$V_t(\theta, \ell \gg \lambda) = \begin{cases} E\lambda & \text{if } \theta = 0^\circ \\ 0 & \text{if } \theta = 90^\circ \\ -E\lambda & \text{if } \theta = 180^\circ \end{cases}$$

Equation 3.

Moreover, when considering the optimal polarization angle the relative axon terminal polarization asymptotically approaches magnitude 1 with increasing branch length (Fig. 13B3).

The analytical solution for a bent axon (Eq. 1) was derived from the cable equation to describe the relationship between axon morphology and terminal coupling constant. For branched axons (Fig. 13C1) the terminal polarization is the sum of: a) The polarization at the branch point (V_0) weighted by the inverse of the final segment's electrotonic length and, b) $E\lambda$, considering the component of EF along the final segment, weighted by the final segment's electronic length. For short branches the terminal membrane potential is coupled with the membrane potential at the bend (V_0) and therefore depends on overall neuronal morphology and where the segment connects to the overall structure (Fig. 13B1, B2, note variability for short branch lengths). For long branches, where $\ell \gg \lambda$, the terminal membrane potential becomes independent of the branch point and approaches $E\lambda\cos\theta$. Equation 1 (using numerically determined branch point voltage) was verified for numerically calculated terminal polarization (Fig. 13D). For the case of final segments oriented parallel to the EF, equation 2 predicts an asymptotic approach to $E\lambda$ for final branch lengths $> 3\lambda$, consistent with numerical simulations (Fig. 13B3). Equation 2 thus explains how overall neuron geometry vs. axon terminal morphology effects resulting terminal polarization, and how maximum expected polarization at a terminal would be $E\lambda$ for a sufficiently long final branch oriented along the field (Fig. 13B3, C3). Importantly, given the density and diversity of afferent axons in the cortex (some with long optimally-oriented final branches) it is reasonable to predict some axon terminals reach the maximal polarization $E\lambda$ for *any* given EF orientation.

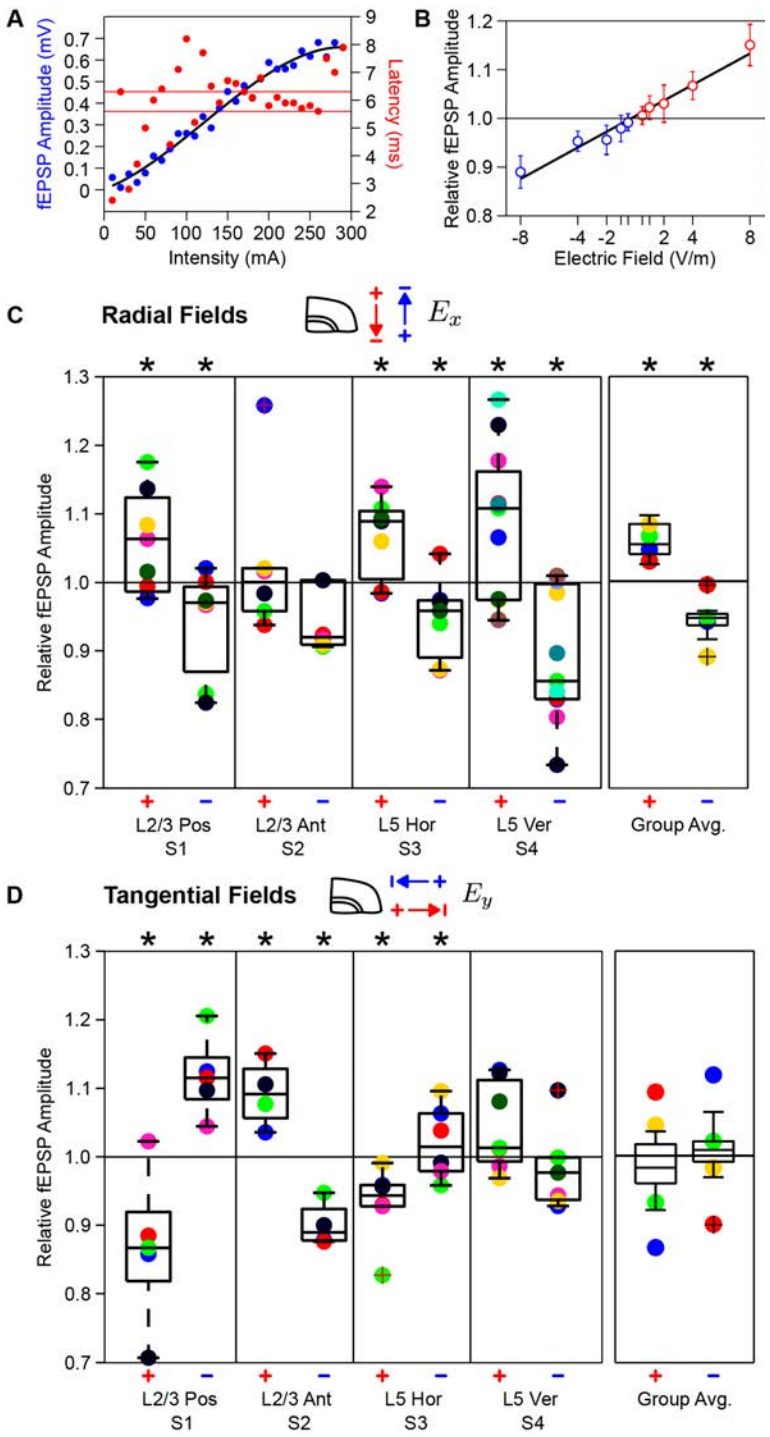

Figure 4. Modulation of pathway-specific synaptic efficacy by radial and tangential DC fields. Application of DC currents in cortical slice demonstrates that tangential current are as effective in modulating pathway-specific synaptic efficacy as radial currents, though pathway-average effects result only for radial electric fields. *A*, Input-output curve of fEPSP response amplitude and peak latency in the horizontal layer V pathway. Horizontal grey bars indicates 25th and 75th percentile of fEPSP peak latency. *B*, Relative fEPSP amplitude in the vertical layer V to II/III pathway at different radially oriented electric field intensities (correlation coefficient R^2 of linear fit=0.96). The fEPSP waveform inset shows a characteristic change in fEPSP amplitude with positive (+8 V/m,

red) and negative radial fields (-8 V/m, blue) from control (no field, black). *C*, fEPSP responses are significantly (P < 0.05, *) facilitated with +8 V/m fields (left) and reduced with -8 V/m (right) in three pathways. In each pathway, individual slice averages are indicated with colored circles. Grouped average fEPSP amplitudes across all synaptic pathways indicate a 7% polarity-specific modulation of synaptic efficacy with 8 V/m radial fields. Circles in the grouped average represent the across slice means of distinct pathways (blue, red, green, and yellow are S1, S2, S3, and S4 pathways, respectively). *D*, fEPSP amplitude was significantly modulated by tangential electric fields in all three horizontal pathways but with direction sensitivity and not in the vertical pathway, all consistent with terminal polarization. Although tangential fields affected individual pathways, grouped average of fEPSP amplitudes across all pathways was not significant.

The relevance of the idealized straight semi-infinite axon (Fig. 13C2), which can be described by a simple analytical solution ($V_t = E\lambda\cos\theta$ or $E\lambda$ for fields oriented along the branch), to realistic tortuous cortical axon morphologies can now be explained with the relationship we have derived (see above). This approximation is relevant for the cases of the branched axon where the final semi-straight segments' electrotonic length is sufficiently long ($> 3\lambda$); these are also the most sensitive terminals to polarization by EFs. Thus the membrane length constant λ reflects the maximal coupling constant of afferent axonal terminals.

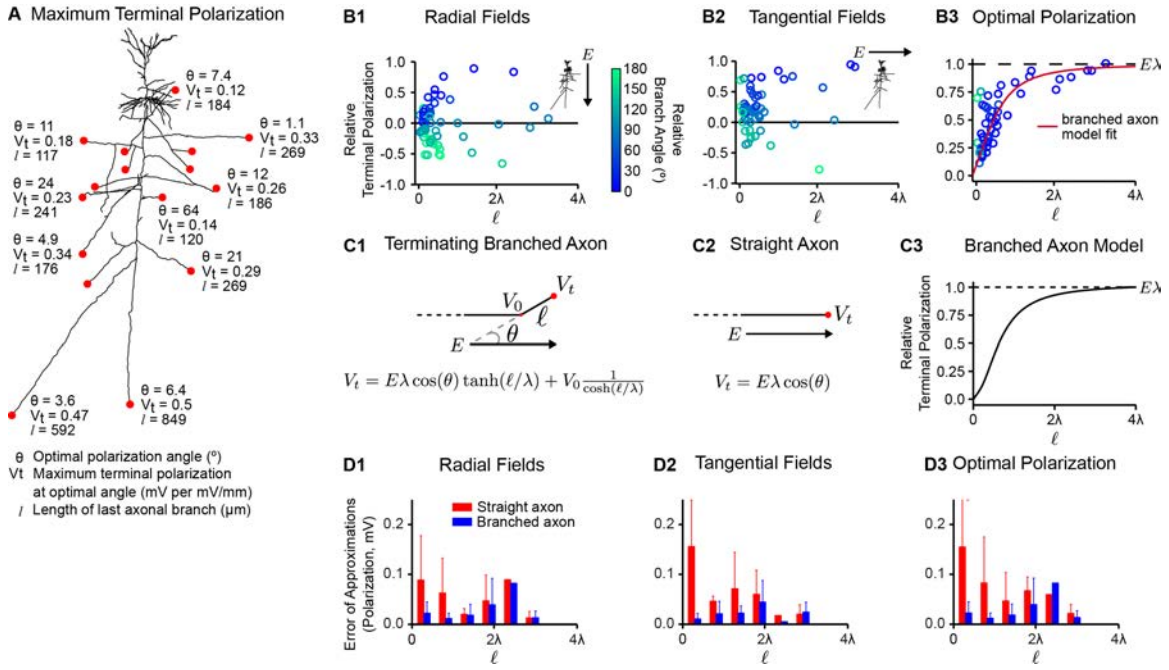

Figure 5. Terminal polarization by uniform DC electric fields using neuron compartment model and analytical/hybrid approximations. Maximum terminal polarization (V_t) depends on the length (ℓ) of the last axonal branch and becomes uncoupled from the bend point at distant terminals (

$\ell > 3\lambda$), however for short branches the terminal membrane potential is coupled with the membrane potential at the bend (V_0). In all cases, numerical simulations applied 1 V/m electric fields. *A*, For a typical cortical pyramidal neuron, the maximum terminal polarization (V_t) is a plotted with the corresponding optimal polarization angle (θ) of the branch relative to the electric field and the length (ℓ) of terminating axon branch. *B1-2*, Relative terminal polarization (Vt normalized by the axonal length constant and by the electric field) as a function of branch electrotonic length and angle (circle color). *B3*, Considering the optimal polarization angle the relative polarization asymptotically approaches magnitude 1 with branch length (equivalently, terminal polarization reaches the maximal polarization $E\lambda$ for increasing lengths). *C1-2*, Schematic of a branched and straight axon in a uniform electric field with analytical solutions (see Methods). The straight axon is a special case of the branched axon with infinite final branch length. For long branches, where $\ell \gg \lambda$, the terminal membrane potential becomes independent of the branch point and approaches $E\lambda\cos\theta$. *C3*, The branched axon model approaches maximal terminal polarization $E\lambda$ for $\ell > 3\lambda$. *D*, Error of approximations (analytical vs. numerical estimates) for branched (blue) and straight (red) axons.

Discussion

The application of tDCS in both clinical and cognitive-neuroscience research has been encouraged by the simplicity of the technique (two electrodes and a battery powered stimulator) and the perception that tDCS protocols can be designed by placing the anode/cathode over the cortex to “excite/inhibit”. The mechanistic question of how acute DCS modulates excitability and ongoing neuronal activity depends on the affected cellular targets.

We characterized DCS generated electric fields, how they polarize cellular compartments, and in turn modulate synaptic efficacy; our approach applied the quasi-uniform assumption (Bikson et al., 2012b) to link finite element models of cortical current flow, brain slices, and neuron compartment models (Fig. 9). On the basis of our findings, the over-arching framework we propose is: During tDCS current crosses the cortex with an electric field vector containing dominantly tangential but also radial components (relative to the cortical surface); whereas the radial component will facilitate/inhibit synaptic efficacy through somatic depolarization/hyperpolarization, the tangential component will concurrently facilitate/inhibit synaptic efficacy, in a pathway specific manner, through terminal hyperpolarization/depolarization. The rationale for this framework in context of prior mechanistic studies is considered.

Animal studies of DCS on spontaneous and evoked cortical activity (Creutzfeldt et al., 1962; Purpura and McMurtry, 1965a; Jefferys, 1981; Chan and Nicholson, 1986; Chan et al., 1988; Gluckman et al., 1996; Fritsch et al., 2010; Reato et al., 2010) demonstrate that typically surface-anode stimulation increases activity while surface-cathode decreases activity, consistent with somatic membrane polarization (Radman et al., 2009a). Similar principles apply in the hippocampus after considering the inverted pyramidal neuron morphology (Gluckman et al., 1996; Bikson et al., 2004; Kabakov et al., 2012). In classical animal studies, by virtue of the stimulation technique (e.g. invasive electrode) and/or cortical anatomy (e.g. reduced cortical folding), electric fields normal to the cortical surface were typically generated (Bindman et al., 1964; Purpura and McMurtry, 1965a). In this vein, we confirm that *purely* inward currents (normal to the cortical surface) during anodal/cathodal DC stimulation in rat cortical slices results in facilitation/inhibition of synaptic efficacy (Fig. 11C, 12C); notably even afferents to the apical dendrites were modulated based on somatic polarization (c.f. (Bikson et al., 2004)). Specifically, polarization along the somatodendritic axis with radial fields modulated cortical synaptic efficacy of orthodromically activated horizontal and vertical afferents, consistent with postsynaptic soma polarization (Fig. 11C, 12C) and in agreement with results in hippocampal slices (Jefferys, 1981; Bikson et al., 2004; Kabakov et al., 2012).

Importantly, in the human case with cortical current flow with *both* a radial and tangential component; one cannot ignore the tangential component and a priori assume modulation simply based on somatic polarization.

Our modeling results (Fig. 10) build on previous efforts (Datta et al., 2009; Salvador et al., 2010) showing that tDCS generates both radial and tangential fields. But surprisingly, quantification on macro and micro-scales demonstrates tangential fields dominate radial fields (4-12x) even under the electrodes (the nominal stimulation target). Most of the cortex will have both a radial and a *larger* tangential component to the current flow (Fig. 10B, C). Tangentially oriented fields do not significantly polarize pyramidal neuron somas (Ranck, 1975; Bikson et al., 2006; Radman et al., 2009a). However, tangential EFs are expected to polarize neuronal elements extending parallel to the cortical surface, notably axons and their synaptic

terminals, including corticocortical afferents (Basser and Roth, 2000; Bikson et al., 2004; Bikson et al., 2006).

Generally, the sensitivity of axon terminals to EFs and the role of terminal membrane potential in synaptic function have been recognized for decades (Purpura and McMurtry, 1965a; Hause, 1975; Bikson et al., 2004; Bikson et al., 2006). Though the polarization of axons and their terminals in the cortex is a complex function of neuronal morphology relative to the EF (Fig. 9C, 13A), we show sufficiently long branch terminals approach the polarization expected for semi-infinite axons: $E\lambda\cos\theta$ (Fig. 13B3, C3). If one considers the diversity and density of axonal afferents, it is reasonable to assume that some axons will have morphology and direction leading to optimal ($E\lambda$) terminal polarization – for any direction EF. λ is thus the effective coupling constant for the most sensitive terminals; ~0.42-0.55 mm for cortical pyramidal axons, (Sasaki et al., 2012). Cortical and hippocampal pyramidal somas have a typical coupling constant ~0.12-0.24 mm (Jefferys, 1981; Bikson et al., 2004; Deans et al., 2007; Radman et al., 2009a; Fröhlich and McCormick, 2010). This *directionless* terminal coupling constant is independent of and 2-3 times more sensitive than cortical pyramid somas under *optimally-oriented* radial EFs (Hause, 1975; Radman et al., 2009a). Thus, even under purely radial fields, afferent axon terminals will polarize more than pyramid somas. Moreover, during tDCS EFs are dominantly tangential (Fig 10), which might indicate a further reduction of pyramid soma polarization, but not afferent axon terminals.

The direction of terminal polarization will depend on the orientation (morphology) of the specific afferent pathway relative to the EF (Fig. 11C, 12D). This is especially relevant for the cortex, where different types of excitatory and inhibitory cells form dense anatomical and functional synaptic circuits that establish routes of information transfer. As a result of the symmetrical orientation of the local synaptic pathways in the primary motor cortex, we demonstrate tangential EFs have no average effect on synaptic efficacy despite pathway specific effects (Fig. 12D) – importantly, given distinct pathway specific functions, a negligible average effect does *not* equate to no net effect on information processing. Concomitant radial and tangential field effects in vivo should be addressed in future studies. Our results in cortical brain slices are consistent with tangential EFs that produce synaptic terminal hyperpolarization/depolarization

leading to facilitation/inhibition of synaptic efficacy (Fig. 11C, 12D). Similar directional sensitivity to electric fields oriented along afferent axons is reported in the hippocampus (Bikson et al., 2004; Kabakov et al., 2012). These results are in agreement with previous findings on the role of synaptic terminal polarization on synaptic strength, as presynaptic hyperpolarization increases presynaptic action potential size and modulates Ca^{2+} current activation and driving force (Hubbard and Willis, 1962b; Takeuchi and Takeuchi, 1962; Miledi and Slater, 1966). Accordingly release is enhanced by terminal hyperpolarization and decreased by terminal depolarization (Bullock and Hagiwara, 1957; Hubbard and Willis, 1962a; Takeuchi and Takeuchi, 1962; Miledi and Slater, 1966; Hubbard and Willis, 1968; Dudel, 1971).

Conclusion

We developed an overarching framework for modulation of synaptic efficacy by acute DCS based on a simple qualitative model where the changes in synaptic efficacy are determined by somatic and afferent axon polarization (Fig. 11C). The results we observed across four pathways for all field orientation and polarities were consistent with this model (Fig 12C, D). Synaptic terminals, therefore, should also be considered as an additional target of modulation during DC stimulation, provided the evidence for a presynaptic contribution to DC stimulation effect (Kabakov et al., 2012; Marquez-Ruiz et al., 2012) and especially given the role of terminals in information processing and plasticity (Malenka and Nicoll, 1999). Indeed, in this last sense the role of somatic vs. terminal effects can be considered analogous to the long-standing debate over pre- and post-synaptic locus of long-term potentiation and depression of synaptic efficacy. Both will likely prove important since during tDCS cortical regions are exposed to EFs with both radial and tangential components, such that the somatic effects produced by the radial component would be modulated by concurrent afferent-specific terminal effects in an antagonistic or complementary fashion.

The cellular locus of acute DCS-induced excitability changes (e.g. somas, dendrites, synaptic terminals) is fundamental to understanding the mechanisms of tDCS and rationalizing stimulation strategies. While this study establishes the principle of axon terminal effects, alongside somatic effects, as a plausible

target of modulation by DC stimulation, it remains to be established where the functional outcomes of DCS (tDCS) originate. For example, this study addressed only the acute synaptic and non-synaptic effects of short duration DC stimulation, thus we did not expect long-term plastic changes. Additionally, interneuronal/inhibitory effects on synaptic function were excluded in the present study, though actions on terminals indicate a potential for modulation if inhibitory function, even if interneuron somata are not significant polarized (Radman 2009). Moreover, brain slices are relatively quiescent compared to the in situ case, with no oscillatory activity or stimulation-matched activation - these factors can be further systematically addressed using brain slice techniques (Nagarajan et al., 1993; Fröhlich and McCormick, 2010; Reato et al., 2010). Notwithstanding these important features, understanding the direct modulation of cortical excitatory transmission by acute DCS is a necessary building block toward a broader mechanistic understanding.

Section 2: Diffuse and sustained electrical stimulation amplifies synaptic cooperativity

Abstract

Transcranial direct current stimulation (tDCS) produces weak and diffuse current flow in the brain with effects that are state-dependent and outlast stimulation when current is sustained. A mechanistic framework for tDCS should capture these spatiotemporal features. It remains unclear how electrical stimulation affects ongoing synaptic dynamics and how modulation of afferent inputs changes synaptic activity at the target brain region. We tested the effect of acute direct current stimulation (DCS; 10-20 V/m for 3-5 s) on constant rate (5-40 Hz) and Poisson-distributed (4 Hz mean) trains of synaptic activity during periods of synaptic adaptation or post-adaptation. Sustained synaptic activity during DCS was polarity-specifically modulated across tested input frequencies. Synaptic depression attenuates the sensitivity to DCS from 1.1% per V/m to 0.55%. Sustained DCS thus facilitates cumulative neuromodulation, potentially reversing endogenous synaptic depression. We establish these effects are mediated by afferent axon fiber polarization, which boosts cooperativity between synaptic inputs when the electric field is oriented along the fibers. This potentially extends the locus of neuromodulation from the nominal brain target to afferent brain regions. Based on these results we hypothesized that the polarization of afferent neurons in upstream brain regions may modulate activity in the target brain region during tDCS. A multiscale model of electrical stimulation including a finite element model of brain current flow, numerical simulations of neuronal activity, and a statistical theory of coincident activity predicts the diffuse and weak profile of current flow can be advantageous.

Introduction

Research into the cognitive and behavioral consequences of transcranial Direct Current Stimulation (tDCS) has outpaced development of cellular models that can explain the diversity of applications, especially in the context of the unique spatiotemporal features of tDCS: sustained flow of weak direct current across large areas of the brain. Computational models of brain current flow during tDCS predict low intensity and diffuse current, which weakly polarizes neurons across the brain. Clinical

neurophysiology and imaging has demonstrated that weak and diffuse current flow produces online changes in cortical excitability that is sustained for the duration of stimulation. It remains unclear how diffuse and low intensity currents can influence connectivity within a local circuit and between brain regions.

Low-intensity direct current stimulation (DCS) produces a small change in membrane potential (< 1 mV, (Radman et al., 2009a)), which is not sufficient to induce spiking activity in resting cortical pyramidal cells. DCS, while weak, modulates synaptic efficacy at rest as measured by single evoked responses in humans ((Nitsche and Paulus, 2000; Priori, 2003)) as well as in animals ((Bikson et al., 2004; Kabakov et al., 2012; Marquez-Ruiz et al., 2012; Rahman et al., 2013)). tDCS is typically applied adjunct to a task (corresponding to sustained neuronal activity) in clinical and performance enhancement applications. In these applications both the DCS and the endogenous activity are sustained. However, the role of DCS acutely on sustained synaptic activity is unclear. In what ways might the dynamics of endogenous activity enhance or dull the effects of sustained DCS?

Acute synaptic modulation by DCS has been linked to both polarization along the somato-dendritic axis (Jefferys, 1981; Bikson et al., 2004; Rahman et al., 2013) and afferent axon terminals (Hause, 1975; Kabakov et al., 2012; Bolzoni et al., 2013a; Rahman et al., 2013; Baczyk and Jankowska, 2014). Neuronal polarization does not have to be limited to just the target brain region during tDCS; activity in the target brain region can be modulated by the simultaneous polarization of neurons and their processes in afferent brain regions. Specifically, synaptic function in the target region will be determined by both local synaptic efficacy and afferent activity in terms of number of active axons and their firing rate – together these set the connectivity between the afferent region and the target. We propose, sustained DCS coupled with endogenous activity may modulate neuronal response in the target brain region through changes in afferent activity as a direct consequence of the diffuse current flow.

We quantified changes in synaptic efficacy in rat brain slices during constant and Poisson rate afferent synaptic activity. We assessed for the first time DCS modulation of synaptic efficacy during adaptation to

ongoing activity and post-adaptation. Our experiments identify a role for afferent axon polarization in driving ongoing activity. Experimental results are integrated into a model of connectivity between brain regions during tDCS which predicts that diffuse and sustained current flow increases the probability of coincident activity and endogenous plasticity between brain regions. Our findings provide a substrate for how weak and diffuse DCS can amplify synaptic activity, modulate synaptic dynamics, and boost synaptic efficacy through cooperativity of afferent inputs.

Methods

Electrophysiology

All animal experiments were carried out in accordance with guidelines and protocols approved by the Institutional Animal Care and Use Committee (IACUC) at The City College of New York, CUNY (Protocol No: 846.3).

Brain slices including a part of the primary motor cortex (M1) were prepared from male young adult Wistar rats aged 3 to 6 weeks old, which were deeply anesthetized with ketamine (7.4 mg/kg) and xylazine (0.7 mg/kg) applied intraperitoneally (i.p.) and sacrificed by cervical dislocation. The brain was removed and immersed in chilled (2-6 °C) artificial cerebrospinal fluid (ACSF) containing (in mM): 126 NaCl, 4.4 KCl, 1.25 NaH_2PO_4, 2 $MgSO_4$, 2 CaCl, 24 $NaHCO_3$ and 10 D-glucose, bubbled with a mixture of 95% O_2-5% CO_2). A slightly modified ACSF composition was used for long-term plasticity experiments (1 mM $MgSO_4$). Coronal slices (400 µm thick) were cut using a vibrating microtome and transferred to a holding chamber for at least 30 min in ambient temperature. Slices were then transferred to a fluid-gas interface chamber perfused with warmed ACSF (30.0±0.5 °C) at 1.9 mL/min. The humidified atmosphere over the slices was saturated with a mixture of 95% O_2-5% CO_2. Recordings started 1-3 h after dissection.

We stimulated the excitatory vertical pathway from L5A→2/3 and the horizontal pathway within the superficial layers (L2/3). A recording electrode was placed 250-400 µm below the pial surface in L2/3 and a bipolar platinum/stainless steel stimulating electrode was positioned ~500 µm vertically below it at the

boundary of L3 and L5. Either 15 (in adaptation experiments) or 200 (in post-adaptation experiments) constant-current pulses (0.2 ms, 10-150 μA) were delivered at 5, 10, 20, or 40 Hz for constant train experiments with an interval of 60 s (15 pulse trains) or 4 min (200 pulse trains) between trains to allow for recovery from synaptic depression. Stimulus intensity was adjusted to produce responses half of the maximum amplitude that could be evoked. In a subset of experiments to evaluate the effect of DCS on a natural train of presynaptic action potentials, 81 pulses were delivered with Poisson distributed interspike intervals (4 Hz mean, 20 sec).

Uniform extracellular EFs (±10 and 20 V/m) were generated by passing constant current (D/A driven analog follower; A-M Systems, WA, USA) between two large Ag-AgCl wires positioned in the bath across the slice starting 0.5 s before a train of constant or Poisson-distributed stimuli. In post-adaptation experiments, the field was applied after 100 pulses for 5 sec that consisted of 50 pulses during-DCS followed by another 50 pulses post-DCS for a total of 200 pulses at a constant frequency of 10 Hz. For all experiments, we used a two-tailed t-test and a bootstrap hypothesis test to test for significance.

Modeling synaptic dynamics and recruitment

The neuronal population response to excitatory presynaptic drive can be modeled as the averaged voltage response $V(t)$ (Richardson et al., 2005). A train of presynaptic spikes arriving down input fiber n over a large population of N_f input fibers at time t evokes excitatory postsynaptic potentials modeled as alpha synapses $\alpha(t)$.

Equation 4. $V(t) = \sum_{n=1}^{N_f} \sum_{\{t_{nk}\}} A_k \alpha(t - t_k)$

The set of amplitudes $\{A_k\}$, reflecting the field potential amplitudes, are modeled using a phenomenological description of dynamic synapses with short-term plasticity (Tsodyks and Markram, 1997; Mongillo et al., 2008). A simple quantitative model of postsynaptic response evoked by multiple synapses can be described as a product of a constant A_0 and two variables F and D:

Equation 5. $A(t) = A_0 \cdot F(t) \cdot D(t)$

$$\frac{dF(t)}{dt} = \frac{F_0 - F(t)}{\tau_F}, t = t_{AP} \Rightarrow F(t) \rightarrow F(t^-) + \Delta$$

$$\frac{dD(t)}{dt} = \frac{1 - D(t)}{\tau_D}, t = t_{AP} \Rightarrow D(t) \rightarrow D(t^-)\left(1 - F(t^-)\right)$$

Synaptic efficacy is modulated by the amount of available resources D and the utilization parameter F that defines the fraction of resources used by each spike. The utilization parameter may reflect residual calcium level in the presynaptic terminal. Upon a spike, an amount FD of the available resources is used to produce the postsynaptic current, thus reducing D; physiologically the process mimics neurotransmitter depletion. The spike also increases F, mimicking presynaptic calcium influx. Experimentally, the field potential amplitude reflects the population averaged synaptic current and is well approximated by this model.

Between spikes, F and D exponentially recover to their baseline levels ($D = 1$ and $F = F_0$, $F \leq 1$) with time constants τ_F (facilitating) and τ_D (depressing). The phenomenological model reproduces behavior of both facilitating ($\tau_F > \tau_D$) and depressing ($\tau_D > \tau_F$) cortical synapses.

We simulated a single postsynaptic integrate-and-fire neuron receiving correlated excitatory input signals. The cell received input through at most 1000 synapses during ongoing synaptic activity at a constant rate (10 Hz). To mimic glutamatergic transmission, synapses were conductance-based with reversal potential $V_{Exc} = 0\, mV$ and time constant $\tau_{Exc} = 5\, ms$. Additionally, every presynaptic spike leads to synaptic depression. Recruitment was modeled as an increase or decrease in the number of active synapses. The number of active synapses was decreased from 1000 to 500 to simulate the dynamics during a decrease in synaptic cooperativity or increased from 500 to 1000 to simulate dynamics during an increase in synaptic cooperativity.

Statistical theory of coincident pre- and postsynaptic spikes

We present a statistical theory (Equation 5) for increasing synaptic strength through changes in the likelihood of pre- or postsynaptic firing by considering the number of presynaptic spikes (N_{pre}) and the number of postsynaptic spikes (N_{post}) in discrete time bins (N_{bins}). The duration of each bin is taken to be 10-20 ms corresponding to the time constant of spike timing dependent plasticity. The hypergeometric distribution is used to estimate the coincidence count probability $P(k|N_{pre}, N_{post}, N_{bins})$ of observing k coincident pre- and postsynaptic spikes from a given number of bins and having observed N_{post} postsynaptic spikes and N_{pre} presynaptic spikes.

Equation 6. $$P(k|N_{pre}, N_{post}, N_{bins}) = \frac{\binom{N_{post}}{k}\binom{N_{bins}-N_{post}}{N_{pre}-k}}{\binom{N_{bins}}{N_{pre}}}$$

Results

A quantitative description of synaptic dynamics during DCS

The effects of DCS on online information processing in the brain can only be understood by considering synaptic dynamics during ongoing activity. A fundamental feature of synaptic transmission is adaptation to continuous afferent inputs (Abbott and Regehr, 2004), which is quantitatively described by short-term plasticity (Equation 1). Adaptation to synaptic activity arising from the depletion of neurotransmitters at the presynaptic terminal underlies important neural functions like gain control (Abbott et al., 1997) and working memory (Mongillo et al., 2008). The short-term plasticity phenomenon regulates synaptic efficacy and is quantified as a gradual decrease (for depressing synapses) or an increase (for facilitating synapses) in the excitatory postsynaptic potential (EPSP, Figure 14B) during continuous presynaptic inputs. Specifically, we quantified how DCS during presynaptic activity leads to a sustained change in the EPSP (Equation 1). A conductance-based neuron model with dynamic synapses suggests that changes in postsynaptic membrane potential during DCS produces a sustained modification in EPSP amplitude

and produces a greater net depolarization when anodal DCS is applied during ongoing synaptic activity (Figure 14C). To test this prediction, we used an in vitro preparation where we could control the frequency of presynaptic inputs and study the effects of DCS on synaptic efficacy through the extracellularly-recorded (field) EPSP (Figure 15A), which we refer to simply as the field potential (FP).

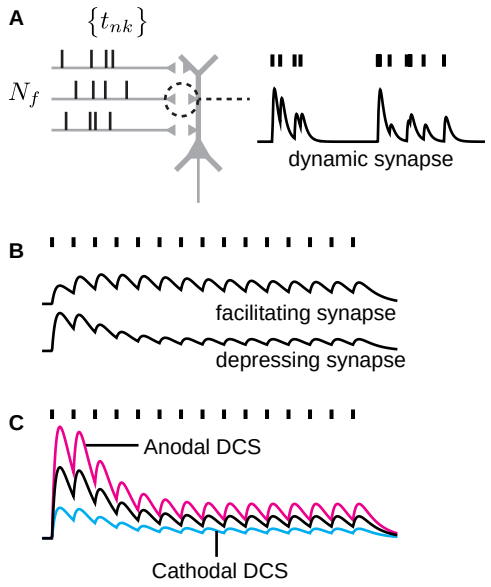

Figure 6. The postsynaptic voltage response during DCS and ongoing presynaptic activity results in sustained and cumulative changes that are regulated by synaptic efficacy, number of active inputs, and rate of presynaptic activity. A) Schematic representing the voltage output of a postsynaptic cell during a train of presynaptic spikes arriving at times $\{t_{nk}\}$ down N_f input fibers. Synaptic transmission at cortical synapses are not static, but are dynamically regulated by the available pool of releasable vesicles. B) Synaptic efficacy during activity is controlled by short-term plasticity based on the initial vesicle release probabilities ($P_{release}$) and vesicle depletion and recovery times. C) Simulation of the postsynaptic response during DCS in a conductance-based model with dynamic synapses. Anodal DCS (red), modeled as a postsynaptic depolarization, facilitates EPSP amplitudes and cathodal DCS (blue), modeled as a postsynaptic hyperpolarization, depresses EPSP amplitudes. The postsynaptic response during DCS is sustained for the duration of DCS.

DCS has a sustained and cumulative effect on synaptic efficacy

The effects of DCS on synaptic efficacy were evaluated during ongoing presynaptic activity in the rat primary motor cortex. Presynaptic afferent axons (L5A→2/3 pathway) were stimulated at 5, 10, 20, and 40 Hz to simulate synaptic activity. Field potentials (FPs) decayed in amplitude over the course of a 15 pulse train as a result of synaptic depression (Figure 15B). Anodal DCS increased (+10 V/m: 13.2±6.9%,

+20 V/m: 20.3±9.8%, n=124, p<0.05) and cathodal DCS decreased (-10 V/m: -13.3±8.7%, -20 V/m: -23.3±11.2%, n=124, p<0.05) the transient FP amplitude when applied during the train of inputs (Figure 15C). Importantly, we show for the first time that the change in synaptic efficacy is maintained for the duration of DCS when there is a constant rate of synaptic activity (Figure 15B, 15C). The steady-state FP amplitude during DCS is significantly greater during anodal DCS and smaller during cathodal DCS, compared to the control case (no-DCS, Figure 15B,C).

Computational models suggest there is cumulative membrane depolarization during ongoing synaptic activity and DCS may amplify the net depolarization (Figure 14C). In vitro, DCS has a greater cumulative increase in synaptic efficacy during activity. Anodal DCS increased and cathodal DCS decreased how fast the cumulative synaptic efficacy changed during synaptic activity, relative to baseline (Figure 14F, 15C). In slices with weak synaptic depression or at low-frequencies of synaptic activity, anodal DCS can reverse synaptic depression towards facilitation for the duration of DCS. This finding is remarkable because it indicates DCS can qualitatively change the nature of gain control in a given brain region, turning depressive dynamics into facilitating ones.

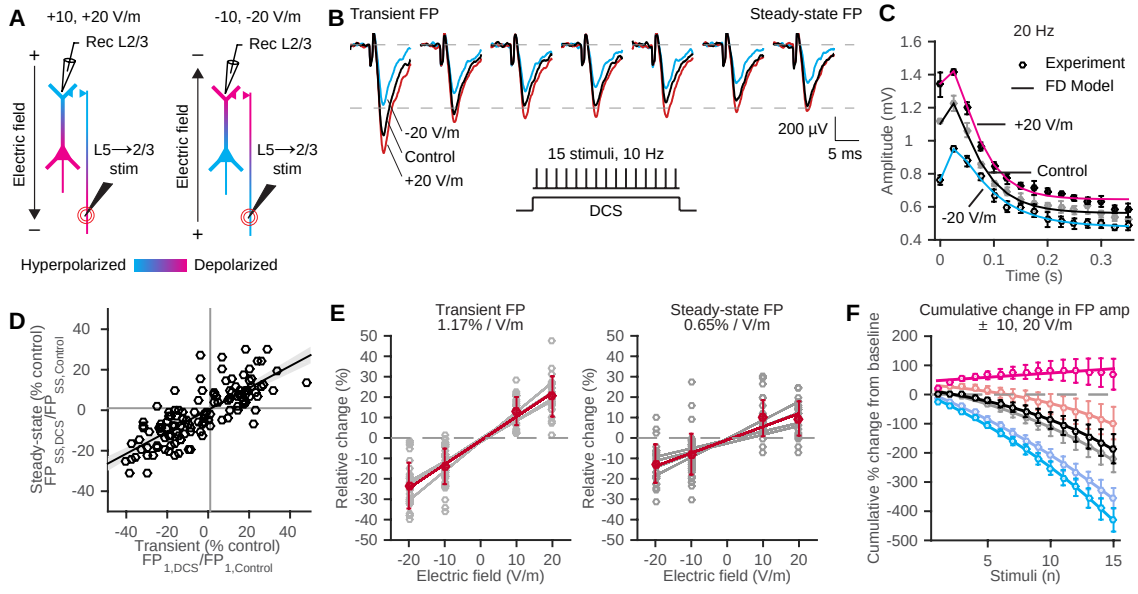

Figure 7. DCS in rat primary motor cortex results in a sustained modulation of synaptic efficacy. A) Schematic of anodal (left) and cathodal (right) DCS with current flow along the somatodendritic axis and the effective membrane polarization of cells and axons in false-color. B) Orthodromic

stimulation of the L5→2/3 pathway at a constant frequency (20 Hz shown) in M1 transiently facilitates synaptic efficacy during anodal DCS and depresses efficacy during cathodal DCS. The DCS effects are sustained for the duration of stimulation. C) DCS modulates synaptic efficacy during continuous afferent inputs despite synaptic depression arising from vesicle depletion in the presynaptic terminals. D) The transient change in field potential (FP) amplitude during DCS is correlated with the steady-state change in FP amplitude. FP amplitudes in the constant-rate train of inputs during DCS are normalized by the corresponding n-th FP amplitude during a train without DCS. E) The sensitivity (% change in FP amplitude per V/m) to DCS of the steady-state FP is less than the sensitivity of the transient FP (n=124). Gray best fit lines are for each of the tested frequencies (5, 10, 20, and 40 Hz) and red is the combined average across frequencies. There was no significant difference in either transient or steady-state sensitivity across frequencies. F) The rate of cumulative change in FP amplitude (the cumulative % change from baseline) is greater during anodal DCS and less during cathodal DCS compared to control. Dark points indicate 20 V/m and light points are 10 V/m. In all cases, magenta indicates anodal DCS and blue is cathodal DCS.

DCS produces frequency-independent changes in synaptic efficacy

A model of dynamic synaptic transmission consisting of a facilitating (F) and a depressing (D) term with first-order decay kinetics (referred to as the FD model) fit to the data predicted the observed EF effects. The most common form of short-term plasticity (>82% of experiments) observed in the rat primary motor cortex was short-term depression ($\tau_D > \tau_F$, τ_D = 0.74 sec, τ_F = 0.23 sec, F_0 = 0.18, Δ = 0.41). DCS had no effect on the time constants for depression or facilitation (Wilcoxon signed-rank test, p > 0.05), suggesting DCS does not have a direct effect on presynaptic transmitter release kinetics. Both in our experiments and in the FD model, ongoing synaptic activity results in a substantial reduction in FP amplitude due to synaptic depression. The change in synaptic efficacy resulting from DCS (and independent of synaptic depression) is quantified by normalizing each n-th FP amplitude during DCS ($FP_{n,DCS}$) by the corresponding n-th FP amplitude without DCS ($FP_{n,Control}$), within-slice. The normalization reveals a sustained increase of synaptic efficacy with anodal DCS and decrease with cathodal DCS for as long as the EF is on (Figure 16A). The sustained change in synaptic efficacy is frequency-independent and persists during a naturalistic pattern of synaptic activity (Figure 17).

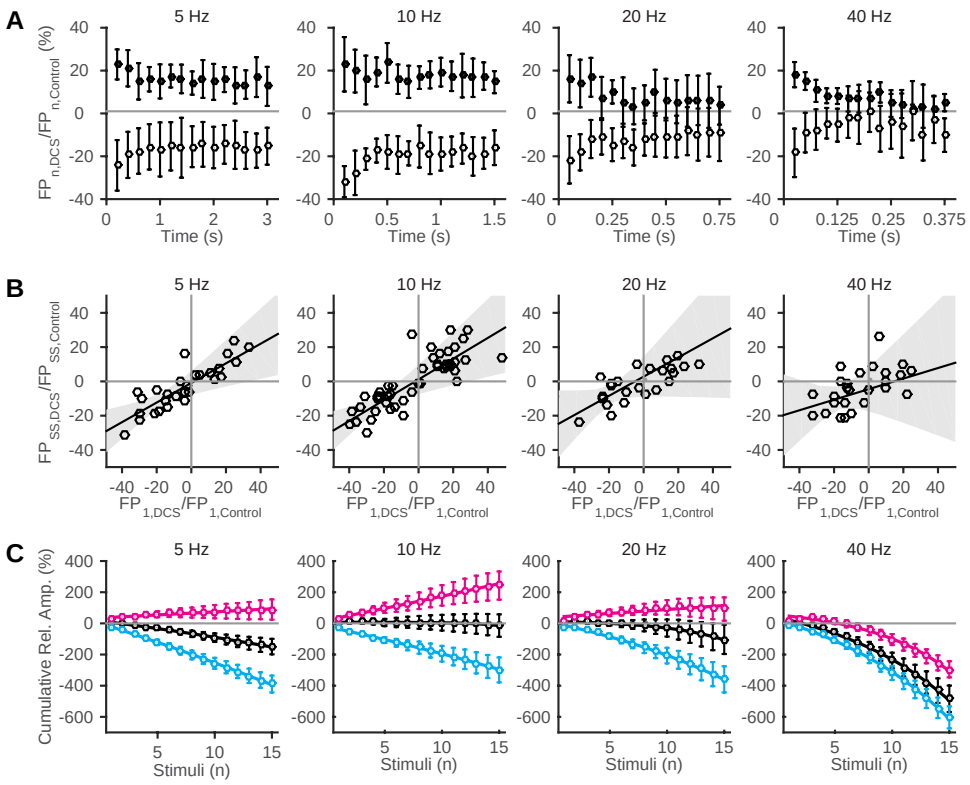

Figure 8. Synaptic efficacy is frequency-independently modulated during DCS, sustained for the duration of stimulation, and is cumulative. A) FP amplitudes during 20 V/m EFs are normalized by the corresponding n-th FP amplitude in a control train, within slice. B) Anodal DCS attenuates synaptic depression. The cumulative percent change from baseline is plotted for anodal (magenta), cathodal (blue), and control (black) conditions. C) The transient change in FP amplitude is correlated with the steady-state change in FP amplitude.

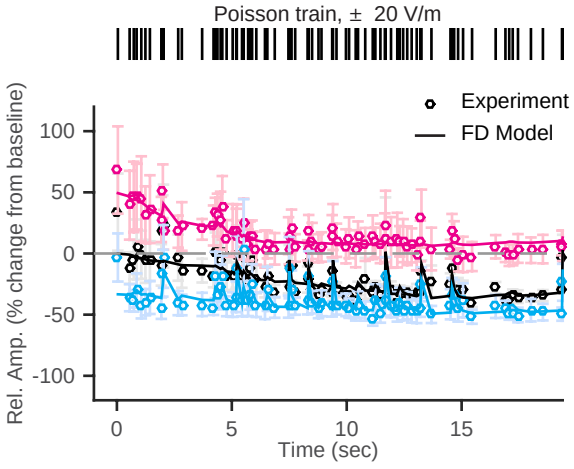

Figure 9. DCS produces a sustained change in synaptic efficacy during a naturalistic pattern of presynaptic activity. Afferent inputs reflecting the Poisson distributed spike train pattern in vivo

(mean rate 4 Hz) is acutely facilitated by anodal DCS (magenta) and depressed by cathodal DCS (blue).

Ongoing synaptic activity changes the synaptic sensitivity to DCS

There is a marked decrease in the sensitivity to DCS over time, quantified as the % change in FP amplitude from control per V/m, from 1.17±0.1% / V/m to 0.65±0.05% / V/m during ongoing synaptic activity (Figure 15E). This change in sensitivity is independent of the rate of synaptic activity (Figure 15E, gray lines indicate different rates of afferent synaptic inputs; rate coefficients: transient: 0.03±0.06% / V/m; steady-state: -0.03±0.07% / V/m). Furthermore, the transient and steady-state change in synaptic efficacy is directly correlated, across all frequencies (Figure 15D, Figure 16B). Synaptic adaptation, therefore, reduces the capacity for DCS to modulate synaptic efficacy.

DCS modulates synaptic efficacy post-adaptation

Modulation of synaptic efficacy after the adaptation period was measured by applying a long-duration train of 200 stimuli at 10 Hz (Figure 18A). 20 V/m EFs were applied for 5 sec after the first 100 pulses in the train. During stimulation, synaptic efficacy transiently decreased with cathodal DCS (-33.5±21%, n=9, $p<0.05$) and increased with anodal DCS (28.8±26.8%, n=11, $p<0.05$). The effect of DCS was sustained for the duration of stimulation but there is an adaptation to DCS during anodal stimulation (Figure 18B).

DCS promotes synaptic cooperativity through recruitment of afferent axons

The negative correlation between the transient change in FP amplitude and the change in FP amplitude during DCS suggests there is an adaptation to the effect of DCS (Figure 18C). We hypothesized the adaptation to DCS may be attributed to recruitment of presynaptic axons during DCS. EFs along the ascending afferent axons may be polarizing presynaptic compartments leading to recruitment of additional afferents (N_f in Equation 1) during orthodromic stimulation. We tested this hypothesis by changing the orthodromic stimulation intensity by ½× or by 2×, thus decreasing or increasing,

respectively, the number of afferent fibers generating the field potential. The protocol is similar to the post-adaptation DCS experiment but here the EF is replaced with a change in stimulus intensity.

Both DCS and changes in orthodromic stimulus intensity result in similar dynamics of the FP (Figure 18D). During cathodal DCS and the analogous ½× stimulus intensity experiments, FP amplitudes were transiently depressed and recovered from depression. During anodal DCS and the analogous 2× orthodromic stimulus intensity experiments, FP amplitudes were transiently facilitated and gradually recovered from facilitation towards baseline. In both cathodal DCS and ½× stimulus intensity experiments we observe a prominent rebound in FP amplitude after DCS was turned off and after stimulus intensity was returned to the probing intensity. These results suggest DCS changes the presynaptic axon membrane potential and modulates the sensitivity to firing action potentials. A model incorporating synaptic depression and recruitment is able to capture the salient features of the experimental data. Recruitment is modeled as an instantaneous increase in the number of active presynaptic inputs for the duration of stimulation. A DCS-induced postsynaptic depolarization alone fails to capture the nonlinear effects of DCS on FP amplitude.

DCS can change synaptic efficacy even without recruitment of afferent fibers during orthodromic stimulation. Axons within L2/3 (L2/3→2/3) were orthodromically stimulated while only polarizing the postsynaptic cells. There is a significant transient change in FP amplitude during DCS (-20 V/m: 3.15±1.18%, n=5; +20 V/m: 6.44±4.78%, n=5). The dynamics of recruitment which would have resulted in an offset of the FP amplitude and a recovery from facilitation or depression towards baseline were not observed. This result, along with previously published work, shows postsynaptic polarization alone can modulate synaptic efficacy. However, the transient change in synaptic efficacy is less than when activating the vertical L5→2/3 pathway (6.44% vs. 28.8% for 20 V/m) suggesting some of the change in synaptic efficacy we observe during stimulation of the L5→2/3 pathway may result from recruitment of afferent axons.

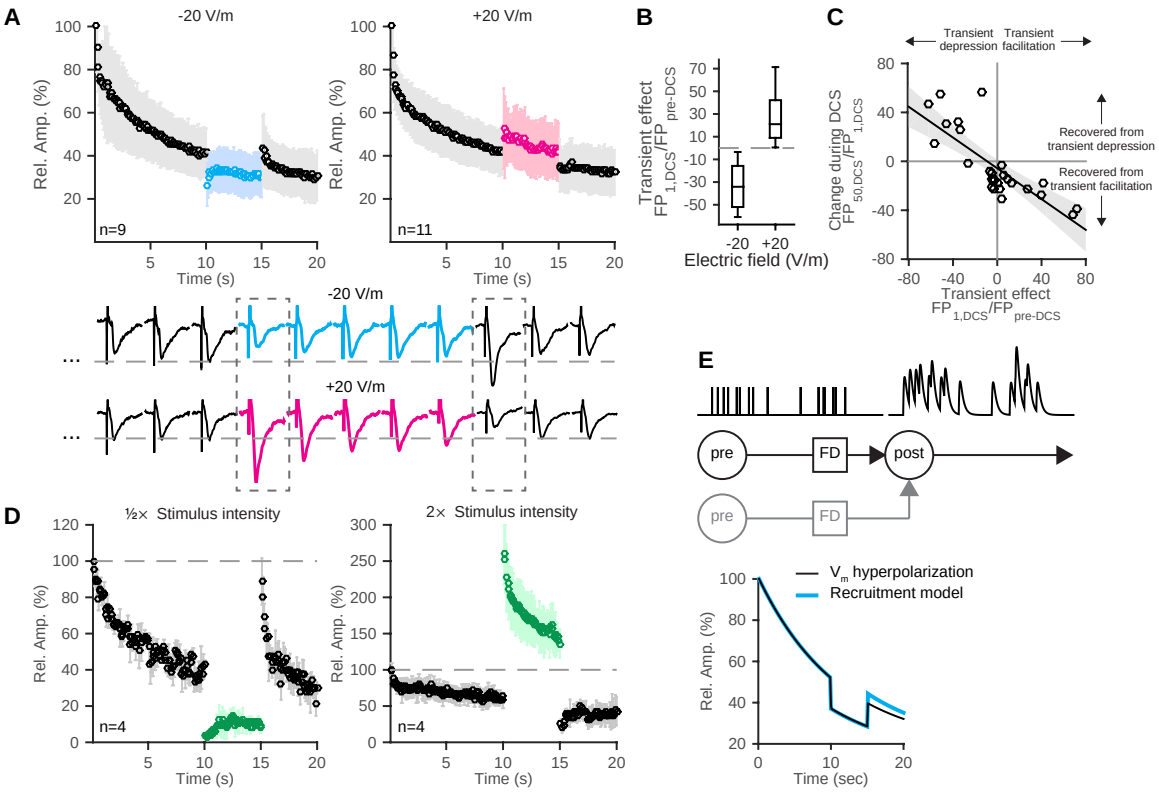

Figure 10. DCS post-adaptation modulates synaptic efficacy and is driven by recruitment of afferent axons. A) Cathodal (blue) and anodal DCS (magenta) during a train of synaptic inputs at 10 Hz modulates synaptic efficacy for the duration of stimulation despite adaptation. B) DCS polarity specifically modulates the transient FP amplitude (first evoked potential during DCS) relative to pre-DCS. C) There is a correlation between the transient change in FP amplitude and the amount of recovery from transient facilitation or depression during DCS. D) Changing the stimulus intensity, instead of applying DCS, results in similar dynamics on FP amplitude. Decreasing stimulus intensity by a half (left) decreases FP amplitudes. There is a pronounced rebound in FP amplitude when the stimulus intensity is returned to the probe intensity. E) A simple dynamic synapse model incorporating recruitment of presynaptic inputs is able to reproduce the effects of DCS on synaptic efficacy and the post-DCS rebound effect.

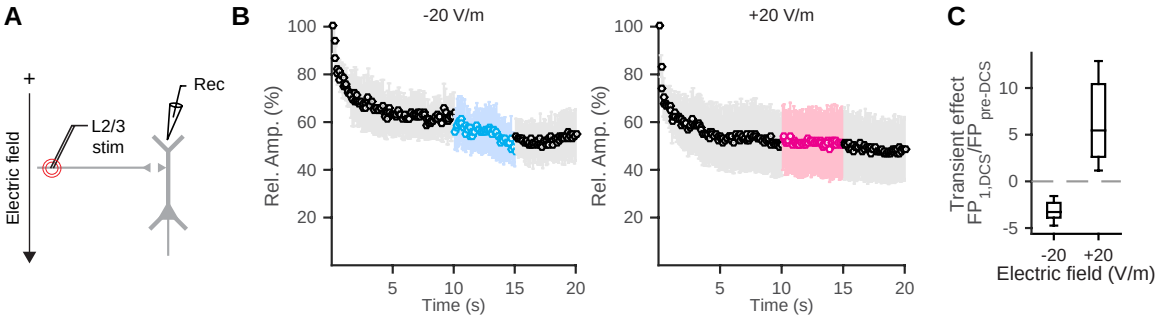

Figure 11. DCS modulates synaptic efficacy post-adaptation through somatic polarization alone. A) Schematic of orthodromic stimulation of L23 during DCS. Current flow along the somatodendritic axis and perpendicular to the horizontally oriented axons selectively polarizes the postsynaptic

cells and not the axons. B) Current flow along the somatodendritic axis during orthodromic stimulation of the horizontal L2/3 pathway modulates synaptic efficacy independent of axonal recruitment. C) Anodal DCS facilitates synaptic efficacy and cathodal DCS depresses efficacy.

A change in the fiber volley (FV) amplitude, which is a compound action potential that reflects the number of activated axons, provides direct evidence for recruitment with DCS. EFs along the ascending fibers in motor cortex (L5→2/3) decreased FV amplitude by -15.5±10% with -20 V/m (n=30) and increased FV amplitude by 13.9±7.1% with +20 V/m (n=30) (Figure 20A). Similarly, in hippocampal CA1 area, EFs along Schaffer collaterals increased FV amplitude by 10.6±10.4% ($p<0.05$) with -20 V/m (n=20) and decreased FV amplitude by -5.5±8% ($p<0.05$) with +20 V/m (n=20) (Figure 20B). The polarity of modulation during DCS reflects axonal polarization such that depolarized regions of the axon (proximal to the negative electrode) correspond to an increase in FV amplitude. In motor cortex, there is a direct positive correlation (r: 0.92, CI: [0.88, 0.95]) between change in FP amplitude and change in FV amplitude. Recruitment of afferent axons during DCS in brain slices may contribute to the modulation of synaptic activity (Figure 20C).

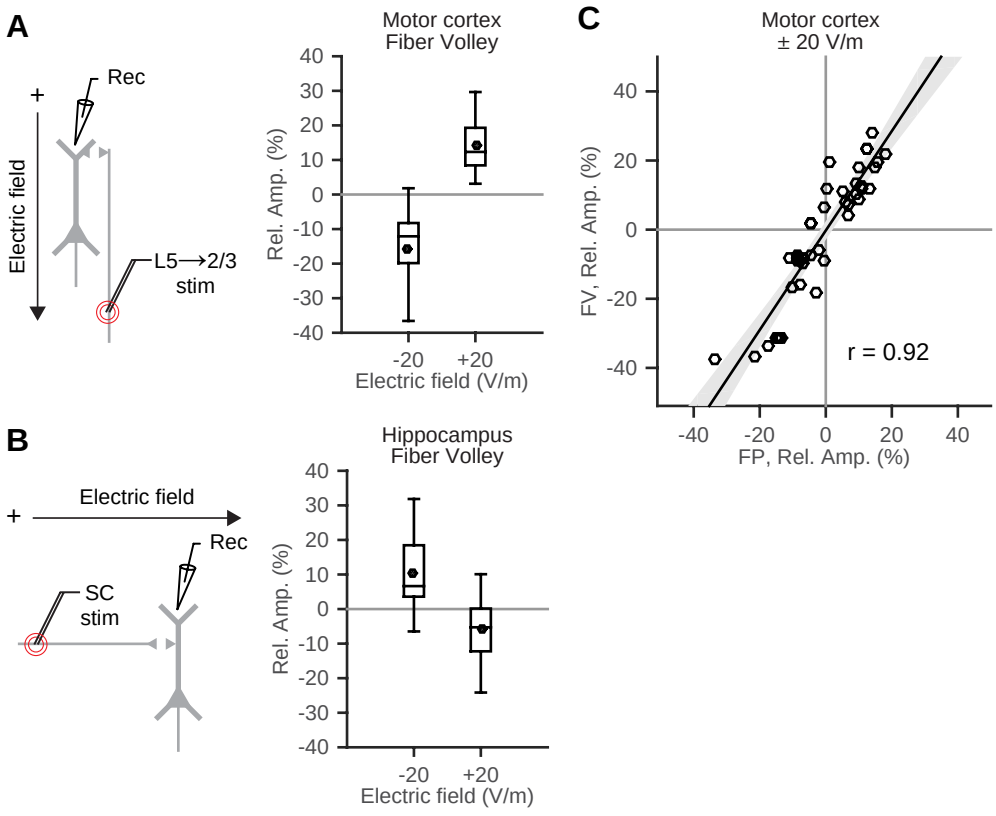

Figure 12. Current flow along axons during DCS modulates fiber volley in rat primary motor cortex and hippocampus. A) Current flow along the somatodendritic axis during orthodromic stimulation of the ascending L5→2/3 pathway polarizes afferent axons and modulates axonal recruitment during DCS. The amplitude of the fiber volley (FV) reflects the number of axons firing action potentials during orthodromic stimulation. B) Similarly, current flow along the afferent axons of the Schaffer collateral pathway modulates the fiber volley amplitude. C) The change in fiber volley amplitudes is directly correlated with the change in postsynaptic field potential amplitude in the rat primary motor cortex. These results show polarizing afferent axons changes the number of active presynaptic inputs and directly modulates synaptic current.

Discussion

Our results show that DCS produces a sustained modulation of synaptic efficacy that is cumulative over the duration of stimulation when applied during ongoing synaptic activity. Ongoing synaptic activity produces well established changes in synaptic dynamics (Abbott et al., 1997; Varela et al., 1997; Zucker and Regehr, 2002; Abbott and Regehr, 2004; Richardson et al., 2005), with depression dominating in motor cortex. We addressed the question if/how synaptic dynamics would affect modulation by DCS (Figure 14). We show synaptic depression contributes to moderate loss in acute sensitivity to DCS (from 1.1% per V/m to 0.55% per V/m; Figure 15E). However, there is a significant modulation that is robust across stimulation frequency (Figure 16) and extends to naturalistic input (Figure 17) and post-adaptation states (Figure 18). Importantly, a cumulative gain in synaptic potentials amplifies the DCS effect because the modulation of synaptic efficacy by DCS is sustained (Figure 15F). Ongoing synaptic activity combined with sustained DCS is an important feature of electrical stimulation – quantified with a model of synaptic dynamics (Figure 17, Figure 18e). We also demonstrate that afferent axon polarization can drive the changes in synaptic activity during DCS (Figure 20), adjunct to traditional somatic polarization (Figure 19) and axon terminal mediated mechanisms (Hause, 1975; Rahman et al., 2013). A targeted brain region may be influenced by both direct modulation of local neuronal processes and by polarizing afferent brain regions. Although our experiments are in vitro, these results have important consequences for how the outcomes of diffuse and weak electrical stimulation are interpreted, and suggest these features can be advantageous.

tDCS using conventional montages with two large pad electrodes produces diffuse current flow through the cortex and subcortical brain regions (Datta et al., 2009; Bikson et al., 2010). For example, the common M1-SO tDCS montage (Datta et al., 2009) produces diffuse current flow not only on the nominal brain target, but also in premotor and supplementary motor cortex (Figure 21A), in addition to other cortical and subcortical brain regions (Bolzoni et al., 2013a; Bolzoni et al., 2013b; Baczyk and Jankowska, 2014). Consequently, the cellular effects of tDCS are not localized to just the targeted brain region but can extend to upstream brain regions. In this way diffuse tDCS may recruit a distributed brain network, for instance the network of brain regions involved in motor planning or execution. However, diffusivity in itself is not a substrate for producing specific behavioral or clinical changes, and needs to be considered in the context of endogenous activity between connected brain regions. Modulation of upstream brain regions can influence the cooperative action of neurons and thus directly affect downstream processes.

The notion of diffuse and sustained current flow being advantageous features of tDCS further extends to how the weak electric fields produced by tDCS are amplified by brain activity. The difference between resting membrane potential and spike threshold for a typical cortical pyramidal cell can be 15-20 mV. DCS, however, results in a small change in membrane potential (~0.2 mV per V/m) at the soma. Amplifying synaptic activity through cooperative inputs during DCS provides a plausible mechanism by which weak EFs can significantly modulate the postsynaptic response (Equation 1). An increase in presynaptic firing rate or the synchronous activation of presynaptic cells during diffuse current flow can directly increase postsynaptic depolarization and firing probability (Figure 21A, 21B).

To formalize our hypothesis that diffuse current flow may be advantageous for neuronal information processing, we present a statistical theory (Equation 5) for increasing synaptic strength through coincident pre- and postsynaptic spikes. We consider the number of presynaptic spikes (N_{pre}) and the number of postsynaptic spikes (N_{post}) in discrete time bins (N_{bins}). The hypergeometric distribution estimates the coincidence count probability $P(k|N_{pre}, N_{post}, N_{bins})$ of observing k coincident pre- and postsynaptic spikes from a given number of bins and having observed N_{post} postsynaptic spikes and N_{pre} presynaptic spikes. By varying the number of presynaptic spikes or postsynaptic spikes we have an

estimate of the number of coincidences. The probability distribution of coincidences closely matches the true number of coincidences in simulations of neuronal activity (Figure 21C, dotted vertical line is estimated number of coincidences from simulations of neuronal activity). During tDCS a change in presynaptic firing rate (as a result of diffuse current flow), or postsynaptic firing rate, or both, can increase the coincidence probability and thus promote synaptic strengthening between connected and active brain regions. While weak electric fields cannot induce firing on their own they exert a modulatory effect on active networks and increase the probability of synaptic strengthening.

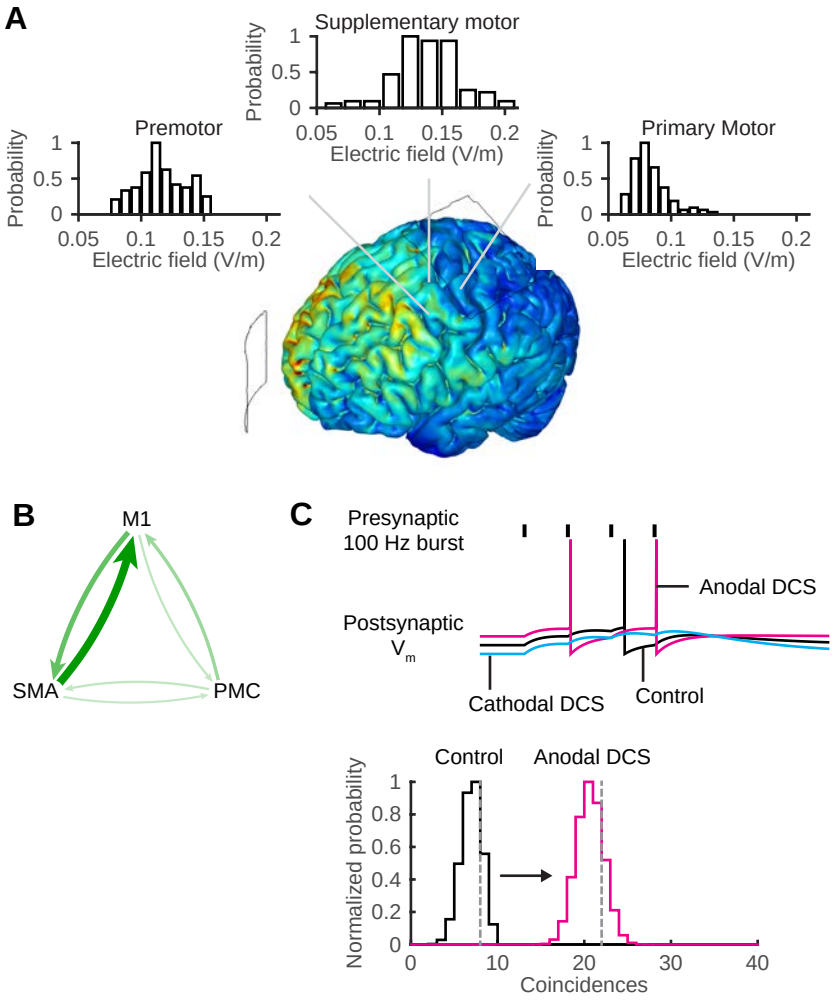

Figure 13. tDCS produces diffuse current flow in the brain which increases the probability of coincident pre- and postsynaptic inputs. A) The electric field magnitude is plotted in a finite element model of tDCS with anode over the primary motor cortex (M1) and cathode over supraorbital region (SO). The electric field magnitude distribution in brain regions adjacent and upstream to M1 is comparable to or higher than in M1. B) The primary motor cortex is synaptically connected to the supplementary motor area (SMA) and premotor cortex (PMC), which drives

motor activity. The thickness of the arrows indicates the relative connection strength from fMRI studies of this functional network. Modulating presynaptic activity in these upstream brain regions during tDCS may drive postsynaptic activity in M1. C) DCS-induced membrane polarization changes the likelihood of firing. An increase in the presynaptic activity (or postsynaptic activity) increases the probability of coincident pre- and postsynaptic action potentials. The vertical grey dotted-line indicates the simulated number of coincidences in a model I&F neuron receiving Poisson distributed synaptic inputs. The hypergeometric probability distribution can be used to approximate the estimated number of coincidences. Combined, these results suggest the probability of coincident inputs can be directly modulated when presynaptic or postsynaptic activity is modulated by diffuse current flow.

Implications and limitations of the theory of diffuse actions of tES

Future studies in both humans and animals will have to address the role of upstream brain regions in regulating the function and output of the target brain region to test our hypothesis. Notable, using convention tDCS montages in humans, peak brain current densities are often between, rather than under electrodes; meaning significant diffuse neuromodulation is expected. Our statistical theory predicts changes in presynaptic firing rate will increase the coincidence of pre- and post-synaptic APs and therefore increase the likelihood of plasticity. Finally, our experimental results can provide some insights into the key features of a typical tDCS protocol. tDCS produces diffuse current flow in the brain, needs to be on for an extended period of time to integrate synaptic activity, and may have to be matched with a task. Our results suggest these features may promote synaptic plasticity because, as we demonstrate, changes in synaptic efficacy are sustained for the duration of DCS and helps synaptic inputs integrate. Additionally, diffuse current flow may enable recruitment of afferent inputs in an active functional network.

Section 3: Electrical stimulation accelerates and boosts the capacity for synaptic learning

Introduction

The functional specificity of local synaptic connections is fundamental to information processing and learning in the brain. Increased connectivity between neurons with similar functional selectivity has been reported across brain regions. Moreover, synaptic strengths within and between these selective populations are experience dependent and modifiable during a training task. Noninvasive electrical brain stimulation may have task-specific effects where learning in a functionally selective population benefits from a combination of training and the increased neuronal excitability during stimulation. How endogenous synaptic plasticity in local circuits is modulated by electrical stimulation is not well understood, especially in the context of task-specific learning.

We found that electric fields produce a voltage- and NMDA-dependent modulation of synaptic strength when applied during theta-burst stimulation in rat hippocampus, accelerates synaptic plasticity with repeated stimulation, and increases the ceiling for synaptic learning. This mechanism provides a means by which repeated stimulation during training can increase the capacity for storing memories and gives rise to the functional specificity of electrical brain stimulation.

Methods

All animal experiments were carried out in accordance with guidelines and protocols approved by the Institutional Animal Care and Use Committee (IACUC) at The City College of New York, CUNY (Protocol No: 846.3).

Brain slices including a part of the hippocampus were prepared from male young adult Wistar rats aged 3 to 5 weeks old, which were deeply anesthetized with ketamine (7.4 mg/kg) and xylazine (0.7 mg/kg)

applied intraperitoneally (i.p.) and sacrificed by cervical dislocation. The brain was removed and immersed in chilled (2-6 °C) artificial cerebrospinal fluid (ACSF) containing (in mM): 126 NaCl, 4.4 KCl, 1.25 NaH2PO4, 1 MgSO4, 2 CaCl, 24 NaHCO3 and 10 D-glucose, bubbled with a mixture of 95% O2-5% CO2). Hippocampal slices (400 µm thick) were cut using a vibrating microtome and transferred to a holding chamber for at least 30 min in ambient temperature. Slices were then transferred to a fluid-gas interface chamber perfused with warmed ACSF (30.0±0.5 °C) at 1.9 mL/min. The humidified atmosphere over the slices was saturated with a mixture of 95% O2-5% CO2. Recordings started 3-4 h after dissection.

Orthodromic stimulation of Schaffer collateral pathway within the CA1 produced field potentials in the LM layer. A recording electrode was placed in the LM layer and a bipolar platinum/stainless steel stimulating electrode was positioned ~500 µm lateral to the recording electrode. Uniform extracellular EFs (±10 and 20 V/m) were generated by passing constant current (D/A driven analog follower; A-M Systems, WA, USA) between two large Ag-AgCl wires positioned in the bath across the slice starting 0.5 s before theta burst stimulation. For all experiments, we used a two-tailed t-test and a bootstrap hypothesis test to test for significance.

LTP was induced along the Schaffer collateral pathway using theta burst stimulation (4 pulses at 100 Hz repeated for 15 bursts at 5 Hz). DCS was applied for 3 seconds during the entire TBS session. For repeated stimulation experiments, DCS and TBS was applied every 40 min – 1 hr until LTP was saturated. Most slices tested were saturated after 3-4 sessions of stimulation. I also tested the effects of AC stimulation when TBS is applied at different phases of stimulation. Each of the 15 bursts in a single TBS session arrived either at the peak, trough, or at another phase of AC stimulation. In functional specificity experiments I simultaneously stimulated both the Schaffer collateral and performant pathways. Schaffer collaterals were stimulated with TBS while the perforant pathway was stimulated with low frequency stimulation (15 pulses at 5 Hz). Each of the 15 pules arrived in the middle of a burst.

Results

DCS modulates endogenous synaptic plasticity

To mimic the learning during a training task, we applied theta-burst stimulation (TBS, 4 pulses at 100 Hz repeated for 15 bursts at 5 Hz) in the hippocampal Schaffer collateral pathway to induce synaptic learning through long-term potentiation (LTP). To test the modulatory effect of electrical stimulation we subjected CA1 pyramidal neurons to depolarizing and hyperpolarizing electric fields (3 sec; 1, 10, 20 V/m; Fig. 1a). We found that, depending on the electric field polarity, the synaptic strength could be either increased or decreased if the field was applied during TBS. Soma depolarizing direct current stimulation (DCS) during LTP induction increased the field EPSP amplitude relative to baseline (control: 1.25±0.04, +20 V/m: 1.46±0.02), whereas soma hyperpolarizing DCS decreased the magnitude of LTP (-20 V/m: 1.22±0.01; Fig. 1b). Weak membrane polarization with DCS alone is not sufficient to induce plasticity along the Schaffer collateral pathway in the absence of synaptic stimulation.

DCS accelerates and boosts the capacity for synaptic learning

The ability to modulate endogenous synaptic plasticity with electrical stimulation provides a substrate for enhancing task-specific learning and prompted us to investigate whether repeated stimulation sessions can accelerate synaptic learning. Indeed, we found that repeated theta burst stimulation (TBS repeated every 60 minutes) combined with DCS increases the rate of synaptic strengthening until local synaptic connections are saturated (Fig. 22e). Inhibiting synaptic current with the selective NMDA receptor antagonist 2-amino-5-phosphonopentanoic acid (AP5) reduced the capacity for synaptic learning and abolished the modulatory effect of DCS. Remarkably, DCS also boosted the ceiling of LTP (Fig. 22e), which could be attributed to the activity-dependent release of extracellular BDNF that has been observed during electrical stimulation (Fritsch et al., 2010; Ranieri et al., 2012). TBS in the presence of extracellular BDNF has also been shown to increase the ceiling of synaptic plasticity.

Timing of synaptic inputs during ACS controls LTP strength

The magnitude of LTP depends both on the postsynaptic membrane potential and the timing of synaptic inputs relative to oscillations in membrane potential. A simple voltage-based learning model showed that membrane polarization controls the postsynaptic firing probability leading to synaptic strengthening through coincident pre- and postsynaptic-spikes (Fig. 22D). Electrical stimulation may directly control the magnitude of LTP through varying degrees of polarization. In order to study the voltage-dependence of LTP during electrical stimulation we applied TBS at different phases of theta-frequency membrane potential oscillation induced by alternating current stimulation (ACS). We found that the timing of synaptic inputs during membrane potential oscillation controls the magnitude of LTP. TBS timed to the peak depolarization phase enhanced LTP with biphasic ACS (figure 22E; control: 1.25±0.6; +20 V/m: 1.59±0.03 relative fEPSP slope) and with monophasic ACS. Synaptic inputs timed to the trough of the membrane potential oscillation, when the cell is maximally hyperpolarized, decreased LTP (Figure 22E; control: 1.25±0.6; -20 V/m: 1.22±0.05 relative fEPSP slope). The dose-response (change in synaptic strength vs electric field intensity) has a monotonic and asymmetric relationship (Figure 22F). These results extend previous findings that timing of synaptic inputs during endogenous membrane potential oscillations control the magnitude of plasticity.

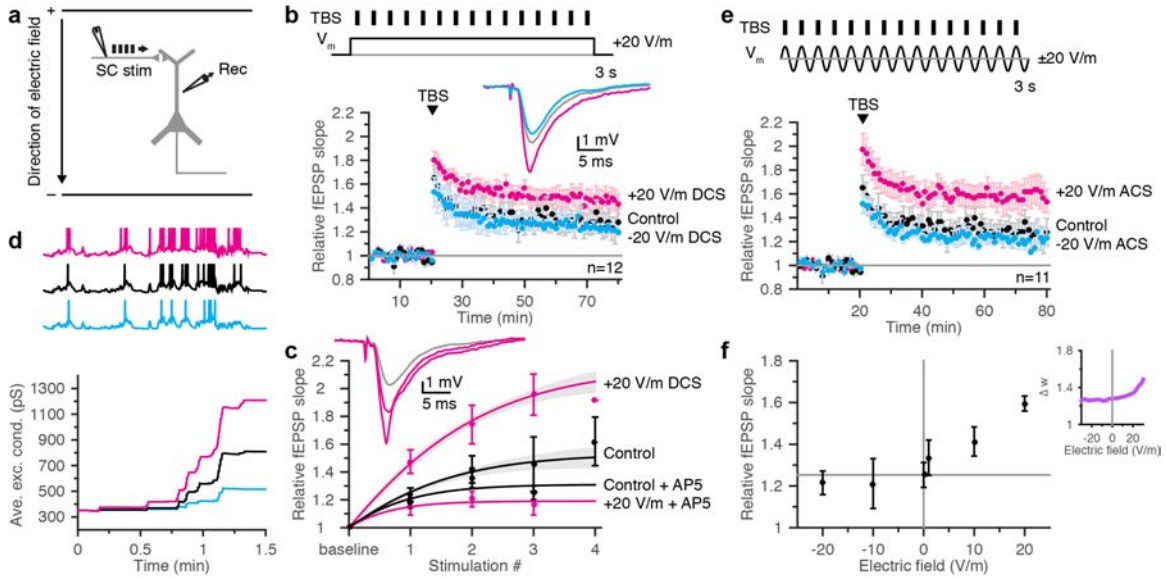

Figure 14. Modulation of LTP with direct and alternating current stimulation accelerates and boosts the ceiling for synaptic learning. A) Schematic of synaptic inputs along the Schaffer collateral pathway during electrical stimulation suing parallel Ag-AgCl electrodes. B) The polarity of direct current stimulation (DCS) controls the magnitude of plasticity induced by theta-burst stimulation (TBS). C) Repeated TBS applied during DCS accelerates synaptic learning towards saturation of synaptic weights. Repeated sessions of TBS with soma depolarizing DCS (+20 V/m) increases the ceiling for synaptic learning. LTP induction and modulation is NMDA-dependent. D) A voltage-based learning rule in a spiking neuron model receiving correlated Poisson-distributed synaptic inputs to induce synaptic learning is able to reproduce the asymmetric and voltage-dependent potentiation observed in-vitro. DCS increases the spiking probability and promotes plasticity. E) TBS is applied at the peak or trough of membrane potential oscillations induced by alternating current stimulation (ACS). Synaptic inputs at the peak of membrane polarization boosts LTP and inputs at the trough decrease LTP. F) Timing of TBS applied at different phases of membrane potential oscillation controls the magnitude of LTP.

Functional specificity and activity-dependent modulation

Transcranial electrical stimulation induces a diffuse electric field in the brain and simultaneously affects multiple brain regions during a training task. TES induces significant and similar magnitude electric fields across multiple brain regions using the traditional electrode montage to target primary motor cortex. How can a diffuse electric field have functionally specific effects? We hypothesized the functional specificity of TES arises from how electric fields affect endogenous synaptic plasticity. Active synaptic pathways during a training task may be modulated more than inactive or weakly active pathways.

We adapted our model to test the functional specificity of electrical stimulation by simulating a single postsynaptic neuron receiving simultaneous input signals from two independent synaptic pathways. The strong pathway was activated with TBS to produce strong synaptic plasticity. The weak pathway was activated at a low-frequency (5 Hz) applied in-phase with the TBS. Synaptic inputs along the weak pathway arrive during a critical period for LTP induction where the TBS has already depolarized the postsynaptic cell and inputs at a low-frequency, which typically induce depression, are now able to evoke a postsynaptic spike and LTP. Under control conditions both pathways showed increased synaptic strength after training with simultaneous TBS and LFS ($\Delta w_{control}^{cond} > \Delta w_{control}^{test}$). Electrical stimulation during training modulated plasticity in both pathways but had a larger modulatory effect on the pathway with stronger synaptic plasticity ($\frac{\Delta w_{field}^{cond}}{\Delta w_{control}^{test}} > \frac{\Delta w_{field}^{test}}{\Delta w_{control}^{test}}$). Active pathways undergoing strong synaptic plasticity

may be preferentially modulated by electrical stimulation during a training task – leading to a discrimination between active and inactive functional networks during diffuse electrical stimulation.

We evaluated the modeling results experimentally by reproducing the stimulation protocol in-vitro. A conditioning stimulus was applied to the Schaffer collateral fibers; the test stimulus was applied to a subicular input on the opposite side of the recording site (Figure 23A). Each shock of the test input was superimposed on the middle of each burst of the conditioning input. The low frequency test stimulus was first applied alone and did not produce long-lasting changes by itself or in the presence of an electric field (Figure 23B). The conditioning site was then stimulated alone, which elicited homosynaptic LTP of the conditioning pathway but did not alter amplitude of responses to the test input (Figure 23C). Stimulating the conditioning site alone during DCS modulated synaptic strength in the conditioning pathway but not in the inactive test pathway (Figure 24D).

When test and conditioning inputs were activated in phase, the conditioning pathway was potentiated as before and there was an additional associative potentiation of the weakly activated test input synapses (conditioning: 1.21±0.06, test: 1.16±0.09). Soma depolarizing DCS boosted synaptic strength in both conditioning and test pathways while the two pathways were simultaneously activated (conditioning: 1.81±0.25, test: 1.45±0.02). Electrical stimulation had a greater effect in modulating synaptic plasticity in the conditioning pathway than the weakly activated test pathway – as predicted by the model. The preferential modulation of active local inputs is especially evident when comparing the change in synaptic weights during DCS against control ($\Delta w_{field}/\Delta w_{control}$) for each pathway.

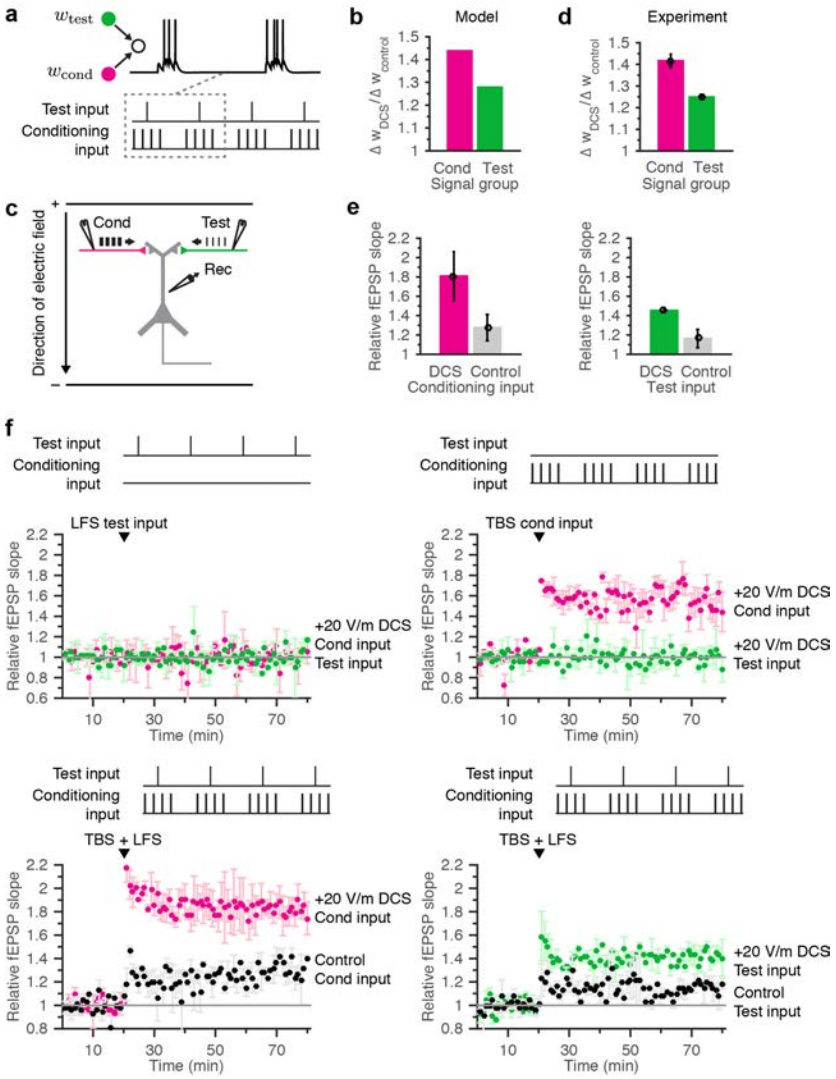

Figure 15. Electrical stimulation differentially modulates strong and weak synaptic plasticity. A) Model neuron receiving simultaneous inputs from two independent signal groups. TBS along the strong pathway induces strong synaptic plasticity and conditions a weak pathway to potentiate during LFS. B) Model prediction of the differential modulation of strong and weak synaptic plasticity during simultaneous synaptic plasticity. C) Schematic of experimental setup where TBS is applied to Schaffer collaterals and LFS to the temporo-ammonic pathway. D) Summary of experimental results. Electrical stimulation has a larger modulatory effect on LTP in strong pathways (conditioning input) than on weak pathways (test input). E) Summary of changes in synaptic strength for each signal group during DCS and in control conditions (no electrical stimulation). F) Changes in synaptic strength for each signal group under all tested conditions.

How weak currents accelerate task specific learning in humans is still not well understood. We found that electric fields produce a voltage- and NMDA-dependent modulation of synaptic strength when applied during theta-burst stimulation in rat hippocampus, accelerates synaptic plasticity with repeated stimulation, and increases the ceiling for synaptic learning. This mechanism provides a means by which

repeated stimulation during training can increase the capacity for storing memories and gives rise to the functional specificity of electrical brain stimulation.

Section 4: Modulation of synaptic plasticity with direct current stimulation is activity-dependent and differs with dendritic location.

Introduction

Transcranial direct current stimulation (tDCS) applies a weak constant current of 2mA or less across the scalp. This apparently simple technique is currently under investigation for a wide variety of conditions, including psychiatric disorders, neurorehabilitation and cognitive enhancement (Coffman et al., 2014; Gomez Palacio Schjetnan et al., 2013; Kuo et al., 2014). Stimulation is often paired with a training task, leading to task-specific enhancements in learning performance (Coffman et al., 2014; Gill et al., 2015). Despite the observation of pharmacological, neuro-physiological and imaging effects in humans (Brunoni et al., 2012) and animals (Pelletier and Cicchetti, 2015), a coherent picture of the relevant cellular mechanisms is yet to emerge.

Long-term learning and memory are thought to be mediated by synaptic plasticity (Takeuchi et al., 2014) and training paradigms in humans presumably influence learning by inducing synaptic plasticity (Draganski and May, 2008). Despite the common practice of applying tDCS during training, cellular effects of DCS applied during endogenous synaptic plasticity induction remain largely unexplored. Instead, the majority of research has analyzed effects when DCS precedes plasticity induction (Podda et al., 2016; Ranieri et al., 2012; Rohan et al., 2015), or is paired with endogenous activity otherwise not known to induce plasticity (Fritsch et al., 2010; Marquez-Ruiz et al., 2012; Monai et al., 2016). Here we are interested in the effects of DCS applied during training, i.e. concurrent with synaptic plasticity induction. As a model of endogenous synaptic plasticity, we induced long-term potentiation (LTP) and depression (LTD) using canonical induction protocols (pulse trains delivered to Schaffer collateral synapses in CA1 of rat hippocampal slices). By sweeping across induction frequencies we capture a frequency-response function (FRF), which has been widely used to study the LTP/LTD threshold and the predictions of the Bienenstock, Cooper and Munro (BCM) theory of synaptic plasticity (Cooper and Bear, 2012).

A prevailing mechanistic explanation is that tDCS produces shifts in cortical excitability, with anodal stimulation increasing excitability and cathodal stimulation decreasing excitability (Brunoni et al., 2012). This cortical excitability hypothesis is rooted in physiological evidence that DCS modulates membrane potential at neuronal somas, leading to changes in firing rate and timing (Bikson et al., 2004; Purpura and Mcmurtry, 1965; Radman et al., 2007, 2009; Reato et al., 2010). Based on these observations, anodal/cathodal tDCS are often assumed to produce LTP/LTD-like effects for an entire brain region (Dayan et al., 2013; Monte-Silva et al., 2013; Ridding and Ziemann, 2010; Stagg and Nitsche, 2011). However, this reasoning ignores the complex gradient of membrane polarization induced in any neuron during DCS. For example, anodal stimulation depolarizes pyramidal neuron somas but will actually hyperpolarize their apical dendrites (Andreasen and Nedergaard, 1996; Bikson et al., 2004). Given the dependence of synaptic plasticity on dendritic membrane potential (Malenka and Bear, 2004), we hypothesized that DCS effects would track the induced dendritic polarization and vary with dendritic location. Consistent with this, we find that cathodal DCS facilitates LTP in apical dendrites only, while anodal DCS facilitates LTP in basal dendrites only. Moreover, we find that both anodal and cathodal DCS reduce LTD in apical dendrites. Importantly, DCS did not induce synaptic plasticity, but rather required an endogenous source of NMDAR plasticity to modulate. For the first time to our knowledge, we directly examine effects on synaptic plasticity when DCS is applied during plasticity induction. We show that these effects are highly variable within a single brain region, with outcomes dependent on the dendritic location and rate of endogenous synaptic activity.

Methods

All animal experiments were carried out in accordance with guidelines and protocols approved by the Institutional Animal Care and Use Committee (IACUC) at The City College of New York, CUNY (Protocol No: 846.3).

Hippocampal brain slices were prepared from male Wistar rats aged 3–5 weeks old, which were deeply anaesthetized with ketamine (7.4 mg kg−1) and xylazine (0.7 mg kg−1) applied I.P., and killed by cervical dislocation. The brain was quickly removed and immersed in chilled (2–6°C) artificial cerebrospinal fluid

(ACSF) containing (in mM): NaCl, 125; KCl, 4.4; NaH2PO4, 1; MgSO4, 1.5; CaCl, 2.5; NaHCO3, 26; D-glucose, 10; bubbled with a mixture of 95% O2–5% CO2. Transverse slices (400 µm thick) were cut using a vibrating microtome (Campden Instruments) and transferred to a holding chamber for at least 1 h at ambient temperature. Slices were then transferred to a fluid–gas interface chamber (Harvard Apparatus) perfused with warmed ACSF (30.0 ± 0.1°C) at 1.0 ml min−1. The humidified atmosphere over the slices was saturated with a mixture of 95% O2–5% CO2. Recordings started 2–3 h after dissection. Field excitatory postsynaptic potentials (fEPSPs) were evoked using a platinum-iridium bipolar stimulating electrode placed in either stratum radiatum or stratum oriens of CA1. Recording electrodes made from glass micropipettes pulled by a Sutter Instruments P-97 and filled with ACSF (resistance 1–8 MΩ), were placed in either stratum radiatum or stratum oriens approximately 250 µm from the stimulating electrode in CA1 to record fEPSPs. fEPSPs were quantified by the average initial slope, taken during the first 0.5 milliseconds after the onset of the fEPSP. Stimulus intensity was set to evoke fEPSPs with 40% of the maximum slope, which was determined at the onset of recording. Stable baseline fEPSPs were recorded every minute for at least 20 minutes before any plasticity induction was applied. fEPSPs were then recorded again every minute for 60 minutes after plasticity induction.

DCS was applied between two parallel Ag-AgCl wires (1 mm in diameter and 12 mm in length) placed in the bath on opposite sides of the brain slice separated by 10 mm with the recording site approximately equidistant from each wire. DCS wires were connected to a current-controlled analog stimulus isolator (A-M Systems) that was controlled by PowerLab hardware and LabChart software (AD Instruments). Slices were oriented such that the somato-dendritic axis of CA1 pyramidal neurons was parallel to the electric field between the DCS wires (Figure 1A). Before each recording, DCS current intensity was calibrated to produce a 20 V/m electric field across each slice (typically 100 - 200 µA) by adjusting the current so that two recording electrodes separated by 0.8 mm in the slice measured a voltage difference of 16 mV (16 mV/0.8 mm = 20 V/m).

For NMDAR antagonist experiments, 100 µM MK-801 (Sigma Aldrich) was included in the ACSF perfused in the recording chamber throughout the experiment. Because MK-801 is an open channel

blocker, baseline fEPSPs were recorded for at least 40 minutes to ensure complete blockade of NMDAR channels (Nabavi et al., 2013a).

Data acquisition and stimulation waveforms were controlled with PowerLab hardware and LabChart software (AD Systems). Extracellular fEPSPs were amplified (100x), low pass filtered (3 kHz), and digitized (10 kHz). Synaptic plasticity was quantified for each slice by taking the average of the last ten fEPSP slopes (51-60 minutes after plasticity induction) and normalizing to the average of baseline fEPSP slopes (20-1 minutes before plasticity induction). Two-tailed student's t-tests were used to determine the significance of differences in synaptic plasticity between conditions, with $p < 0.05$ considered significant.

Here we name the polarity of stimulation based on the orientation of DCS relative to pyramidal neurons. Following convention in human tDCS, DCS with the anode closer to CA1 apical dendrites is referred to as anodal stimulation. Conversely, DCS with the cathode closer to CA1 apical dendrites is referred to cathodal stimulation. Importantly, apical dendrites are polarized oppositely from basal dendrites and somas, regardless of DCS polarity (Andreasen and Nedergaard, 1996; Bikson et al., 2004; Rahman et al., 2013). So anodal DCS will depolarize somas and basal dendrites, while hyperpolarizing apical dendrites. Conversely, cathodal DCS will hyperpolarize somas and basal dendrites, while depolarizing apical dendrites (Figure 1A).

Acute effects were determined based on the first response (two responses for paired pulse data) during DCS and were normalized to the average of baseline responses. Fiber volley amplitude was taken as the difference between the trough of the fiber volley and the mean of the two surrounding peaks. Paired pulse ratio was taken as ratio of the second and first fEPSP slopes during 20 Hz HFS (50 ms inter-pulse interval) in each condition.

Frequency-response functions in figure 1B were each fit with a double exponential function with five parameters: S= c_1 e^(c_2 x)+ c_3 e^(c_4 x)+c_5 where x is the induction frequency, S is the resulting synaptic plasticity, and c_1…c_5 are free parameters.

Results

DCS shifts the frequency-response function

Trains of synaptic activity have conventionally been used to induce synaptic plasticity in hippocampal slices (Malenka and Bear, 2004). As a model of endogenous synaptic plasticity, trains of 900 pulses at varying frequencies (0.5, 1, 5, 20 Hz) were applied to the Schaffer collateral pathway synapsing on CA1 apical dendrites. Low frequency stimulation (LFS) generated LTD (0.5 Hz: 84.1±2.7%, $p<0.001$, n=10; 1 Hz: 78.9±2.9%, $p<0.0001$, n=9), while high frequency stimulation (HFS) generated LTP (20 Hz: 114.1±2.7%, $p<0.001$, n=13), and an intermediate frequency marked the transition between LTD and LTP (5 Hz: 95.9±3.7%, p=0.30, n=9). The resulting FRF (Figure 1B) maps the degree of synaptic activity during induction to the degree of resulting synaptic plasticity and is consistent with existing literature (Cooper and Bear, 2012).

DCS was then applied during plasticity induction at each frequency. Our previous experiments with the present preparation demonstrate that cathodal DCS depolarizes CA1 apical dendrites (Figure 1A; Bikson et al. 2004, figure 10), and was therefore expected to facilitate LTP in this dendritic region (Malenka and Bear, 2004). DCS significantly attenuated LTD induced by 0.5 Hz (Figure 1C; 97.5±5.9%, p = 0.04, n = 8) and 1 Hz LFS (Figure 1D; 89.2±3.1%, p = 0.03, n = 10) and enhanced LTP induced by 20 Hz HFS (Figure 1F; 128.8±4.7%, p = 0.01, n = 14). The DCS effect at 5 Hz trended towards significance (Figure 1E; 102.3±2.2%, p = 0.14, n = 11), consistent with smaller effects observed previously at the threshold between LTP and LTD (Hulme et al., 2012; Ikegaya et al., 2002; Lisman, 2001). The resulting DCS FRF was significantly shifted compared to control ($F=17.93$, $df=1$, $p<0.0001$). Fitting a double exponential to the means of each FRF highlights the DCS-induced reduction in LTP threshold, biasing synapses toward

potentiation (Figure 1B). Similar shifts of the FRF have been associated with enhanced learning in cortex (Cooper and Bear, 2012; Hulme et al., 2013).

DCS effects on LTP depend on dendritic location

DCS is known to modulate the membrane potential of neuronal compartments (Andreasen and Nedergaard, 1996; Bikson et al., 2004; Chan et al., 1988; Radman et al., 2009; Rahman et al., 2013) and dendritic membrane potential is known to be a critical determinant of NMDAR-dependent plasticity (Malenka and Bear, 2004). Other DCS effects in humans and animals have been shown to be NMDAR-dependent, and it is widely speculated that tDCS exerts long-term effects through membrane polarization and NMDARs (Stagg and Nitsche, 2011). An important subtlety that is often lost in this discussion is that DCS will simultaneously depolarize and hyperpolarize different compartments within the same neuron. Indeed, previous work from our own group with a similar experimental setup showed that cathodal DCS simultaneously depolarizes CA1 apical dendrites while hyperpolarizing their basal dendrites and soma. Conversely, anodal DCS hyperpolarizes CA1 apical dendrites while depolarizing their basal dendrites and soma (Bikson et al., 2004). We therefore expected that the effects of anodal and cathodal stimulation would vary with dendritic location. To test this we paired both anodal and cathodal DCS with 20 Hz HFS in both CA1 apical and basal dendrites. In apical dendrites, cathodal DCS enhanced LTP, while anodal DCS had no significant effect (Figure 2C,D; control: 114.1±2.7%,n=13; cathodal: 128.8±4.7%,p=0.01,n=14; anodal: 111.7±4.5%,p=0.63, n=8). In basal dendrites, anodal DCS now enhanced LTP while cathodal DCS had no significant effect (Figure 2E,F; control: 148.6±3.6%,n=10; cathodal:142.5±5.2%, p=0.34,n=10; anodal: 180.4±9.1%, p<0.01,n=5). As expected, the effects of anodal and cathodal DCS were dependent on dendritic location.

DCS effects are polarity dependent for LTP but not LTD

Anodal and cathodal DCS apply stimulation with opposite polarity and are canonically expected to produce opposite effects (Nitsche et al., 2008). As reported above, we find that cathodal and anodal DCS have asymmetric effects on LTP for a given dendritic location. Moreover, when paired with 1Hz LFS we

observe no polarity dependence of effects. LTD is reduced by both anodal and cathodal DCS, i.e. synaptic strength is increased compared to control (Figure 2G,H; control: 78.9±2.9%,n=9; cathodal: 89.2±3.1%,p=0.03,n=10; anodal: 95.6±5.9%,n=8,p=0.04). These results reveal that modulation of synaptic plasticity by DCS depends on both the physical location of concurrently active synapses (basal or apical dendrites) and the rate of their activity (LFS or HFS) (Figure 2B).

DCS effects require a concurrent endogenous source of NMDAR plasticity

tDCS is often applied under the assumption that stimulation alone is sufficient to induce plasticity (Brunoni et al., 2012; Pelletier and Cicchetti, 2015; Ridding and Ziemann, 2010). However, given the modest effects on membrane potential for typical stimulation intensities (Andreasen and Nedergaard, 1996; Radman et al., 2009; Rahman et al., 2013), we propose that DCS instead acts as a modulator of NMDAR plasticity. DCS would therefore require a concurrent endogenous source of plasticity to modulate. To test this requirement we again applied cathodal DCS, but removed endogenous NMDAR-dependent plasticity in two ways: first by weakening synaptic activity to well below the plasticity threshold, and second by directly blocking NMDAR current during strong synaptic activity. When applied during weak synaptic activity (30 pulses, 1/60 Hz), cathodal DCS had no effect (Figure 3C; control: 99.3±1.1%, n=9; cathodal DCS: 100.8±4.0%, n=7; p = 0.68). When paired with strong synaptic activity (20 Hz HFS) but NMDARs were blocked with antagonist MK-801, cathodal DCS also had no effect (Figure 3B, control: 92.0±1.6%, n=10; cathodal DCS: 94.3±2.3%, n=9; p = 0.42). These results suggest that DCS may act as a modulator of endogenous synaptic plasticity, rather than an inducer of de novo synaptic plasticity.

Acute effects of DCS on synaptic transmission

To gain insight into potential mechanisms by which DCS may modulate synaptic plasticity, we examined the effects of DCS on several measures of baseline synaptic transmission. However, one-way ANOVAs yielded no significant effect of stimulation on fEPSP slope (Figure 4A; F=0.23,df=1,p=0.63), fiber volley amplitude (Figure 4B, F=0.33,df=1,p=0.57), or paired pulse ratio (Figure 4C; F=0.11,df=1,p=0.74).

Discussion

LTP, LTD, and learning

There is now strong evidence for a role of both LTP and LTD-like processes in various types of learning and memory (Broussard et al., 2016; Connor and Wang, 2015; Dong et al., 2013; Kuhlman et al., 2014; Nabavi et al., 2014; Rioult-Pedotti, 2000). At the behavioral level, learning is likely to involve both of these processes, with the precise degree of each depending on the specific behavior. For example, some learned behaviors directly require habituation to a familiar stimulus and are specifically dependent on LTD (Griffiths et al., 2008; Massey and Bashir, 2007). Other learned behaviors involve formation of new associations and responses to the environment, which require LTP and are eliminated by LTD (Broussard et al., 2016; Nabavi et al., 2014). We observed that LTP is facilitated in dendrites that are depolarized by DCS. This cellular DCS effect may contribute to enhanced learning when tDCS is paired with training that induces plasticity, such as motor rehabilitation (Kang et al., 2016; Rioult-Pedotti, 2000). Indeed, similar shifts in the FRF have been linked to facilitation of learning on both theoretical and experimental grounds (Cooper and Bear, 2012). We also observed a reduction of LTD for both stimulation polarities (Figure 2B). One may therefore expect that these effects would inhibit learning that requires LTD.

Plasticity dependence may underlie task-specific effects

When tDCS is paired with training, the observed effects are often specific to the trained task (Bikson et al., 2013; Gill et al., 2015; Sipolins et al., in review). While electrodes are typically placed over an intended target region, it is unlikely that task specificity is solely the result of spatial selectivity of current flow. Even in the most focal tDCS applications (e.g. HD-tDCS), current flow through the brain is diffuse, reaching large swaths of cortex and subcortical structures (Borckardt et al., 2012; Datta et al., 2009). Moreover, within any particular brain region, there are likely to be neurons involved in many disparate memory engrams or behaviors. The common assumption that tDCS induces plastic effects indiscriminately (Nitsche et al., 2008), or even at weakly active synapses (Fritsch et al., 2010), therefore

implies broad effects on any cognitive output in the stimulated brain regions. This is at odds with the observed specificity of effects. Instead, to explain task-specificity tDCS may act as a selective modulator of endogenous synaptic plasticity. Our results support this hypothesis, as DCS had no effect when synaptic input was too weak (Figure 3C) or when NMDARs were blocked during strong synaptic input (Figure 3B), indicating that synaptic efficacy is modulated by DCS only when NMDAR-dependent plasticity is present. This provides a basis for effects to be task-specific, as synapses associated with the paired task are more likely to be undergoing plasticity and therefore subject to modulation during tDCS. Moreover, this predicts that tDCS effects should be enhanced when paired with tasks that induce synaptic plasticity. Indeed, there is some evidence for this (Gill et al., 2015; Martin et al., 2014). The precise role of endogenous synaptic activity in DCS effects remains an important area for future research.

Dendritic polarization determines dependence on DCS polarity and pathway

Under the conventional excitability hypothesis, ‘anodal tDCS’ is assumed to produce inward cortical current flow, which depolarizes pyramidal neuron somas and hence increases cortical excitability. ‘Cathodal tDCS’ is soma-hyperpolarizing and thus should reduce cortical excitability (Nitsche et al., 2008). However, it is becoming increasingly clear that this reasoning is an oversimplification, particularly when it comes to long-term effects and learning (Antal et al., 2007; Jacobson et al., 2012; Vines et al., 2008). While effects on somatic membrane potential must still be considered, our results here point to a role for dendritic membrane polarization in determining DCS effects on synaptic plasticity.

Membrane polarization due to DCS can in principle affect the function of all voltage-dependent channels distributed throughout a neuron, particularly the relief of NMDARs from magnesium blockade. This influence may be most pronounced in dendrites, where DCS has been shown to modulate excitability involving multiple voltage-dependent channels (Andreasen and Nedergaard, 1996). While we do not directly measure membrane polarization in the present experiments, our group has done this previously with the same preparation, showing membrane polarization to be maximal in dendrites (Bikson et al.

2004, figure 10), with opposite polarization in apical and basal dendrites. Indeed we observe modulation of synaptic plasticity that is consistent with this variable dendritic, rather than a singular somatic polarization effect (Figure 2).

Given that DCS effects can vary with dendritic location, tasks that activate pathways with different dendritic locations may respond differently to the same stimulation. A lack of control over the location of active pathways could therefore lead to highly variable results in clinical studies. Attention to dendritic polarization may therefore help to explain mixed effects observed in tDCS outcomes (Antal et al., 2007; Horvath et al., 2014; Jacobson et al., 2012; Saucedo Marquez et al., 2013). This motivates a shift away from the conventional focus on somatic polarization, which implies fixed excitability changes for an entire brain region.

While our results are consistent with a role for DCS-induced dendritic polarization, we cannot rule out the involvement of other cellular DCS effects, such as on inhibitory interneurons, glia, neuromodulators systems, or immune response (Pelletier and Cicchetti, 2015). Further investigation into the involvement of these systems is an important area for future work. The lack of effects on fiber volleys and paired pulse ratio suggest that DCS does not affect recruitment or vesicle release probability at presynaptic terminals. This is expected, as Schaffer collateral fibers are oriented perpendicular to the applied DCS electric field vector. While previous studies have reported effects on fEPSP slope, the lack of an effect here may result from a smaller sample size and weaker fields (Bikson et al., 2004; Kabakov et al., 2012; Rahman et al., 2013).

Low frequency stimulation effects

The horizontal axis of the FRF is often equated with the degree of postsynaptic calcium influx during induction. HFS leads to strong calcium influx and triggers LTP, while LFS leads to moderate calcium influx and LTD. Based on this calcium control hypothesis, we expected DCS-induced dendritic polarization to modulate calcium influx through NMDARs and produce horizontal shifts in the FRF (Cooper and Bear, 2012). The effects we observe with 1 Hz LFS may therefore be expected, as a

horizontal shift of the FRF in either direction would result in less LTD if 1 Hz is near the point of maximum LTD (minimum synaptic strength). This interpretation is less adequate in accounting for the effect observed at 0.5 Hz LFS (Figure 1C), as a left horizontal shift would produce more LTD at 0.5 Hz. However, recent evidence suggests a deviation from the calcium control hypothesis, as LTD can be induced by metabotropic NMDAR function rather than calcium influx (Aow et al., 2015; Dore et al., 2015; Nabavi et al., 2013a, 2013b; Stein et al., 2015). The calcium and voltage dependence of LTD remains controversial though (Babiec et al., 2014; Nabavi et al., 2013b), making it more difficult to interpret results with LFS. We also note that the duration of DCS was particularly long with 0.5 Hz LFS (30 minutes), potentially producing effects that occur on longer time scales, such as on protein synthesis. For example, priming of BDNF synthesis at the start of DCS (Podda et al., 2016) may lead to increased BDNF release later on during DCS, which reduces LTD (Ikegaya et al., 2002). Future experiments directly measuring calcium influx during these induction protocols may provide some resolution to these issues.

Effect asymmetry

Our results demonstrate an asymmetric DCS effect on synaptic plasticity, such that DCS was only able to increase synaptic strength (enhance LTP, reduce LTD). Asymmetries have been found in other animal studies (Marquez-Ruiz et al., 2012; Ranieri et al., 2012) and human studies (Coffman et al., 2014; Jacobson et al., 2012). In parallel work in our lab, we find an asymmetry in acute DCS effects on cellular excitability. This nonlinearity could be the result of the nonlinear voltage dependence of NMDARs (Jahr and Stevens, 1990). Similarly, these asymmetries may reflect floor or ceiling effects of any number of cellular processes, where the endogenous state is such that it can only be modulated in one direction.

Conclusions and context

DCS is likely to affect many cellular processes simultaneously (Pelletier and Cicchetti, 2015). To improve tDCS applications it will be important to parse which of these cellular effects are most relevant under various clinical conditions, such that desirable outcomes can be reliably produced. Previous studies in animals (Fritsch et al., 2010; Marquez-Ruiz et al., 2012; Monai et al., 2016; Podda et al., 2016; Ranieri et

al., 2012; Reato et al., 2015; Rohan et al., 2015) and humans (Liebetanz, 2002; Nitsche et al., 2003; Rroji et al., 2015) have implicated various effects related to synaptic plasticity (NMDAR, BDNF, adenosine, norepinephrine). However, it remains unknown exactly how the DCS electric field vector interacts with cellular activity to produce these effects. The brain slice preparation used here allows for precise control over the electric field vector with respect to neuronal morphology and synaptic activity, facilitating a bottom-up approach. It will be important for future work to relate the effects observed here to in vivo tDCS in both rodent models and humans.

DCS-induced membrane polarization is often cited as a source of effects (Stagg and Nitsche, 2011), but the polarization profile of a neuron during DCS will be as complex as its morphology (Rahman et al., 2013) and the effects of polarization are likely to vary with the endogenous activity of the neuron. We demonstrate here that the effects of DCS vary with the spatial and temporal properties of the endogenous synaptic activity that it is paired with (Figure 2). These results highlight the complexity of DCS interactions with neuronal morphology and activity, motivating a departure from the canonical excitability hypothesis, which implies singular effects for an entire brain region.

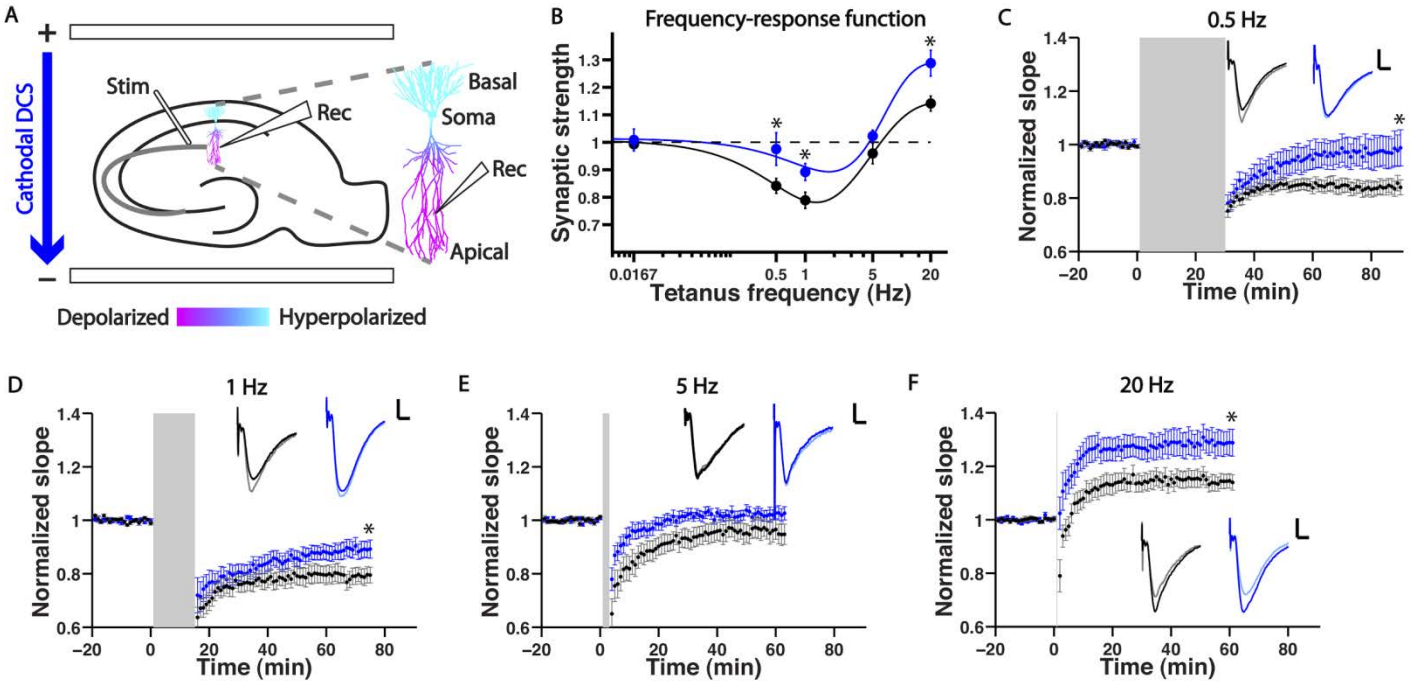

Figure 1. DCS shifts synaptic plasticity in apical dendrites towards potentiation. A: Schematic depicts cathodal DCS of a hippocampal slice, with expected membrane polarization of CA1 pyramidal neuron (enlarged at right; prediction based on computational model as in Rahman et al. 2013). Arrow indicates the direction of positive current flow between electric field wires placed in the recording chamber (horizontal bars above and below hippocampal slice). **B:** Cathodal DCS (blue) shifts the frequency-response function towards potentiation. Data are fit with a double exponential function to highlight the change LTP threshold. **C-F:** DCS applied during plasticity-inducing LFS attenuated LTD (**C,D**) and enhanced LTP (**F**), but the effect was not significant near the crossover point between LTD and LTP (**E**). Sample fEPSP traces are provided for each condition (grey/black: before/after control; light blue/blue: before/after cathodal; scale bars: 1 mV, 4 ms). Synaptic strength in (**B**) is the average of the last ten normalized fEPSP slopes in each condition (51-60 minutes post-induction). Data for 0.0167 Hz is shown in figure 3C. Grey bars indicate the duration of plasticity induction and concurrent DCS. Data are represented as mean ± SEM across slices. * = $p < 0.05$.

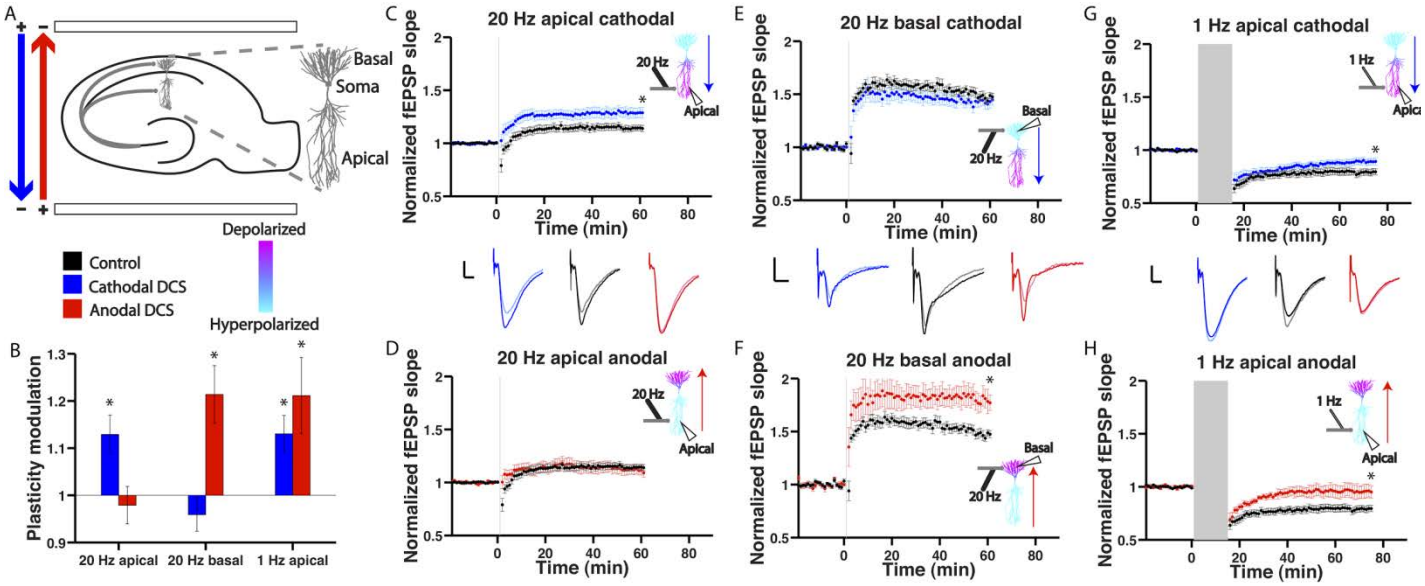

Figure 2. Mixed of effects of anodal and cathodal DCS depend on dendritic location. A: Schematic depicts anodal (red) and cathodal (blue) DCS of a hippocampal slice. Arrows indicate the direction of positive current flow between DCS electrodes. Reconstruction of a CA1 pyramidal neuron with dendritic compartments labeled at right. **B:** Modulation of synaptic plasticity depends on polarity, dendritic location and rate of induction. **C-D:** In apical dendrites cathodal DCS enhances LTP, but anodal has no significant effect. **E-F:** Changing dendritic location to basal dendrites, anodal DCS now enhances LTP, but cathodal DCS has no effect. **G-H:** Changing induction frequency to 1 Hz LFS (in apical dendrites), both anodal and cathodal reduce LTD. **C-H:** For comparison, DCS polarity is the same across each row of panels, while dendritic recording location is the same within each column of panels. Example traces for each condition are given in the center of each column (grey/light blue/pink traces are before plasticity induction; black/blue/red traces are after plasticity induction; scale bars: 1 mV, 4 ms). Insets depict the reconstructed CA1 pyramidal neuron in (**A**) with expected membrane polarization (prediction based on computational model as in Rahman et al. 2013), induction and recording sites, and orientation of DCS electric field vector. Grey bars indicate the duration of plasticity induction and concurrent DCS. Plasticity modulation in (**B**) is the resulting plasticity in each DCS condition normalized to the mean of the plasticity in the corresponding control condition. Data are represented as mean ± SEM across slices. * = $p < 0.05$.

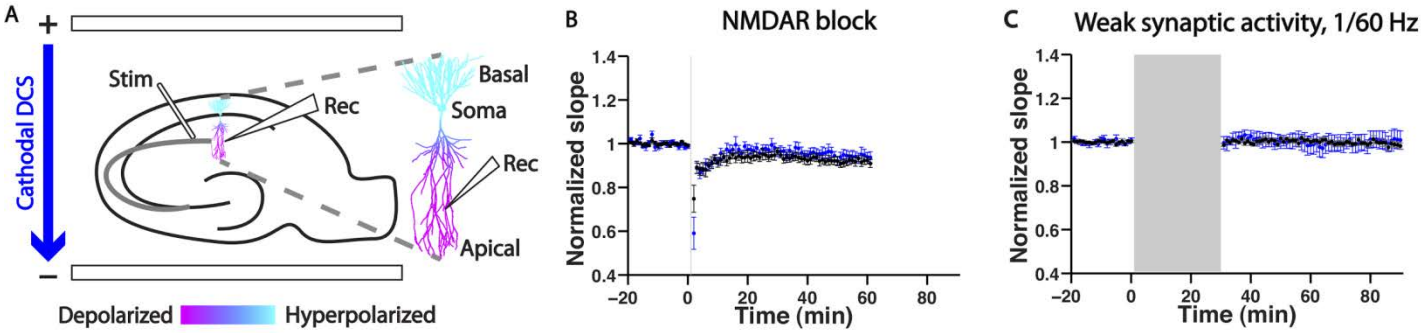

Figure 3. DCS requires an endogenous source of NMDAR plasticity. A: Schematic depicts cathodal DCS (blue) of a hippocampal slice, with expected membrane polarization of CA1 pyramidal neuron (enlarged at right; prediction based on computational model created as described in Rahman et al. 2013). **B**: Cathodal DCS with 20 Hz HFS has no effect on synaptic strength when NMDARs are blocked with antagonist MK-801 **C**: Cathodal DCS applied during synaptic activity that is too weak to induce plasticity (30 pulses at 1/60 Hz) has no effect on synaptic strength. Grey bars indicate duration of induction and concurrent DCS. Data are represented as mean ± SEM across slices.

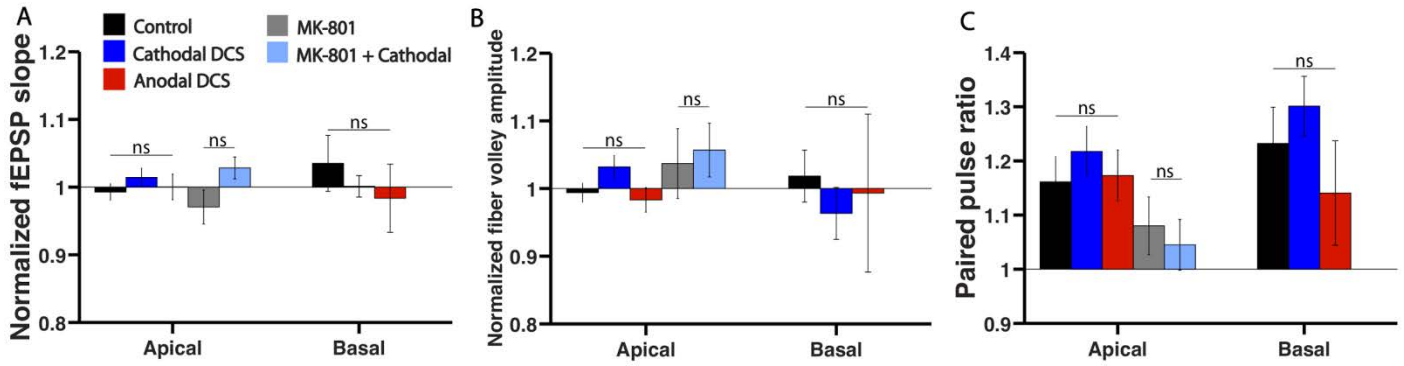

Figure 4. No significant effects on baseline synaptic transmission. DCS had no significant effect on fEPSP slope (**A**), fiber volley amplitude (**B**), or paired pulse ratio (**C**), in apical or basal dendrites, or when NMDARs were blocked with MK-801. Data are represented as mean ± SEM across slices. ns = $p > 0.05$.

References

Abbott LF, Regehr WG (2004) Synaptic computation. Nature 431:796-803.

Abbott LF, Varela JA, Sen K, Nelson SB (1997) Synaptic depression and cortical gain control. Science 275:220-224.

Ali MM, Sellers KK, Frohlich F (2013) Transcranial alternating current stimulation modulates large-scale cortical network activity by network resonance. J Neurosci 33:11262-11275.

Anastassiou CA, Montgomery SM, Barahona M, Buzsaki G, Koch C (2010) The effect of spatially inhomogeneous extracellular electric fields on neurons. J Neurosci 30:1925-1936.

Andreasen M, Nedergaard S (1996) Dendritic electrogenesis in rat hippocampal CA1 pyramidal neurons: functional aspects of Na+ and Ca2+ currents in apical dendrites. Hippocampus 6:79-95.

Antal A, Varga ET, Kincses TZ, Nitsche MA, Paulus W (2004) Oscillatory brain activity and transcranial direct current stimulation in humans. Neuroreport 15:1307-1310.

Antal A, Boros K, Poreisz C, Chaieb L, Terney D, Paulus W (2008) Comparatively weak after-effects of transcranial alternating current stimulation (tACS) on cortical excitability in humans. Brain Stimul 1:97-105.

Ardolino G, Bossi B, Barbieri S, Priori A (2005) Non-synaptic mechanisms underlie the after-effects of cathodal transcutaneous direct current stimulation of the human brain. Journal of Physiology-London 568:653-663.

Arlotti M, Rahman A, Minhas P, Bikson M (2012) Axon Terminal Polarization Induced by Weak Uniform DC Electric Fields: A Modeling Study. Conf Proc IEEE Eng Med Biol Soc.

Aroniadou VA, Keller A (1993) The patterns and synaptic properties of horizontal intracortical connections in the rat motor cortex. J Neurophysiol 70:1553-1569.

Aroniadou VA, Keller A (1995) Mechanisms of LTP induction in rat motor cortex in vitro. Cereb Cortex 5:353-362.

Ascoli GA (2006) Mobilizing the base of neuroscience data: the case of neuronal morphologies. Nat Rev Neurosci 7:318-324.

Atallah BV, Scanziani M (2009) Instantaneous modulation of gamma oscillation frequency by balancing excitation with inhibition. Neuron 62:566-577.

Baczyk M, Jankowska E (2014) Presynaptic actions of transcranial and local direct current stimulation in the red nucleus. J Physiol 592:4313-4328.

Basser PJ, Roth BJ (2000) New currents in electrical stimulation of excitable tissues. Annu Rev Biomed Eng 2:377-397.

BeMent SL, Ranck JB, Jr. (1969) A quantitative study of electrical stimulation of central myelinated fibers. Exp Neurol 24:147-170.

Bikson M, Radman T, Datta A (2006) Rational modulation of neuronal processing with applied electric fields. Conference proceedings : Annual International Conference of the IEEE Engineering in Medicine and Biology Society IEEE Engineering in Medicine and Biology Society Conference 1:1616-1619.

Bikson M, Reato D, Rahman A (2012a) Cellular and Network Effects of Transcranial Direct Current Stimulation: Insights from Animal Models and Brain Slice. In: Transcranial Brain Stimulation, 1 Edition (Miniussi C, Paulus W, Rossini PM, eds), p 456. New York: CRC Press.

Bikson M, Dmochowski J, Rahman A (2012b) The "quasi-uniform" assumption in animal and computational models of non-invasive electrical stimulation. Brain Stimul.

Bikson M, Ghai RS, Baraban SC, Durand DM (1999) Modulation of burst frequency, duration, and amplitude in the zero-Ca(2+) model of epileptiform activity. J Neurophysiol 82:2262-2270.

Bikson M, Datta A, Rahman A, Scaturro J (2010) Electrode montages for tDCS and weak transcranial electrical stimulation: Role of "return" electrode's position and size. Clinical Neurophysiology 121:1976-1978.

Bikson M, Inoue M, Akiyama H, Deans JK, Fox JE, Miyakawa H, Jefferys JG (2004) Effects of uniform extracellular DC electric fields on excitability in rat hippocampal slices in vitro. J Physiol 557:175-190.

Bikson M, Bulow P, Stiller JW, Datta A, Battaglia F, Karnup SV, Postolache TT (2008) Transcranial direct current stimulation for major depression: a general system for quantifying transcranial electrotherapy dosage. Curr Treat Options Neurol 10:377-385.

Bindman LJ, Lippold OC, Redfearn JW (1962) Long-lasting changes in the level of the electrical activity of the cerebral cortex produced by polarizing currents. Nature 196:584-585.

Bindman LJ, Lippold OC, Redfearn JW (1964) The Action of Brief Polarizing Currents on the Cerebral Cortex of the Rat (1) during Current Flow and (2) in the Production of Long-Lasting after-Effects. J Physiol 172:369-382.

Bolzoni F, Baczyk M, Jankowska E (2013a) Subcortical effects of transcranial direct current stimulation in the rat. J Physiol 591:4027-4042.

Bolzoni F, Pettersson LG, Jankowska E (2013b) Evidence for long-lasting subcortical facilitation by transcranial direct current stimulation in the cat. J Physiol 591:3381-3399.

Brignani D, Ruzzoli M, Mauri P, Miniussi C (2013) Is transcranial alternating current stimulation effective in modulating brain oscillations? PLoS One 8:e56589.

Brown P, Oliviero A, Mazzone P, Insola A, Tonali P, Di Lazzaro V (2001) Dopamine dependency of oscillations between subthalamic nucleus and pallidum in Parkinson's disease. J Neurosci 21:1033-1038.

Brunoni AR, Nitsche MA, Bolognini N, Bikson M, Wagner T, Merabet L, Edwards DJ, Valero-Cabre A, Rotenberg A, Pascual-Leone A, Ferrucci R, Priori A, Boggio PS, Fregni F (2012) Clinical research with transcranial direct current stimulation (tDCS): challenges and future directions. Brain Stimul 5:175-195.

Bullock TH, Hagiwara S (1957) Intracellular recording from the giant synapse of the squid. J Gen Physiol 40:565-577.

Buzsaki G, Draguhn A (2004) Neuronal oscillations in cortical networks. Science 304:1926-1929.

Buzsaki G, Wang XJ (2012) Mechanisms of gamma oscillations. Annu Rev Neurosci 35:203-225.

Cambiaghi M, Velikova S, Gonzalez-Rosa JJ, Cursi M, Comi G, Leocani L (2010) Brain transcranial direct current stimulation modulates motor excitability in mice. Eur J Neurosci 31:704-709.

Cano T, Morales-Quezada JL, Bikson M, Fregni F (2013) Methods to focalize noninvasive electrical brain stimulation: principles and future clinical development for the treatment of pain. Expert review of neurotherapeutics 13:465-467.

Carlson C, Devinsky O (2009) The excitable cerebral cortex Fritsch G, Hitzig E. Uber die elektrische Erregbarkeit des Grosshirns. Arch Anat Physiol Wissen 1870;37:300-32. Epilepsy Behav 15:131-132.

Castro-Alamancos MA, Donoghue JP, Connors BW (1995) Different forms of synaptic plasticity in somatosensory and motor areas of the neocortex. J Neurosci 15:5324-5333.

Chan CY, Nicholson C (1986) Modulation by applied electric fields of Purkinje and stellate cell activity in the isolated turtle cerebellum. J Physiol 371:89-114.

Chan CY, Hounsgaard J, Nicholson C (1988) Effects of electric fields on transmembrane potential and excitability of turtle cerebellar Purkinje cells in vitro. J Physiol 402:751-771.

Creutzfeldt OD, Fromm GH, Kapp H (1962) Influence of transcortical d-c currents on cortical neuronal activity. Exp Neurol 5:436-452.

Datta A, Elwassif M, Battaglia F, Bikson M (2008) Transcranial current stimulation focality using disc and ring electrode configurations: FEM analysis. Journal of Neural Engineering 5:163-174.

Datta A, Baker JM, Bikson M, Fridriksson J (2011) Individualized model predicts brain current flow during transcranial direct-current stimulation treatment in responsive stroke patient. Brain Stimul 4:169-174.

Datta A, Truong D, Minhas P, Parra LC, Bikson M (2012) Inter-Individual Variation during Transcranial Direct Current Stimulation and Normalization of Dose Using MRI-Derived Computational Models. Frontiers in psychiatry / Frontiers Research Foundation 3:91.

Datta A, Bansal V, Diaz J, Patel J, Reato D, Bikson M (2009) Gyri-precise head model of transcranial direct current stimulation: Improved spatial focality using a ring electrode versus conventional rectangular pad. Brain Stimulation 2:201-207.

Dayan E, Censor N, Buch ER, Sandrini M, Cohen LG (2013) Noninvasive brain stimulation: from physiology to network dynamics and back. Nat Neurosci 16:838-844.

Deans JK, Powell AD, Jefferys JG (2007) Sensitivity of coherent oscillations in rat hippocampus to AC electric fields. J Physiol 583:555-565.

Domingo JL, Llobet JM, Corbella J (1990) Toxic effects of vanadium in streptozotocin-treated rats after administration of vanadate to normalize blood glucose levels. Diabetologia 33:62-63.

Dudel J (1971) The effect of polarizing current on action potential and transmitter release in crayfish motor nerve terminals. Pflugers Arch 324:227-248.
Durand DM, Bikson M (2001) Suppression and control of epileptiform activity by electrical stimulation: A review. Proceedings of the Ieee 89:1065-1082.
Edwards DJ, Krebs HI, Rykman A, Zipse J, Thickbroom GW, Mastaglia FL, Pascual-Leone A, Volpe BT (2009) Raised corticomotor excitability of M1 forearm area following anodal tDCS is sustained during robotic wrist therapy in chronic stroke. Restorative neurology and neuroscience 27:199-207.
Eldar E, Cohen JD, Niv Y (2013) The effects of neural gain on attention and learning. Nat Neurosci.
Francis JT, Gluckman BJ, Schiff SJ (2003) Sensitivity of neurons to weak electric fields. J Neurosci 23:7255-7261.
Fritsch B, Reis J, Martinowich K, Schambra HM, Ji Y, Cohen LG, Lu B (2010) Direct current stimulation promotes BDNF-dependent synaptic plasticity: potential implications for motor learning. Neuron 66:198-204.
Fritsch GT HE (1870) On the electrical excitability of the cerebrum In: Von Bonin G (1960) trans. Some Papers on the Cerebral Cortex.
Fröhlich F, McCormick DA (2010) Endogenous electric fields may guide neocortical network activity. Neuron 67:129-143.
Fujisawa S, Matsuki N, Ikegaya Y (2004) Chronometric readout from a memory trace: gamma-frequency field stimulation recruits timed recurrent activity in the rat CA3 network. J Physiol 561:123-131.
Gartside IB (1968) Mechanisms of sustained increases of firing rate of neurones in the rat cerebral cortex after polarization: reverberating circuits or modification of synaptic conductance? Nature 220:382-383.
Gasca F, Richter L, Schweikard A (2010) Simulation of a conductive shield plate for the focalization of transcranial magnetic stimulation in the rat. Conf Proc IEEE Eng Med Biol Soc 2010:1593-1596.
Gerstner W, Kreiter AK, Markram H, Herz AV (1997) Neural codes: firing rates and beyond. Proc Natl Acad Sci U S A 94:12740-12741.
Ghai RS, Bikson M, Durand DM (2000) Effects of applied electric fields on low-calcium epileptiform activity in the CA1 region of rat hippocampal slices. J Neurophysiol 84:274-280.
Gluckman BJ, Neel EJ, Netoff TI, Ditto WL, Spano ML, Schiff SJ (1996) Electric field suppression of epileptiform activity in hippocampal slices. J Neurophysiol 76:4202-4205.
Gomez PSA, Faraji J, Metz GA, Tatsuno M, Luczak A (2013) Transcranial direct current stimulation in stroke rehabilitation: a review of recent advancements. Stroke research and treatment 2013:170256.
Guleyupoglu B, Schestatsky P, Edwards D, Fregni F, Bikson M (2013) Classification of methods in transcranial electrical stimulation (tES) and evolving strategy from historical approaches to contemporary innovations. J Neurosci Methods 219:297-311.
Haider B, Duque A, Hasenstaub AR, McCormick DA (2006) Neocortical network activity in vivo is generated through a dynamic balance of excitation and inhibition. J Neurosci 26:4535-4545.
Hause L (1975) A mathematical model for transmembrane potentials secondary to extracellular fields., in Electroanaesthesia: Biomedical and Biophysical Studies. New York: Academic Press.
Herrmann CS, Rach S, Neuling T, Struber D (2013) Transcranial alternating current stimulation: a review of the underlying mechanisms and modulation of cognitive processes. Front Hum Neurosci 7:279.
Hess G, Donoghue JP (1994) Long-Term Potentiation of Horizontal COnnections Provides A Mechanism To Reorganize Cortical Motor Maps. Journal of Neurophysiology 71:2543-2547.
Hess G, Aizenman CD, Donoghue JP (1996) Conditions for the induction of long-term potentiation in layer II/III horizontal connections of the rat motor cortex. Journal of Neurophysiology 75:1765-1778.
Holt GR, Koch C (1999) Electrical interactions via the extracellular potential near cell bodies. Journal of computational neuroscience 6:169-184.
Hubbard JI, Willis WD (1962a) Mobilization of transmitter by hyperpolarization. Nature 193:174-175.
Hubbard JI, Willis WD (1962b) Hyperpolarization of mammalian motor nerve terminals. J Physiol 163:115-137.
Hubbard JI, Willis WD (1968) The effects of depolarization of motor nerve terminals upon the release of transmitter by nerve impulses. J Physiol 194:381-405.
Islam N, Aftabuddin M, Moriwaki A, Hori Y (1997) Effects of anodal polarization on protein kinase Cgamma (PKCgamma) in the rat brain. Indian J Physiol Pharmacol 41:204-210.
Jefferys JGR (1981) Influence of electric fields on the excitability of granule cells in guinea-pig hippocampal slices. J Physiol 319:143-152.

Joucla S, Yvert B (2009) The "mirror" estimate: an intuitive predictor of membrane polarization during extracellular stimulation. Biophys J 96:3495-3508.
Joucla S, Yvert B (2011) Modeling extracellular electrical neural stimulation: From basic understanding to MEA-based applications. J Physiol Paris.
Kabakov AY, Muller PA, Pascual-Leone A, Jensen FE, Rotenberg A (2012) Contribution of axonal orientation to pathway-dependent modulation of excitatory transmission by direct current stimulation in isolated rat hippocampus. J Neurophysiol.
Kar K, Krekelberg B (2012) Transcranial electrical stimulation over visual cortex evokes phosphenes with a retinal origin. J Neurophysiol 108:2173-2178.
Keller A (1993) Intrinsic synaptic organization of the motor cortex. Cereb Cortex 3:430-441.
Kim GW, Ko MH (2013) Facilitation of corticospinal tract excitability by transcranial direct current stimulation combined with voluntary grip exercise. Neurosci Lett.
Koch C (1984) Cable theory in neurons with active, linearized membranes. Biological cybernetics 50:15-33.
Krause B, Márquez-Ruiz J, Cohen Kadosh R (2013) The effect of transcranial direct current stimulation: a role for cortical excitation/inhibition balance? Front Hum Neurosci 7.
Kronberg G, Bikson M (2012) Electrode assembly design for transcranial Direct Current Stimulation: a FEM modeling study. Conf Proc IEEE Eng Med Biol Soc 2012:891-895.
Kuo MF, Nitsche MA (2012) Effects of transcranial electrical stimulation on cognition. Clinical EEG and neuroscience : official journal of the EEG and Clinical Neuroscience Society 43:192-199.
Kwag J, Paulsen O (2009) The timing of external input controls the sign of plasticity at local synapses. Nat Neurosci 12:1219-1221.
Lapenta OM, Minati L, Fregni F, Boggio PS (2013) Je pense donc je fais: transcranial direct current stimulation modulates brain oscillations associated with motor imagery and movement observation. Front Hum Neurosci 7:256.
Lesniak M, Polanowska K, Seniow J, Czlonkowska A (2013) Effects of Repeated Anodal tDCS Coupled With Cognitive Training for Patients With Severe Traumatic Brain Injury: A Pilot Randomized Controlled Trial. The Journal of head trauma rehabilitation.
Liebetanz D, Fregni F, Monte-Silva KK, Oliveira MB, Amancio-dos-Santos A, Nitsche MA, Guedes RC (2006) After-effects of transcranial direct current stimulation (tDCS) on cortical spreading depression. Neurosci Lett 398:85-90.
Lopez-Quintero SV, Datta A, Amaya R, Elwassif M, Bikson M, Tarbell JM (2010) DBS-relevant electric fields increase hydraulic conductivity of in vitro endothelial monolayers. J Neural Eng 7:16005.
Madhavan S, Shah B (2012) Enhancing motor skill learning with transcranial direct current stimulation - a concise review with applications to stroke. Frontiers in psychiatry / Frontiers Research Foundation 3:66.
Malenka RC, Nicoll RA (1999) Long-term potentiation--a decade of progress? Science 285:1870-1874.
Markram H, Wang Y, Tsodyks M (1998) Differential signaling via the same axon of neocortical pyramidal neurons. Proceedings of the National Academy of Sciences of the United States of America 95:5323-5328.
Marquez-Ruiz J, Leal-Campanario R, Sanchez-Campusano R, Molaee-Ardekani B, Wendling F, Miranda PC, Ruffini G, Gruart A, Delgado-Garcia JM (2012) Transcranial direct-current stimulation modulates synaptic mechanisms involved in associative learning in behaving rabbits. Proc Natl Acad Sci U S A.
Marshall L, Helgadottir H, Molle M, Born J (2006) Boosting slow oscillations during sleep potentiates memory. Nature 444:610-613.
McNeal DR (1976) Analysis of a model for excitation of myelinated nerve. IEEE Trans Biomed Eng 23:329-337.
Medina J, Beauvais J, Datta A, Bikson M, Coslett HB, Hamilton RH (2013) Transcranial direct current stimulation accelerates allocentric target detection. Brain Stimul 6:433-439.
Merrill DR, Bikson M, Jefferys JGR (2005) Electrical stimulation of excitable tissue: design of efficacious and safe protocols. Journal of Neuroscience Methods 141:171-198.
Miledi R, Slater CR (1966) The action of calcium on neuronal synapses in the squid. J Physiol 184:473-498.
Minhas P, Bansal V, Patel J, Ho JS, Diaz J, Datta A, Bikson M (2010) Electrodes for high-definition transcutaneous DC stimulation for applications in drug delivery and electrotherapy, including tDCS. Journal of Neuroscience Methods 190:188-197.
Miranda PC, Lomarev M, Hallett M (2006) Modeling the current distribution during transcranial direct current stimulation. Clin Neurophysiol 117:1623-1629.

Miranda PC, Faria P, Hallett M (2009) What does the ratio of injected current to electrode area tell us about current density in the brain during tDCS? Clin Neurophysiol 120:1183-1187.
Miranda PC, Correia L, Salvador R, Basser PJ (2007a) Tissue heterogeneity as a mechanism for localized neural stimulation by applied electric fields. Phys Med Biol 52:5603-5617.
Miranda PC, Correia L, Salvador R, Basser PJ (2007b) The role of tissue heterogeneity in neural stimulation by applied electric fields. Conf Proc IEEE Eng Med Biol Soc 2007:1715-1718.
Moliadze V, Atalay D, Antal A, Paulus W (2012) Close to threshold transcranial electrical stimulation preferentially activates inhibitory networks before switching to excitation with higher intensities. Brain Stimul 5:505-511.
Mongillo G, Barak O, Tsodyks M (2008) Synaptic theory of working memory. Science 319:1543-1546.
Montez T, Poil SS, Jones BF, Manshanden I, Verbunt JP, van Dijk BW, Brussaard AB, van Ooyen A, Stam CJ, Scheltens P, Linkenkaer-Hansen K (2009) Altered temporal correlations in parietal alpha and prefrontal theta oscillations in early-stage Alzheimer disease. Proc Natl Acad Sci U S A 106:1614-1619.
Morrell F (1961) Effect of anodal polarization on the firing pattern of single cortical cells. Annals of the New York Academy of Sciences 92:860-876.
Nagarajan SS, Durand DM, Warman EN (1993) Effects of induced electric fields on finite neuronal structures: a simulation study. IEEE Trans Biomed Eng 40:1175-1188.
Nitsche MA, Paulus W (2000) Excitability changes induced in the human motor cortex by weak transcranial direct current stimulation. J Physiol 527 Pt 3:633-639.
Nitsche MA, Paulus W (2001) Sustained excitability elevations induced by transcranial DC motor cortex stimulation in humans. Neurology 57:1899-1901.
Nitsche MA, Seeber A, Frommann K, Klein CC, Rochford C, Nitsche MS, Fricke K, Liebetanz D, Lang N, Antal A, Paulus W, Tergau F (2005) Modulating parameters of excitability during and after transcranial direct current stimulation of the human motor cortex. J Physiol 568:291-303.
Ochi M, Saeki S, Oda T, Matsushima Y, Hachisuka K (2013) Effects of anodal and cathodal transcranial direct current stimulation combined with robotic therapy on severely affected arms in chronic stroke patients. Journal of rehabilitation medicine : official journal of the UEMS European Board of Physical and Rehabilitation Medicine 45:137-140.
Olma MC, Dargie RA, Behrens JR, Kraft A, Irlbacher K, Fahle M, Brandt S (2013) Long-term effects of serial anodal tDCS on motion perception in subjects with occipital stroke measured in the unaffected visual hemifield. Frontiers in Human Neuroscience 7.
Ozen S, Sirota A, Belluscio MA, Anastassiou CA, Stark E, Koch C, Buzsaki G (2010) Transcranial electric stimulation entrains cortical neuronal populations in rats. J Neurosci 30:11476-11485.
Park EH, Barreto E, Gluckman BJ, Schiff SJ, So P (2005) A model of the effects of applied electric fields on neuronal synchronization. Journal of computational neuroscience 19:53-70.
Peterchev AV, Wagner TA, Miranda PC, Nitsche MA, Paulus W, Lisanby SH, Pascual-Leone A, Bikson M (2011) Fundamentals of transcranial electric and magnetic stimulation dose: definition, selection, and reporting practices. Brain Stimul.
Pinsky PF, Rinzel J (1994) Intrinsic and network rhythmogenesis in a reduced Traub model for CA3 neurons. Journal of computational neuroscience 1:39-60.
Pirulli C, Fertonani A, Miniussi C (2013) The role of timing in the induction of neuromodulation in perceptual learning by transcranial electric stimulation. Brain Stimul.
Plonsey R, Barr RC (2000) Bioelectricity: a quantitative approach: Springer.
Prescott SA, De Koninck Y, Sejnowski TJ (2008) Biophysical basis for three distinct dynamical mechanisms of action potential initiation. PLoS computational biology 4:e1000198.
Priori A (2003) Brain polarization in humans: a reappraisal of an old tool for prolonged non-invasive modulation of brain excitability. Clin Neurophysiol 114:589-595.
Purpura DP, McMurtry JG (1965a) Intracellular Activities And Evoked Potential Changes During Polarization of Motor Cortex. Journal of Neurophysiology 28:166-&.
Purpura DP, McMurtry JG (1965b) INTRACELLULAR POTENTIALS OF CORTICAL NEURONS DURING APPLIED TRANSCORTICAL POLARIZING CURRENTS. Electroencephalography and Clinical Neurophysiology 18:203-&.
Radman T, Ramos RL, Brumberg JC, Bikson M (2009a) Role of cortical cell type and morphology in subthreshold and suprathreshold uniform electric field stimulation in vitro. Brain Stimulation 2:215-228.

Radman T, Su Y, An JH, Parra LC, Bikson M (2007) Spike timing amplifies the effect of electric fields on neurons: implications for endogenous field effects. J Neurosci 27:3030-3036.
Radman T, Datta A, Ramos RL, Brumberg JC, Bikson M (2009b) One-dimensional representation of a neuron in a uniform electric field. Conf Proc IEEE Eng Med Biol Soc 2009:6481-6484.
Rahman A, Reato D, Arlotti M, Gasca F, Datta A, Parra LC, Bikson M (2013) Cellular Effects of Acute Direct Current Stimulation: Somatic and Synaptic Terminal Effects. J Physiol.
Rall W (1959) Branching dendritic trees and motoneuron membrane resistivity. Exp Neurol 1:491-527.
Ranck JB, Jr. (1975) Which elements are excited in electrical stimulation of mammalian central nervous system: a review. Brain Res 98:417-440.
Ranieri F, Podda MV, Riccardi E, Frisullo G, Dileone M, Profice P, Pilato F, Di Lazzaro V, Grassi C (2012) Modulation of Ltp at Rat Hippocampal Ca3-Ca1 Synapses by Direct Current Stimulation. J Neurophysiol.
Rattay F (1989) Analysis of models for extracellular fiber stimulation. IEEE Trans Biomed Eng 36:676-682.
Reato D, Bikson M, Parra LC (2015) Lasting modulation of in vitro oscillatory activity with weak direct current stimulation. J Neurophysiol 113:1334-1341.
Reato D, Rahman A, Bikson M, Parra LC (2010) Low-Intensity Electrical Stimulation Affects Network Dynamics by Modulating Population Rate and Spike Timing. Journal of Neuroscience 30:15067-15079.
Reato D, Gasca F, Datta A, Bikson M, Marshall L, Parra LC (2013) Transcranial electrical stimulation accelerates human sleep homeostasis. PLoS computational biology 9:e1002898.
Redfearn JW, Lippold OC, Costain R (1964) A Preliminary Account of the Clinical Effects of Polarizing the Brain in Certain Psychiatric Disorders. Br J Psychiatry 110:773-785.
Reis J, Fritsch B (2011) Modulation of motor performance and motor learning by transcranial direct current stimulation. Current opinion in neurology 24:590-596.
Richardson AG, McIntyre CC, Grill WM (2000) Modelling the effects of electric fields on nerve fibres: influence of the myelin sheath. Medical & Biological Engineering & Computing 38:438-446.
Richardson MJ, Melamed O, Silberberg G, Gerstner W, Markram H (2005) Short-term synaptic plasticity orchestrates the response of pyramidal cells and interneurons to population bursts. Journal of computational neuroscience 18:323-331.
Rioult-Pedotti MS, Friedman D, Hess G, Donoghue JP (1998) Strengthening of horizontal cortical connections following skill learning. Nat Neurosci 1:230-234.
Roth BJ (1994) Mechanisms for electrical stimulation of excitable tissue. Crit Rev Biomed Eng 22:253-305.
Rubinstein JT (1993) Axon termination conditions for electrical stimulation. IEEE Trans Biomed Eng 40:654-663.
Ruffini G, Wendling F, Merlet I, Molaee-Ardekani B, Mekkonen A, Salvador R, Soria-Frisch A, Grau C, Dunne S, Miranda P (2012) Transcranial Current Brain Stimulation (tCS):Models and Technologies. IEEE transactions on neural systems and rehabilitation engineering : a publication of the IEEE Engineering in Medicine and Biology Society.
Salvador R, Mekonnen A, Ruffini G, Miranda PC (2010) Modeling the electric field induced in a high resolution realistic head model during transcranial current stimulation. Conf Proc IEEE Eng Med Biol Soc 2010:2073-2076.
Salvador R, Silva S, Basser PJ, Miranda PC (2011) Determining which mechanisms lead to activation in the motor cortex: a modeling study of transcranial magnetic stimulation using realistic stimulus waveforms and sulcal geometry. Clin Neurophysiol 122:748-758.
Sasaki T, Matsuki N, Ikegaya Y (2011) Action-potential modulation during axonal conduction. Science 331:599-601.
Sasaki T, Matsuki N, Ikegaya Y (2012) Effects of axonal topology on the somatic modulation of synaptic outputs. J Neurosci 32:2868-2876.
Saucedo Marquez CM, Zhang X, Swinnen SP, Meesen R, Wenderoth N (2013) Task-specific effect of transcranial direct current stimulation on motor learning. Frontiers in Human Neuroscience 7.
Schroeder CE, Lakatos P (2009) Low-frequency neuronal oscillations as instruments of sensory selection. Trends Neurosci 32:9-18.
Shu Y, Hasenstaub A, Badoual M, Bal T, McCormick DA (2003) Barrages of synaptic activity control the gain and sensitivity of cortical neurons. J Neurosci 23:10388-10401.
Stagg CJ, Nitsche MA (2011) Physiological basis of transcranial direct current stimulation. Neuroscientist 17:37-53.
Takeuchi A, Takeuchi N (1962) Electrical changes in pre- and postsynaptic axons of the giant synapse of Loligo. J Gen Physiol 45:1181-1193.

Tang MF, Hammond GR (2013) Anodal transcranial direct current stimulation over auditory cortex degrades frequency discrimination by affecting temporal, but not place, coding. Eur J Neurosci.

Terzuolo CA, Bullock TH (1956) Measurement of Imposed Voltage Gradient Adequate to Modulate Neuronal Firing. Proc Natl Acad Sci U S A 42:687-694.

Toleikis JR, Sances A, Jr., Larson SJ (1974) Effects of diffuse transcerebral electrical currents on cortical unit potential activity. Anesth Analg 53:48-55.

Tranchina D, Nicholson C (1986) A model for the polarization of neurons by extrinsically applied electric fields. Biophys J 50:1139-1156.

Tsodyks MV, Markram H (1997) The neural code between neocortical pyramidal neurons depends on neurotransmitter release probability. Proc Natl Acad Sci U S A 94:719-723.

Turkeltaub PE, Benson J, Hamilton RH, Datta A, Bikson M, Coslett HB (2012) Left lateralizing transcranial direct current stimulation improves reading efficiency. Brain Stimul 5:201-207.

Varela JA, Sen K, Gibson J, Fost J, Abbott LF, Nelson SB (1997) A quantitative description of short-term plasticity at excitatory synapses in layer 2/3 of rat primary visual cortex. J Neurosci 17:7926-7940.

Wang Y, Gupta A, Toledo-Rodriguez M, Wu CZ, Markram H (2002) Anatomical, physiological, molecular and circuit properties of nest basket cells in the developing somatosensory cortex. Cerebral Cortex 12:395-410.

Ward LM (2003) Synchronous neural oscillations and cognitive processes. Trends in cognitive sciences 7:553-559.

Worrell GA, Parish L, Cranstoun SD, Jonas R, Baltuch G, Litt B (2004) High-frequency oscillations and seizure generation in neocortical epilepsy. Brain 127:1496-1506.

Yi GS, Wang J, Wei XL, Tsang KM, Chan WL, Deng B (2014a) Neuronal spike initiation modulated by extracellular electric fields. PLoS One 9:e97481.

Yi GS, Wang J, Wei XL, Tsang KM, Chan WL, Deng B, Han CX (2014b) Exploring how extracellular electric field modulates neuron activity through dynamical analysis of a two-compartment neuron model. Journal of computational neuroscience 36:383-399.

Yoon KJ, Oh BM, Kim DY (2012) Functional improvement and neuroplastic effects of anodal transcranial direct current stimulation (tDCS) delivered 1day vs. 1week after cerebral ischemia in rats. Brain Res.

Zimerman M, Nitsch M, Giraux P, Gerloff C, Cohen LG, Hummel FC (2013) Neuroenhancement of the aging brain: restoring skill acquisition in old subjects. Ann Neurol 73:10-15.

Zucker RS, Regehr WG (2002) Short-term synaptic plasticity. Annual review of physiology 64:355-405.

1.

1. Report Type

Final Report

Primary Contact E-mail

Contact email if there is a problem with the report.

bikson@ccny.cuny.edu

Primary Contact Phone Number

Contact phone number if there is a problem with the report

9173062381

Organization / Institution name

The City College of New York

Grant/Contract Title

The full title of the funded effort.

Cellular Mechanisms of tDCS

Grant/Contract Number

AFOSR assigned control number. It must begin with "FA9550" or "F49620" or "FA2386".

FA9550-13-1-0073

Principal Investigator Name

The full name of the principal investigator on the grant or contract.

Marom Bikson

Program Manager

The AFOSR Program Manager currently assigned to the award

Dr. Patrick O. Bradshaw

Reporting Period Start Date

03/15/2013

Reporting Period End Date

03/14/2016

Abstract

Executive Summary: The overall aim of this proposal (FA9550-13-1-0073) was to address the cellular mechanisms of transcranial Direct Current Stimulation (DCS). Indeed, the scale and pace on tDCS trials in humans (hundreds published per year, and hundreds ongoing) has vastly outpaced our understanding of cellular mechanisms. There are so many human trials because various investigators have proposed that tDCS may be used to enhanced wide range of cognitive functions and also treat a wide range of neuro-psychiatric disease. The breadth of these applications is almost unbelievable – it is based on the general concept that tDCS is paired with a task (some kind of training) and that tDCS produces an enhancement in only that task. The ability of tDCS to selectively promote performance on trained tasks is essential but unaddressed at the cellular level. The combination of tDCS with training implies interactions of DCS with ongoing task-specific activity leading to task-specific plasticity. This proposal showed that DCS can induce lasting (plastic) changes selectivity in co-activated synaptic processes and provided a cellular substrate for these changes. This proposal therefore provided a detailed cellular-level explanation for how tDCS can enhance (theoretically) any task it is paired with. This proposal thus not only provides a cellular explanation for tDCS, it also showed why tDCS could be applied to so many applications. This is a fundamental advance in rationalizing the use of tDCS, and together is a new theory we call "functional targeting".

Distribution Statement

This is block 12 on the SF298 form.

Distribution A - Approved for Public Release

Explanation for Distribution Statement

If this is not approved for public release, please provide a short explanation. E.g., contains proprietary information.

SF298 Form

Please attach your SF298 form. A blank SF298 can be found here. Please do not password protect or secure the PDF The maximum file size for an SF298 is 50MB.

BiksonFinalReport_SB.pdf

Upload the Report Document. File must be a PDF. Please do not password protect or secure the PDF . The maximum file size for the Report Document is 50MB.

BiksonFinalReportmain.pdf

Upload a Report Document, if any. The maximum file size for the Report Document is 50MB.

Archival Publications (published) during reporting period:

Rahman A, Bikson M. et al. Diffuse and sustained electrical stimulation amplifies synaptic cooperativity. Submitted. In review.

Rahman A, Bikson M. et al. Electrical stimulation accelerates and boosts the capacity for synaptic learning . In preparation.

Kronberg G, Bikson M. et al. Modulation of synaptic plasticity with direct current stimulation is activity-dependent and differs with dendritic location. Submitted. In review.

Rahman A, Reato D, Arlotti M, Gasca F, Datta A, Parra LC, Bikson M. Cellular Effects of Acute Direct Current Stimulation: Somatic and Synaptic Terminal Effects. Journal of Physiology 2013; 591.10: 2563-2578

Rahman A, Lafon B, Bikson M. Multilevel computational models for predicting the cellular effects of noninvasive brain stimulation. Prog Brain Res. 2015;222:25-40. doi:10.1016/bs.pbr.2015.09.003

Bikson M, Truong DQ, Mourdoukoutas AP, Aboseria M, Khadka N, Adair D, Rahman A. Modeling sequence and quasi-uniform assumption in computational neurostimulation. Prog Brain Res. 2015;222:1-23 doi:10.1016/bs.pbr.2015.08.00

Rahman A, Bikson M. Origins of specificity during tDCS: anatomical, activity-selective, and input-bias mechanisms Frontiers of Human Neuroscience 2013; doi 10.3389/fnhum.2013.00688

Reato D, Rahman A, Bikson M, Parra LC. Effects of weak transcranial Alternating Current Stimulation on brain activity – a review of known mechanisms from animal studies. Frontiers of Human Neuroscience 2013; doi 10.3389/fnhum.2013.00687

2. New discoveries, inventions, or patent disclosures:

Do you have any discoveries, inventions, or patent disclosures to report for this period?

No

Please describe and include any notable dates

Do you plan to pursue a claim for personal or organizational intellectual property?

Changes in research objectives (if any):

None.

Change in AFOSR Program Manager, if any:

None.

Extensions granted or milestones slipped, if any:

None.

AFOSR LRIR Number

LRIR Title

Reporting Period

Laboratory Task Manager

Program Officer

Research Objectives

Technical Summary

Funding Summary by Cost Category (by FY, $K)

	Starting FY	FY+1	FY+2
Salary			
Equipment/Facilities			
Supplies			
Total			

Report Document

Report Document - Text Analysis

Report Document - Text Analysis

Appendix Documents

2. Thank You

E-mail user

Jun 13, 2016 17:09:53 Success: Email Sent to: bikson@ccny.cuny.edu